

**EFFECT OF ALLOYING ELEMENTS ON FERRITE GROWTH IN
FE-C-X TERNARY ALLOYS**

**EFFECT OF ALLOYING ELEMENTS ON FERRITE GROWTH IN
FE-C-X TERNARY ALLOYS**

By

DAMON PANAHI

B.Eng, M.Eng, M.Sc,

A Thesis Submitted to the School of Graduate Studies in Partial Fulfilment of the
Requirements for the Degree Doctor of Philosophy

McMaster University

© Copyright by Damon Panahi, July 2013

Doctor of Philosophy (2013)

McMaster University (Materials Science &
Engineering),
Hamilton, Ontario

TITLE: Effect of Alloying Elements on Ferrite Growth in Fe-C-X Ternary Alloys

AUTHOR: Damon Panahi, M. E. Sc. (McMaster University), M. Eng. (Iran University of
Science and Technology), B. Eng (Imam Khomeini International University)

SUPERVISORS: Dr. Gary Purdy and Dr. Hatem Zurob,

NUMBER OF PAGES: XIV, 159

Abstract

A self-consistent model for non-partitioning planar ferrite growth from alloyed austenite is developed. The model captures the evolution with time of interfacial contact conditions for substitutional and interstitial solutes. Substitutional element solute drag is evaluated in terms of the dissipation of free energy within the interface, and an estimate is provided for the rate of buildup of the alloying element “spike” in austenite.

The transport of the alloying elements within the interface region is modeled using a discrete-jump model, while the bulk diffusion of C is treated using a standard continuum treatment.

The model is validated against ferrite precipitation and decarburization kinetics in the Fe-Ni-C, Fe-Mn-C, Fe-Mo-C, Fe-Si-C, Fe-Cr-C and Fe-Cu-C systems.

Acknowledgment

My foremost thank goes to my supervisors Dr. Gary Purdy and Dr. Hatem Zurob. I thank them for their patience and encouragement that carried me on through difficult times, and for their insights and suggestions that helped to shape my research skills. Their valuable feedback contributed greatly to this dissertation.

I would also like to express my sincere gratitude to Dr. Chris Hutchinson and Dr. Yves Brechet for their fruitful collaboration and invaluable ideas. Their suggestions in research discussions provided me great opportunities to look at the challenging problems from different angles.

I especially would like to express my appreciation to Dr. Dmitri Malakhov for his invaluable guidance and support during my journey at McMaster University. I learned a lot from him.

Appreciation also goes out to Doug Culley, Ed McCaffery, Diana Maltese and Nancy Cole for all the instances at which their assistance helped me along the way.

The generous support from The Natural Sciences and Engineering Research Council of Canada (NSERC) is also greatly appreciated.

My deepest gratitude goes to my parents for their unflagging love and support throughout my life. I am indebted to my father, Jalil Panahi, and my mother, Pourandokht Mohammad-Hosseini, for their unconditional care and love.

Last but not the least I must acknowledge my beautiful wife and best friend, Tannaz, for her patience and understanding during this research. Without her love, encouragement and generous support this dissertation was simply impossible.

Contents

1. LITERATURE REVIEW	1
1.1 Introduction	1
1.2 Thermodynamic treatment of kinetics of internal processes	4
1.2.1 Irreversible thermodynamic of bulk phases	4
1.2.2 Phenomenological equations for mobility and diffusion	12
1.2.3 Free energy of precipitation	19
1.2.4 Partitioning and partitionless transformations	20
1.3 Theoretical analysis of growth of ferrite in austenite matrix	22
1.3.1 Interface-controlled growth	23
1.3.2 Diffusion-controlled growth	26
1.3.2.1 Binary systems (Fe-C)	27
a) Calculation of velocity in Fe-C system.....	31
1.3.2.2 Ternary systems (Fe-C-X).....	39
a) Local Equilibrium (LE and LENP).....	40
b) Para Equilibrium (PE)	43
c) Transition Models (PE to LENP)	47
1.3.3 Model developed by Hutchinson et.al.....	49
1.3.4 Solute drag and dissipation of free energy.....	57
1.3.4.1 Force-based models (Solute drag)	61
1.3.4.2 Free energy dissipation approach	68
1.3.4.3 Solute drag and free energy dissipation during phase transformation	71
1.3.5 Model developed by Odqvist et.al.....	75
1.4 Experimental observations on $\gamma \rightarrow \alpha$ transformation kinetics	78
1.4.1 Classical precipitation experiments.....	79
1.4.2 Controlled decarburization experiments.....	81
1.4.3 Evidences on boundary segregation and spike build-up	83
2. MODEL DEVELOPMENT	89
2.1 Self-Consistent Model for Ferrite growth	90
2.1.1 Key Physical Processes.....	90
2.1.2 Alloying Element Diffusion	90

2.1.3	Evolution of Carbon Concentrations at the Interface	94
2.1.4	Carbon Diffusion in the Bulk-phases	97
2.1.5	Growth Rate:.....	98
2.2	Model Parameters:.....	99
2.3	Application of the model	101
2.3.1	Fe-Ni-C and Fe-Mn-C.....	102
2.3.2	Fe-Mo-C system	113
2.3.3	General cases (Fe-Si-C, Fe-Cr-C and Fe-Cu-C)	114
2.3.4	Temperature-Jump experiments:.....	122
2.3.4.1	Temperature jump in Binary system (Fe-C)	123
2.3.4.2	Ternary system (Fe-C-Mo).....	127
a)	Fast forward motion	127
b)	Fast backward motion.....	130
3.	DISCUSSION	133
3.1	Key Features of the Model:	133
3.2	Critical Assessment of the Model:	136
3.3	Grain Size Effect in Precipitation:.....	139
4.	CONCLUSIONS	143
5.	FUTURE WORKS	146
APPENDIX 1:	148
THE MODIFIED THERMODYNAMIC DESCRIPTION OF FE-MN-C AT HIGH		
TEMPERATURES		148
APPENDIX 2: TWO-JUMP VS. THREE-JUMP MODEL		150
REFERENCES:.....		154

List of Figures

FIGURE 1-1. SCHEMATIC OF ENERGY BARRIER AND DRIVING FORCE FOR A REACTION BETWEEN TWO STATES.....	14
FIGURE 1-2. SCHEMATIC OF A MOLAR GIBBS ENERGY DIAGRAM FOR CALCULATION OF DRIVING FORCE FOR PRECIPITATION OF A NEW PHASE [4].....	20
FIGURE 1-3. MOLAR GIBBS FREE ENERGY DIAGRAM FOR A PARTITIONLESS TRANSFORMATION [4]	21
FIGURE 1-4. SCHEMATIC OF CONCENTRATION PROFILE DURING A DIFFUSIONLESS TRANSFORMATION [4].....	22
FIGURE 1-5. SCHEMATIC OF GIBBS FREE ENERGY DIAGRAM SHOWING A) DRIVING FORCES FOR DIFFUSION AND FRICTION B) POSSIBLE RANGE OF CONCENTRATIONS FOR A PRECIPITATE DURING MASSIVE TRANSFORMATION [4]	25
FIGURE 1-6. GROWTH OF THE FERRITE LAYER DURING DECARBURIZATION OF BINARY FE-0.57 WT% C SYSTEM AT DIFFERENT TEMPERATURES SHOWING A PERFECT MATCH WITH CALCULATIONS CONSIDERING LOCAL EQUILIBRIUM AT THE INTERFACE [10].....	28
FIGURE 1-7: COMPARISON OF THE MIXED-MODE MODEL (CURVED LINES) WITH THE DIFFUSION-CONTROLLED MODEL (THE STRAIGHT LINE). CALCULATED BY KRIELAART ET.AL. [11].....	29
FIGURE 1-8: COMPARISON OF EVOLUTION OF CARBON PROFILES IN A) INTERFACE-CONTROLLED MODEL B) DIFFUSION-CONTROLLED MODEL AND C) MIXED-MODE MODEL [11] IN A FE-C ALLOY	30
FIGURE 1-9. SCHEMATIC OF GENERAL TECHNIQUES FOR INVESTIGATING FERRITE GROWTH IN STEELS [17], [18].....	32
FIGURE 1-10 (A) CARBON CONCENTRATION PROFILE DURING CLASSICAL PRECIPITATION (B) AREAS TO BE CONSIDERED IN MASS BALANCE EQUATION	34
FIGURE 1-11. FE-C PHASE DIAGRAM [19].....	35
FIGURE 1-12. CARBON PROFILE DURING DECARBURIZATION PROCESS IN DIFFERENT REGION 1 [19]	37
FIGURE 1-13. VARIATION OF CARBON DIFFUSIVITY IN AUSTENITE AS A FUNCTION OF A) CONCENTRATION AND B) TEMPERATURE [21].....	38
FIGURE 1-14. (A) I/C CONTOURS FOR EACH TIE-LINE [26] (B) ENVELOPE OF ZERO PARTITIONING [3]	40
FIGURE 1-15. SCHEMATIC OF A) LOCAL EQUILIBRIUM WITH NEGLIGIBLE PARTITIONING, B) LOCAL EQUILIBRIUM WITH FULL PARTITIONING [3]	42
FIGURE 1-16. HILLERT’S THERMODYNAMIC APPROACH FOR FINDING LENP LINE IN FE-C-X SYSTEMS [26]	43
FIGURE 1-17. PARA EQUILIBRIUM TIE-LINES [3]	45
FIGURE 1-18. SCHEMATIC OF FE-C-X PHASE DIAGRAM SHOWING THE PARA-EQUILIBRIUM PHASE BOUNDARIES [35], ISOTHERMAL SECTION OF THE PHASE DIAGRAM	45
FIGURE 1-19. KINETICS OF FERRITE GROWTH DURING DECARBURIZATION OF FE-MN-C AT DIFFERENT TEMPERATURES [41]	54
FIGURE 1-20. SCHEMATIC PRESENTATION OF TWO-JUMP MODEL BY ZUROB ET.AL [41].....	55
FIGURE 1-23. SCHEMATIC CHARACTERIZATION OF INTERFACE MODELS [2].....	58
FIGURE 1-24. CLASSIFICATION OF THE COMMON ALLOYING ELEMENTS IN STEEL [13]	58
FIGURE 1-25. BALANCE OF FORCES ACTING ON THE GRAIN BOUNDARY DURING GRAIN GROWTH [47]	62
FIGURE 1-26. ATTRACTING POTENTIAL WELL AROUND A BOUNDARY [19].....	63
FIGURE 1-27. (A) COMPOSITION PROFILES FOR AN ATTRACTIVE POTENTIAL WELL AT DIFFERENT INTERFACE VELOCITIES $V_A < V_B < V_C < V_D < V_E$ (B) IMPURITY DRAG FOR VARIOUS VELOCITIES [44].....	65

FIGURE 1-28. SCHEMATIC OF ATOMISTIC TREATMENT OF SOLUTE DRAG PROPOSED BY LUCKE AND STUEW [45].....	66
FIGURE 1-29. ENERGY BALANCE AT THE BOUNDARY DURING GRAIN GROWTH [47].....	69
FIGURE 1-30: SCHEMATIC OF CONCENTRATION PROFILE ACROSS THE PHASE INTERFACE IN THE THERMODYNAMIC APPROACH DEVELOPED BY LIU ET.AL [50] A) THREE-ZONE MODEL USED FOR ANALYZING THE EFFECT OF NIOBIUM ON MASSIVE TRANSFORMATION [51] AND B) TWO ZONES MODEL USED FOR ANALYZING EFFECT OF MO ON BAY FORMATION IN TTT DIAGRAMS [53].....	72
FIGURE 1-31. SUGGESTED POTENTIAL WELL AT THE INTERFACE USED BY PURDY AND BRECHET [31] FOR CALCULATING SOLUTE DRAG DURING PHASE TRANSFORMATION	73
FIGURE 1-21. SCHEMATIC PRESENTATION OF A) THE VARIATION THERMODYNAMIC PROPERTIES AND B) CONCENTRATION GRADIENT IN ODQVIST'S MODEL.....	77
FIGURE 1-22. A+ Γ PHASE FIELD IN FE-C-NI PHASE DIAGRAM AT 973 K (700 °C). PF LINE IS SHOWING THE POSSIBLE TRANSITION PATH FROM PE TO LENP GROWTH CONDITION [37][38].....	78
FIGURE 1-32. EXPERIMENTALLY OBTAINED BOUNDARY FOR TRANSITION FROM FAST GROWTH RATE TO SLOW GROWTH RATE OBTAINED USING CLASSICAL PRECIPITATION TECHNIQUE A) ISOPLETH FOR ALLOY CONTAINING 2 WT% MN B) ISOPETH FOR ALLOY CONTAINING 2.5 WT% NI [59].....	80
FIGURE 1-33. KINETICS OF FERRITE LAYER GROWTH IN DECARBURIZING EXPERIMENTS ON FE-0.54 WT% C-0.51 WT% MO ALLOY, BY HUTCHINSON <i>ET.AL</i> [16]	82
FIGURE 1-34. STEM RESULTS ON MO ACCUMULATION AT Γ /A INTERPHASE BOUNDARIES OF PRECIPITATION EXPERIMENTS ON FE-0.24 WT PCT C-0.93 WT PCT MO ALLOY AT DIFFERENT TIMES AND TEMPERATURES (EACH POINT IS AN AVERAGE OF DIFFERENT MEASUREMENTS ON A SINGLE BOUNDARY) [62]	84
FIGURE 1-35: THE HEAT TREATMENT PROCEDURES USED BY CHEN <i>ET.AL</i> [64] FOR THEIR EXPERIMENT	85
FIGURE 1-36: THE DILATION RESULTS BY CHEN <i>ET.AL</i> [64] IN FE-0.17Mn-0.023C ALLOY AS A FUNCTION OF TEMPERATURE (A) THE CYCLIC PROCEDURE BETWEEN 860 °C AND 885 °C. THE GROWTH RETARDATION IS OBSERVED DURING THE FINAL STAGE COOLING STEP (IN SOLID AND RED LINE) AND (B) THE USUAL $\Gamma \rightarrow$ A TRANSFORMATION IN WHICH NO GROWTH RETARDATION IS OBSERVED DURING COOLING (IN SOLID AND RED LINE).....	86
FIGURE 1-37: Γ /A INTERFACE POSITION SIMULATED BY CHEN <i>ET.AL</i> [64] IN FE-0.17Mn-0.023C ALLOY UNDER (A) LOCAL EQUILIBRIUM CONDITIONS AND (B) PARAEQUILIBRIUM CONDITIONS AS A FUNCTION OF TEMPERATURE AFTER THE CYCLIC PHASE TRANSFORMATIONS BETWEEN 860 °C AND 885 °C.	87
FIGURE 1-38: THE EVOLUTION OF MN PROFILES BY LOCAL EQUILIBRIUM MODEL DURING THE CYCLIC PHASE TRANSFORMATION (BY CHEN ET.AL [64]). IT SHOWS HOW THE Γ /A INTERFACE ENCOUNTERS THE BURIED MN SPIKE IN THE MATRIX (INHERITED FROM PREVIOUS THERMAL CYCLES) DURING THE FINAL COOLING DOWN STEP. THE PLOTS (A)–(D) CORRESPOND TO THE POINTS MARKED A, B, C, D IN FIGURE 1-37.	88
FIGURE 2-1. SCHEMATIC OF X CHEMICAL POTENTIAL PROFILES ACROSS THE INTERFACE:.....	91
FIGURE 2-2. INTERFACE MODEL IN TERMS OF ATOMIC PLANES (0,1,2,3) AND DEFINITION OF THE VARIOUS DIFFUSIVITIES (D_1, D_2, D_3), JUMPS AND FLUXES (J_1, J_2, J_3).....	92
FIGURE 2-3. : ISOTHERMAL SECTIONS FOR A) FE-NI-C AND B) FE-MO-C AT 775 °C, PLOTTED AS U_x VS. U_c	96
FIGURE 2-4. SCHEMATICS OF C PROFILES IN A) DECARBURIZATION AND B) PRECIPITATION; ALONG WITH VELOCITY EQUATIONS FOR THE TWO DIFFERENT CASES	98
FIGURE 2-5. A) 2.5 WT% NI ISOPLETH WITH ALLOY COMPOSITIONS (BLACK CIRCLES) EXAMINED BY OI, LUX AND PURDY [59], B) ISOTHERMAL SECTION OF FE-NI-C PHASE DIAGRAM AT 700 °C WITH FIVE ALLOY COMPOSITIONS	

EXAMINED BY HUTCHINSON *ET AL.* [16], c) 2.0 wt% MNISOPLETSHWITH DIFFERENT ALLOY COMPOSITIONS EXAMINED BY OI, LUX AND PURDY [59] d) SCHEMATIC OF THE INITIAL CHEMICAL POTENTIAL PROFILES USED FOR CALCULATIONS IN Fe-Ni-C AND Fe-Mn-C SYSTEMS 105

FIGURE 2-6. EVOLUTION OF CARBON CONCENTRATION, CARBON FLUX, AND SUBSTITUTIONAL ALLOYING ELEMENT CONCENTRATION ON THE AUSTENITE SIDE OF THE INTERFACE AS A FUNCTION OF TIME IN A) 3.14% Ni-0.062% C ALLOY, B) Fe-2.08%Mn-0.095%C ALLOY, EVOLUTION OF THE FREE ENERGY DISSIPATION FOR EACH ALLOY AS FUNCTION OF TIME IS ALSO PRESENTED IN THE LAST ROW 107

FIGURE 2-7: FERRITE LAYER GROWTH KINETICS DURING DECARBURIZATION OF Fe-1.46 Ni-0.74C ALLOY : A) 735 C, B) 755 C, c) 775 C. COMPARISONS WITH THE PE, LENP AND THE DEVELOPED MODEL ARE SHOWN IN EACH CASE AS WELL AS THE FREE ENERGY DISSIPATION DURING REACTION, 109

FIGURE 2-8. KINETICS OF DECARBURIZATION (LEFT) AND EVOLUTION OF FREE ENERGY DISSIPATION (RIGHT) IN Fe-0.94%Mn-0.57%C ALLOY AT A) 755 °C B) 775 °C, THE SECONDARY AXIS IN THE LEFT COLUMN IS PRESENTING THE LENP SPIKE BULDUP PARAMETER (P_{Spike}) WHICH IS DEFINED IN THE TEXT AND VARIES FROM 0 IN THE CASE OF PE TO 1 IN THE CASE OF LENP. 110

FIGURE 2-9. KINETICS OF DECARBURIZATION (LEFT) AND EVOLUTION OF FREE ENERGY DISSIPATION (RIGHT) IN Fe-0.94%Mn-0.57%C ALLOY AT A) 806 °C B) 825 °C, THE SECONDARY AXIS IN THE LEFT COLUMN IS PRESENTING THE LENP SPIKE BULDUP PARAMETER (P_{Spike}) WHICH IS DEFINED IN THE TEXT AND VARIES FROM 0 IN THE CASE OF PE TO 1 IN THE CASE OF LENP. 111

FIGURE 2-10: FREE ENERGY DISSIPATION ASSOCIATED WITH ATOMIC JUMPS FROM FERRITE INTO THE INTERFACE ,1, WITHIN THE INTERFACE ,2, AND FROM AUSTENITE INTO THE INTERFACE, 3, DURING INTERFACE MIGRATION IN Fe-1.46Ni-0.74C ALLOY AT (A) 735 °C AND (B) 775 °C. THE SHADED AREA IS REPRESENTING THE RANGE OF THE VELOCITIES ENCOUNTERED DURING THE DECARBURIZING EXPERIMENTS OF THIS ALLOY..... 112

FIGURE 2-11. KINETICS OF DECARBURIZATION AND EVOLUTION OF FREE ENERGY DISSIPATION IN Fe-0.51%Mo-0.54%CALLOY AT A) 775 °C B) 806 °C AND C) 825 °C. 114

FIGURE 2-12: EXPERIMENTAL FERRITE LAYER GROWTH KINETICS MEASUREMENTS FROM Fe-0.88 Si-0.58C ALLOY EXAMINED BY ZUROB *ET.AL* [18]: A) 775 C, B) 806 C, c) 825 C D) 850 C . COMPARISONS WITH THE PE, LENP AND THE DEVELOPED MODEL ARE SHOWN IN EACH CASE AS WELL AS THE FREE ENERGY DISSIPATION DURING REACTION..... 115

FIGURE 2-13: EXPERIMENTAL FERRITE LAYER GROWTH KINETICS MEASUREMENTS FROM Fe-2.00 Cr-0.58C ALLOY EXAMINED BY BECHE *ET.AL* [23] : A) 775 C, B) 806 C, c) 825 C, D) 850 C. COMPARISONS WITH THE PE, LENP AND THE DEVELOPED MODEL ARE SHOWN IN EACH CASE AS WELL AS THE FREE ENERGY DISSIPATION DURING REACTION..... 116

FIGURE 2-14: EXPERIMENTAL FERRITE LAYER GROWTH KINETICS MEASUREMENTS FROM Fe-0.97 Cu-0.56C ALLOY [75]: A) 755 C, B) 775 C, c) 806 C D) 830 C E) 855 C. COMPARISONS WITH THE PE, LENP AND THE DEVELOPED MODEL ARE SHOWN IN EACH CASE AS WELL AS THE FREE ENERGY DISSIPATION DURING REACTION. 118

FIGURE 2-15: DECARBURIZING SETUP FOR TEMPERATURE-JUMP EXPERIMENTS IN Fe-C SYSTEM 124

FIGURE 2-16: TEMPERATURE-JUMP DATA IN Fe-C SYSTEM. SAMPLES WERE DECARBURIZED FOR 20 MINUTES AT 850 °C AND THEN WERE MOVED TO 750 °C. THE PREDICTED KINETICS ASSUMING FULL EQUILIBRIUM AT 750 °C IS SHOWN BY THE DOTTED LINE. 125

FIGURE 2-17: A) INTERFACIAL CARBON CONCENTRATIONS AND CARBON PROFILES IMMEDIATELY AFTER TEMPERATURE JUMP FROM 850 °C TO 750 °C IN Fe-0.65 C B) SCHEMATIC OF CARBON FLUXES IN FERRITE AND AUSTENITE AFTER CHANGING THE TEMPERATURE 126

FIGURE 2-18: A) DICTRA PREDICTIONS FOR T-JUMP EXPERIMENT IN Fe-C SYSTEM A) LAYER THICKNESS BEFORE AND AFTER TEMPERATURE JUMP B) CARBON PROFILES IN AUSTENITE AND FERRITE AFTER TEMPERATURE-JUMP 126

FIGURE 2-19: (Fe-4.72 Mo)-C BINARY PHASE DIAGRAM SHOWING THE TEMPERATURES AT WHICH DECARBURIZATION WAS CONDUCTED 128

FIGURE 2-20: EXPERIMENTAL RESULTS FOR TEMPERATURE JUMP FROM 1178 °C TO 578 °C IN Fe-0.27 C-4.72 Mo ALLOY 129

FIGURE 2-21: MODELING RESULTS FOR TEMPERATURE-JUMP EXPERIMENT IN Fe-0.27C-4.72 Mo ALLOY. A) VARIATION OF CARBON CONCENTRATION AT AUSTENITE INTERFACE ($X_{CINTAUST}$), B) CARBON PROFILES IN FERRITE AND AUSTENITE AFTER SUDDEN CHANGE OF CARBON ON THE AUSTENITE SIDE OF THE INTERFACE 129

FIGURE 2-22: EXPERIMENTAL OBSERVATION FOR TEMPERATURE-JUMP FROM 850 °C TO 600 °C IN Fe-0.65C-1.85 Mo ALLOY. A) 45 MINUTES AT 850 °C AND JUMP TO 600 °C, B) 5 MINUTES AT 850 °C AND THEN JUMP TO 600 °C 131

FIGURE 2-23: A) INTERFACE LOCATION BEFORE AND AFTER TEMPERATURE JUMP FROM 850 C TO 600 C IN Fe-0.65C-1.85 Mo ALLOY. IT SHOWS THAT SOME FERRITE ISLANDS ARE LEFT BEHIND WHEN THE INTERFACE MOVES BACKWARD B) (Fe-1.86 Mo)-C PHASE DIAGRAM SHOWING POSSIBILITY OF CARBIDE FORMATION DURING THE T-JUMP EXPERIMENT FROM 850 °C TO 600 °C 132

FIGURE 3-1: PREDICTED EVOLUTION OF FERRITE LAYER IN AN ALLOY CONTAINING 2.41% Ni AND 0.078% C TRANSFORMED AT 700 °C FOR GRAIN SIZE OF 10, 20, 50, 100 AND 500 MM. A) THICKNESS OF THE FERRITE LAYER VS. TIME B) INTERFACE VELOCITY VS. TIME C) EVOLUTION OF AUSTENITE NICKEL AND CARBON CONCENTRATION VS. INTERFACE VELOCITY 141

FIGURE 3-2: EFFECT OF THE PRECIPITATION TEMPERATURE AND PRIOR AUSTENITE GRAIN SIZE ON FINAL FERRITE VOLUME FRACTION IN Fe-2Mn-0.05C ALLOY [77] 142

FIGURE AP1-1: PORTION OF THE Fe-Mn-C PHASE DIAGRAM. EXPERIMENTAL DATA POINTS ALONG WITH THE CALCULATED PHASE BOUNDARIES USING THERMODYNAMIC MODELS BY HUANG [82], SRIVASTAVA AND KIRKALDY [81] AND THE MODIFIED VERSION OF HUANG'S DESCRIPTION. 149

FIGURE AP2-2: EFFECT OF THE SECOND JUMP WITHIN THE INTERFACE ON FREE ENERGY DISSIPATION DURING AUSTENITE TO FERRITE TRANSFORMATION IN Fe-0.51 Mo-0.54 C SYSTEM AT 717 °C. THE DOTTED-LINE REPRESENTS RESULTS WITHOUT THE SECOND JUMP (TWO-JUMP MODEL) AND THE SOLID LINE REPRESENTS RESULTS INCLUDING THE SECOND JUMP (THREE-JUMP MODEL). A) $E=15$ KJ/MOLE B) $E=20$ KJ/MOLE 152

FIGURE AP2-3: EFFECT OF THE SECOND JUMP WITHIN THE INTERFACE ON FREE ENERGY DISSIPATION DURING FERRITE GRAIN GROWTH IN Fe-0.51 Mo-0.54 C SYSTEM AT 717 °C. THE DOTTED-LINE REPRESENTS RESULTS WITHOUT THE SECOND JUMP (TWO-JUMP MODEL) AND THE SOLID LINE REPRESENTS RESULTS INCLUDING THE SECOND JUMP (THREE-JUMP MODEL). A) $E=15$ KJ/MOLE B) $E=20$ KJ/MOLE 152

FIGURE AP2-4: EFFECT OF THE SECOND JUMP WITHIN THE INTERFACE ON FREE ENERGY DISSIPATION DURING AUSTENITE TO FERRITE TRANSFORMATION IN Fe-0.51 Mo-0.54 C SYSTEM AT 806 °C. THE DOTTED-LINE REPRESENTS RESULTS WITHOUT THE SECOND JUMP (TWO-JUMP MODEL) AND THE SOLID LINE REPRESENTS RESULTS INCLUDING THE SECOND JUMP (THREE-JUMP MODEL). A) $E=15$ KJ/MOLE B) $E=20$ KJ/MOLE 153

FIGURE AP2-5: EFFECT OF THE SECOND JUMP WITHIN THE INTERFACE ON FREE ENERGY DISSIPATION DURING AUSTENITE TO FERRITE TRANSFORMATION IN Fe-0.51 Mo-0.54 C SYSTEM AT 825 °C. THE DOTTED-LINE REPRESENTS

RESULTS WITHOUT THE SECOND JUMP (TWO-JUMP MODEL) AND THE SOLID LINE REPRESENTS RESULTS INCLUDING THE SECOND JUMP (THREE-JUMP MODEL). A) $E=15$ KJ/MOLE B) $E=20$ KJ/MOLE 153

List of Tables

TABLE 2-1. EXPERIMENTALLY OBTAINED FERRITE VOLUME FRACTION AND NEW MODEL PREDICTIONS FOR DIFFERENT FE-NI-C AND FE-MN-C ALLOYS AT DIFFERENT TEMPERATURES.....	105
TABLE 2-2: SUMMARY OF THE PARAMETERS USED FOR MODELLING OF THE INTERFACE MIGRATION IN DIFFERENT SYSTEMS.....	120
TABLE 2-3: ACTIVITY COEFFICIENT OF THE INVESTIGATED ELEMENT IN AUSTENITE AND FERRITE MATRIX OF FE-X-C ALLOYS AT DIFFERENT TEMPERATURES.....	121
TABLE 3-1: SUMMARY OF THE PARAMETERS USED IN THE PRESENT MODEL COMPARED TO EARLIER MODELS BY ODQVIST <i>ET</i> <i>AL.</i> [33, 34] AND HUTCHINSON <i>ET AL.</i> [6] FOR THE CASE OF PRECIPITATION IN FE-NI-C AT 700 °C.....	134

1. Literature review

1.1 Introduction

Transformation of austenite into ferrite is one of the most studied problems in materials science. This transformation, which usually happens under non-equilibrium conditions, is probably the most important step in production of steels for industrial uses. Controlling and manipulating this transition step provides a great opportunity for development of new generation of advanced steels with unique mechanical and physical properties.

Subsequently, development of a physically based model with predictive capability of γ to α transformation in different alloying systems has been a subject of many investigations in the last 70-80 years. Specially, extensive advancements in the area of computational thermodynamics during last 20-30 years, has provided a great opportunity for researchers to combine thermodynamic and kinetics theories and develop new computational methods for design and improvement of new alloying steels.

In line with such efforts, one can point, for example, to Johnson-Mehl-Avrami-Kolmogorov (JMAK) equation as one of the oldest empirical modeling tools used in industries for explaining the kinetics of $\alpha \rightarrow \gamma$ transition. Modified version of JMAK approach can be written as:

$$X = 1 - \exp \left\{ - \frac{1}{d_{\gamma}^m} \left(\int_T^{T_s} \frac{\beta(T)^{1/k}}{\varphi(T)} dT \right)^k \right\}$$

Where X denotes the fraction transformed, d_γ the prior austenite grain size, T the temperature, $\varphi=dT/dt$ the instantaneous cooling rate and T_s the transformation start temperature. The parameters m , k and β are those which depend on alloy composition. m is the grain size exponent and β , is the temperature dependent rate parameter.

Despite usefulness and popularity of JMAK equation, it should be emphasised that using this equation requires availability of several parameters which can only be determined experimentally for each specific alloy. It means that, introduction of even small changes in composition of an alloy necessitates new arrays of experiments to obtain these governing parameters and this, in fact, introduces a great limitation to generality of this equation. Beside this, it is also worth noticing that JMAK equation only deals with fraction of the new phase in the structure and does not give any insight regarding nature of the phase transformation.

Considering the growing needs for production and development of modern multi-alloyed steels, which usually contain more than one alloying element, it would be of primary significant for steel industries to have better physically-based models which can adequately address interactions of each of these components together and with phase boundaries during phase transformation.

In this regard, even though precipitation of ferrite from austenite involves both nucleation and growth steps but, an overall look at the available literature shows that

most of the attention in this area has been directed toward the later step - precipitation growth - which occurs irreversibly.

The influence of alloying elements on the kinetics of ferrite growth in steel has been the subject of investigation and debate for over a century. In the binary Fe-C system, the relaxation times of ferrite growth are necessarily related to the diffusion of carbon, either in austenite or in ferrite or in the interface joining them. Thus, for example, in the isothermal growth of planar grain boundary ferrite from supersaturated austenite, one finds that a local equilibrium model of the kind initially proposed by Zener [1] gives an adequate first order representation of the thickening kinetics. In contrast, it has been recognized for more than a half-century that the simple extension of the Zener model to the thickening of grain boundary ferrite allotriomorphs in ternary and higher order iron alloys is not so straightforward. The roots of the problem lie almost entirely in the huge differences in mobilities of the substitutional and interstitial solutes (*e.g.* Mn and C) in steel.

In fact, accurate understanding of evolution of alloying elements across the interface boundary and selection of the appropriate interfacial tie-line, is a key parameter for a successful modelling of the $\gamma \rightarrow \alpha$ transformation kinetics.

According to the conventional picture for phase transformation, migration of an interface involves three basic steps: 1) individual atoms feel a driving force for joining to the structure of the growing phase on the other side of the boundary and as a result leave

the parent phase, 2) diffuse through the interface boundary 3) and finally join to the structure of the growing phase [2]. All these kinetics processes during ferrite growth happen spontaneously and are intrinsically irreversible.

In general, in order to deal with addition of substitutional alloying elements in steels and model the kinetics of ferrite growth, as a priory, one needs to have a fundamental understanding of different parameters involved in the transformation process. Atomic diffusion, boundary mobility, thermodynamic driving forces, energy dissipation associated with different kinetic processes and structure of the interface region are of such parameters which should be fully understood. Some of these processes will be described in detail in sections 1.2.

1.2 Thermodynamic treatment of kinetics of internal processes

1.2.1 Irreversible thermodynamic of bulk phases

According to the second law of thermodynamic progress of any spontaneous reaction in a system is associated with net increase in entropy of the universe[3]. In isolated systems this is equivalent to the increase of entropy in that system.

According to the irreversible thermodynamics a non-equilibrium system can be divided into small sub-units within which equilibrium condition is satisfied and Gibbs fundamental relation is valid:

$$TdS_m^{total} = dU_m + PdV_m - \sum_i \mu_i dX_i \quad (1.1)$$

where, P is pressure, V_m is molar volume, μ_i is chemical potential of component i and X_i is mole fraction. This situation is called “*quasi equilibrium*” state.

In this equation dS^{total} is representing the changes in total entropy of the system. It includes contribution of different processes such as Internal processes, heat transfer (dQ) or addition of matter (dN), *i.e.*:

$$dS^{total} = d_{ip}S + \frac{dQ}{T} + S_m dN \quad (1.2)$$

In a closed system, dN is equal to zero and as a result, for an irreversible transformation, eq.(1.2) can be simplified to:

$$dS^{total} = d_{ip}S + \frac{dQ}{T} \quad (1.3)$$

Following eq.(1.3) rate of the entropy change can be written as :

$$\frac{dS^{total}}{dt} = \frac{d_{ip}S}{dt} + \frac{1}{T} \frac{dQ}{dt} \quad (1.4)$$

It means that, in a closed system with constant temperature and volume, the rate of entropy change consists of a term for contribution of heat transfer across the boundary of that system and a term which considers the contribution of internal irreversible processes, $d_{ip}S$, inside that system.

In theoretical treatment of precipitation growth, one should pay attention that, there are some important assumptions which are justified to be made in each subunit:

- 1) Volume change associated with diffusional processes in solid state can be neglected.
- 2) Usually $\gamma \rightarrow \alpha$ transformation occurs at high temperatures where thermal equilibrium assumption for vacancies is completely reasonable.
- 3) Much higher rate of heat conduction compare to the growth rate of a precipitate in diffusional solid state phase transformation makes it reasonable to assume a uniform temperature during transformation, *i.e.* temperature gradient and effect of the heat transfer can be neglected.
- 4) Constant energy
- 5) Constant number of moles

Assumptions 2 and 3, allow us to consider contribution of heat transfer across the boundary equal to zero. In other words we can write:

$$\frac{dQ}{dt} = 0 \quad \Rightarrow \quad \frac{dS^{total}}{dt} = \frac{d_{ip}S}{dt}$$

Moreover, following the derivation by Van der Ven and Delay [3], entropy in irreversible processes can be assumed as a fluid which not only crosses these units (entropy flux) but

also, can be created per unit volume (entropy production). In other words, one can also write the following entropy balance equation within each sub-unit of a closed system:

$$\frac{\partial(S^{total}/V_m)}{\partial t} = \sigma - div J_s \quad (1.5)$$

Where the term on the left represent rate of the entropy change per unit volume and the right side is presenting the difference between entropy production (σ) and flux of entropy across that unit ($div J_s$).

Assumptions 4 and 5, allow us to write the following balance equation for energy, U_m , and mass, X_i , in a subunit:

$$\frac{1}{V_m} \frac{dU_m}{dt} + div J_u = 0 \quad (1.6)$$

$$\frac{1}{V_m} \frac{dX_i}{dt} + div J_i = 0 \quad (1.7)$$

where, J_i is flux of atoms and J_u is flux of energy.

By some mathematical manipulation and Integrating equations (1.6) into the derivative of eq. (1.1) one can get an expression similar to the equation (1.5) for each subunit:

$$TdS^{total} = dU_m + \overbrace{PdV_m}^{\text{constant volume}} - \overbrace{\sum_i \mu_i dX_i}^{\text{closed system}}$$

⇓

$$\frac{dS^{total}}{dt} = \frac{1}{T} \frac{dU_m}{dt}$$

⇓ Integrating equations (1.6)

$$\frac{1}{V_m} \frac{dS^{total}}{dt} = \underbrace{\left[J_u \cdot \text{grad} \frac{1}{T} \right]}_{\sigma} - \underbrace{\text{div} \frac{1}{T} (J_u)}_{\text{div} J_s} \quad (1.8)$$

As seen in eq.(1.8), for a system, the entropy production term (σ) relates to the flux of internal processes consists:

$$\sigma = J_u \cdot \text{grad} \frac{1}{T} \quad (1.9)$$

From equation (1.9) one can conclude that the rate of entropy production (σ_i) due to internal processes for each process will retain the same form and can be written as the product of flux (J_i) and thermodynamic force (Z_i) in that process:

$$\sigma_i = J_i Z_i \quad (1.10)$$

As a result, in the presence of N irreversible processes, total rate of the entropy production will be:

$$\sigma = \sum_{i=1}^N J_i Z_i \quad (1.11)$$

By integrating over the total volume of a subunit and comparing *eq.(1.4)* with *eq.(1.8)*, one can write the following expression for the total production of entropy in a closed system:

$$d_{ip}S = \sigma dt \quad (1.12)$$

According to the second law of thermodynamics for a spontaneous reaction:

$$d_{ip}S \geq 0 \Rightarrow \sigma \geq 0$$

Generally, if advancement of a certain internal process is represented by ξ then $d_{ip}S/d\xi$ may define as a new state variable which is called '*generalized thermodynamic force*' [4] and will be denoted by Z . This variable can be used more specifically to introduce an expression for the *driving force* (D) of any internal process at constant T [4] as following:

$$D \equiv T \frac{d_{ip}S}{d\xi} = T Z \quad (1.13)$$

This driving force (D) can be evaluated in different ways, for example [4]:

$$-D = \left(\frac{\partial U}{\partial \xi} \right)_{S,V,N_i} = \left(\frac{\partial F}{\partial \xi} \right)_{T,V,N_i} = \left(\frac{\partial H}{\partial \xi} \right)_{S,P,N_i} = \left(\frac{\partial G}{\partial \xi} \right)_{T,P,N_i} = \left(\frac{\partial \Omega}{\partial \xi} \right)_{S,V,N_i}$$

Where U, F, H, G and Ω are representatives for internal energy, Helmholtz free energy, enthalpy, Gibbs free energy and grand potential, respectively. The negative sign of D is

explained by the second law of thermodynamics which requires that the entropy production rate to be positive for a spontaneous process.

The choice of an appropriate expression for driving force strongly depends on the availability of any of these fundamental equations in the system under consideration. For example, Gibbs free energy (G) is a very common choice in solid state phase transformation under constant temperature and pressure.

Here, it is also worth mentioning that for an isothermal reaction one can write:

$$\frac{d_{ip}S}{d\xi} = \frac{D}{T}$$

$$d_{ip}S = \frac{D}{T} d\xi$$

$$\Delta_{ip}S = \int d_{ip}S = \int \left(\frac{D}{T} \right) d\xi$$

$$\Delta_{ip}S = \left(\frac{1}{T} \right) \int D d\xi$$

Hillert [4] mentions that “*the quantity $\int D d\xi$ could be called **integrated driving force** but unfortunately it is often called simply ‘driving force’.*”

Under constant T, P and N_i this integrated driving force is equal to reduction of Gibbs free energy (*i.e.* dissipation of Gibbs free energy):

$$\int D d\xi = -\Delta G^{dissipated} \quad (1.14)$$

Generally, in view of these relationships between entropy production rate (σ), and driving forces for internal processes (D), rate of the energy consumption (ψ) in a closed system due to an internal process can be expressed as:

$$\psi = T.\sigma \quad (1.15)$$

$$\psi_i = T.(J_i Z_i) = J_i D_i \quad (1.16)$$

In this context, it is often said that the energy has been ‘dissipated’ during transformation and ψ_i will be equivalent to the energy dissipation per unit of time and per unit of volume at temperature T .

As mentioned, in solid state phase transformations it may be often more convenient to use Gibbs free energy to describe different processes in the system. Consequently, dissipation of free energy can be denoted by \dot{G} which is expressed in J/s as following:

$$-\dot{G}_i = J_i D_i$$

$$-\dot{G} = \sum J_i D_i$$

Obviously, to compare this dissipation rate, \dot{G} , with the total changes of the Gibbs energy, it would be necessary to express both parameters in a same dimension. Generally, this can be done by dividing \dot{G} by a flux, J_o , which is expressed in mol/sec :

$$-\Delta G_m = -\frac{\dot{G}}{J_o} = \sum f_i D_i$$

Where $f_i = J_i/J_o$.

Here ΔG_m represents the total change of the properties (or total driving force) in that system while $f_i D_i$ represents sink of the energy (dissipation of energy). For simple cases, one can define J_o to be equal to J_i [4]:

$$J_o = J_i \quad \Rightarrow \quad -\Delta G_m = \sum D_i \quad (1.17)$$

1.2.2 Phenomenological equations for mobility and diffusion

It is observed experimentally that reaction rate, $J = d\xi/dt$, in most of irreversible processes, is proportional to the thermodynamic force, $Z = dS/d\xi$ and can be described as:

$$J = L \cdot Z \quad (1.18)$$

Where L is a kinetic coefficient which is positive by definition [4].

If there are several reactions happening simultaneously in a system, then not only direct contribution of them in entropy production should be taken into account (eq.(1.11)), but also effect of possible interactions between these processes on the reaction rate should be considered (*i.e.* indirect effect).

This can be done by introducing a **phenomenological relation**:

$$J_i = \sum L_{ik} Z_k$$

$$J_i = L_{ii} Z_i + \sum_{k \neq i} L_{ik} Z_k \quad (1.19)$$

Where L_{ik} are phenomenological coefficients which describe interaction between different processes [3].

In many cases (*e.g.* atomic diffusion), we are interested in a reaction rate between two states. Having Q as the height of the energy barrier between the two states, it is again experimentally seen that in many cases rate of the reaction is closely tied to the temperature through Arrhenius equation:

$$J = K \exp\left(\frac{-Q}{RT}\right) \quad (1.20)$$

Where K is a pre-factor and R is the universal gas constant.

If the reference point for measuring Q is located on the average value between the two states (Figure 1-1), then it will be clear that the thermodynamic driving force for the reaction, D , has a direct effect on the effective activation energy (for moving the reaction in both forward and backward directions).

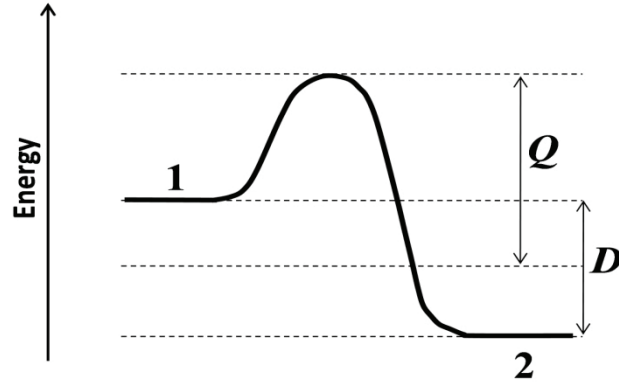


Figure 1-1. Schematic of energy barrier and driving force for a reaction between two states

As a result, according to absolute reaction rate theory, the net rate of the reaction (difference between forward and backward directions) can be expressed in the following form:

$$J = K \left[\exp\left(-\frac{Q-D/2}{RT}\right) - \exp\left(-\frac{Q+D/2}{RT}\right) \right] \quad (1.21)$$

If the driving force is very low compare to RT , then

$$\sinh(D/2RT) \approx D/2RT$$

and consequently, eq.(1.21) can be simplified to:

$$J = K \exp\left(-\frac{Q}{RT}\right) \cdot 2 \sinh\left(\frac{D}{2RT}\right) \cong \underbrace{K' \exp\left(-\frac{Q}{RT}\right)}_M \cdot D$$

$$\Rightarrow J = M \cdot D \quad (1.22)$$

Where the phenomenological coefficients in eq.(1.22), M , is called “mobility” and has the dimension $mol^2/J s$:

$$M = M_0 \exp\left(-\frac{Q}{RT}\right) \quad (1.23)$$

As an example, flux of interstitial atoms (*e.g.* Carbon in steels), occur through jumping of atoms from interstitial sites to available vacancies in a host lattice.

Driving force for this jumping at a constant temperature is chemical potential gradient of the interstitial atoms ($\nabla\mu_C$). Moreover, these atoms exchange their positions with vacancies and as a result, fractions and driving forces of these vacancies is another factor which should be also taken into account.

So, using eq. (1.22), one can drive an expression for flux of interstitial atoms (in a lattice fixed frame of reference):

$$J_C = -M y_C y_{Va} \cdot \nabla(\mu_C - \mu_{Va}) \quad (1.24)$$

Where y_C and y_{Va} are fraction of C atoms and vacancies per mole of host atoms, respectively.

$M y_C y_{Va}$ is the phenomenological coefficient and it's dimension is $mol^2/J s m$.

Similarly, flux of substitutional atoms, X , through vacancy mechanism at a high temperature, at which equilibrium number of vacancies is maintained everywhere ($\Delta\mu_{Va} = 0$), can be expressed as:

$$J_X = -M x_X \cdot \nabla \mu_X \quad (1.25)$$

Where, x_X is mole fraction of X atoms in the system. The equilibrium fraction of vacancies (x_{Va}) is incorporated in M coefficient.

For the less probable cases where substitutional diffusion happens through ring mechanism (*i.e.* substitutional atoms A and B diffuse by exchanging positions with each other), the flux expression will be:

$$J = -M_{AB} x_A \cdot x_B \nabla (\mu_A - \mu_B) \quad (1.26)$$

Here it is worth mentioning that, any movement inside a system (*e.g.* atomic flux), should be defined relative to a reference point (frame of reference) and all the expressions mentioned so far for atomic fluxes are given in *a lattice-fixed frame of reference*. Andersson and Agren mention in [5] that “*atomistic models of diffusion are usually formulated relative to the lattice and the fluxes are then expressed in the so-called lattice fixed frame*”. However, in some cases it might be more convenient to define fluxes in a *volume-fixed frame of reference*, where there is no net flow of volume in the system due to diffusion. For example, Hillert [4] states that “*The situation is different in a substitutional solution.... A lattice-fixed frame may thus expand or contract locally if the*

solute atoms diffuse with a different rate to that of the solvent atoms. Experimentally, it may be easiest to study substitutional diffusion in a volume-fixed frame”.

Nevertheless, if it is needed, one can always transfer fluxes from one frame of reference to another one [5]. For example, if flux of substitutional atoms, A , through vacancy mechanism, is expressed in the volume-fixed frame, then eq.(1.25) will get the form of eq.(1.26). In other words, “*the net effect will be the same as if atoms exchange position with each other*” [4]:

$$J = -M_{AB} x_A \cdot x_B \nabla (\mu_A - \mu_B)$$

Where:

$$M_{AB} = x_A M_A + x_B M_B \quad (1.27)$$

Here, it is of relevance to mention that according to definition of volume-fixed frame in a system (phase) with n components:

$$\sum_{k=1}^n J_k V_k = 0 \quad (1.28)$$

Where J_k and V_k are flux and partial molar volume of component k respectively.

Molar volume of a phase (V_m) is also related to the partial molar volume of its component through the following expression:

$$V_m = \sum_{k=1}^n x_k V_k \quad (1.29)$$

Where, x_k is mole fraction of each component.

Generally, in a volume-fixed frame of reference the main contribution in the volume of a phase comes from substitutional elements and as a result, one may divide all elements into two categories: those that contribute to the volume of a phase, such as substitutional elements, and those which do not contribute ($V_k = 0$), such as interstitial atoms.

For the sake of simplicity, in solid state phase transformation, one can consider the same partial molar volume (V_s) for all substitutional atoms in the system. As a result [5]:

$$V_m = \sum_{k=1}^n x_k V_s = V_s \left(\sum_{j \in \text{substitutional atoms}} x_j \right)$$

Under this condition, the concentration variable, C_k , which is defined as moles of k (x_k) per unit volume, can be presented as following [5]:

$$C_k = \frac{x_k}{V_m} = \frac{x_k}{V_s \sum_{j \in S} x_j} = \frac{1}{V_s} \cdot \frac{x_k}{\sum_{j \in S} x_j} \quad (1.30)$$

Here $\frac{x_k}{\sum_{j \in S} x_j}$ can be denoted by U_k which is called “U-fraction” and, in fact, is mole

fraction of component k on the substitutional lattice [6].

1.2.3 *Free energy of precipitation*

As mentioned before, the integrated driving force under constant T, P and N_i is expressed by eq.(1.14). For a spontaneous precipitation reaction, the extent of the process, $d\xi$, is equivalent to the amount of the precipitation:

$$D = -\left(\frac{\partial G}{\partial \xi}\right)_{T,P,N_i} = -\left(\frac{\partial G}{\partial N^\alpha}\right)_{T,P,N_i} = -\Delta G_m^\alpha$$

where N^α is number of moles of the precipitate and ΔG_m^α is decrease of Gibbs free energy accompanying the precipitation reaction:

$$\Delta G_m^\alpha = G_m^{\text{products}} - G_m^{\text{reactants}}$$

for a binary system of A and B atoms this energy is schematically presented in Figure 1-2a and can be written as:

$$\Delta G_m^\alpha = G_m^\alpha(x_B^\alpha) - [x_A^\alpha \cdot \mu_A^\gamma(x^\circ) + x_B^\alpha \cdot \mu_B^\gamma(x^\circ)] \quad (1.31)$$

if the new phase has the potential of μ_A^α and μ_B^α , then eq.(1.31) takes the following form (Figure 1-2b):

$$\Delta G_m^\alpha = x_A^\alpha (\mu_A^\alpha - \mu_A^\gamma) + x_B^\alpha (\mu_B^\alpha - \mu_B^\gamma) \quad (1.32)$$

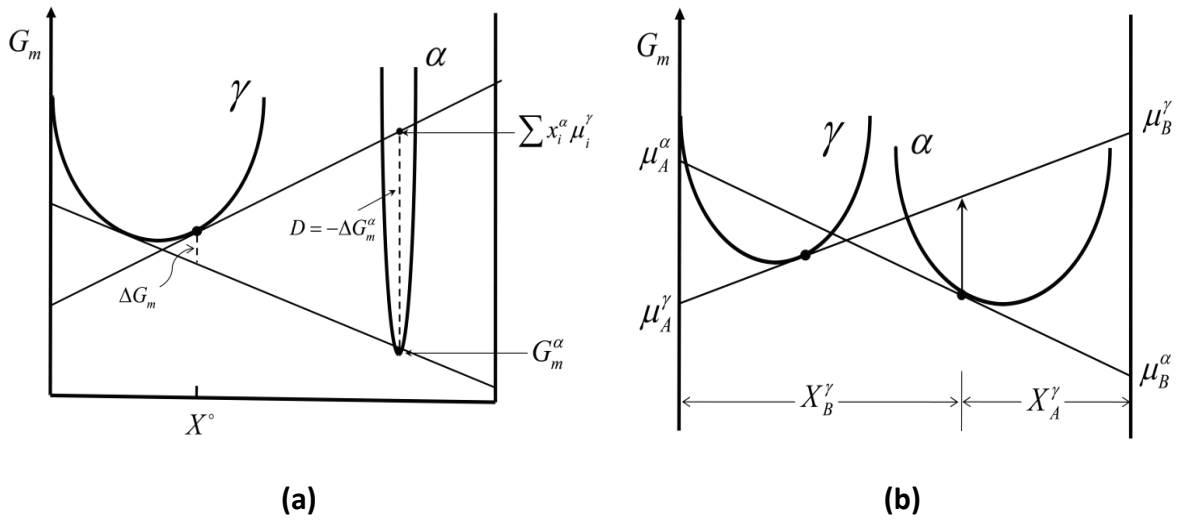


Figure 1-2. Schematic of a molar Gibbs energy diagram for calculation of driving force for precipitation of a new phase [4]

ΔG_m^α is the integrated driving force for onset of the precipitation and is the one which is usually used in the literature for precipitation discussions. Here it is very important to understand that, there is a difference between ΔG_m^α and the integrated driving force for the whole process of transformation after completion (ΔG_m). The later one, which represents the average force for transformation, is also presented in Figure 1-2b.

1.2.4 Partitioning and partitionless transformations:

When composition of both phases fall on the left hand side of the intersecting point of the Gibbs energy curves, both reactant and the product phase can have the same composition (Figure 1-3). This situation, which is usually called partitionless transformation, may occur when the parent phase is highly supersaturated.

Depending upon partitioning of the components between parent and daughter phases, the transformation can be categorized as either completely *diffusionless*, such as martensitic transformation, or *quasi-diffusionless*, such as massive transformation [4].

As demonstrated in Figure 1-4, local equilibrium assumption at the interface during phase transformation implies a spike formation and partitioning of some of the components ahead of the migration interface.

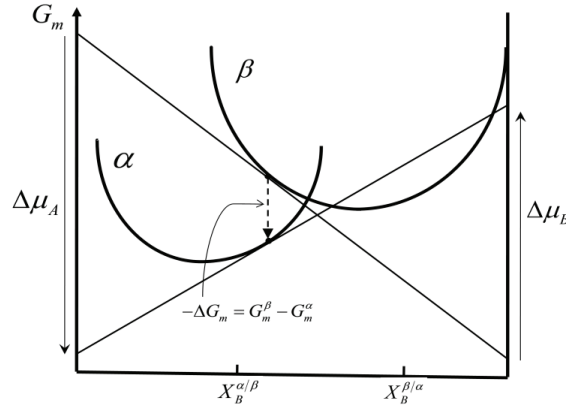


Figure 1-3. Molar Gibbs free energy diagram for a Partitionless transformation [4]

It is shown that in order to avoid complete diffusion during formation of a new phase, the growth rate of the precipitating phase should be of the order of D/d or higher (D is diffusion coefficient and d is about 10^{-10} m). Under this condition, width of the spike ahead of the interface will be less than an inter-atomic distance. In other words, pile-up formation will become physically impossible [4].

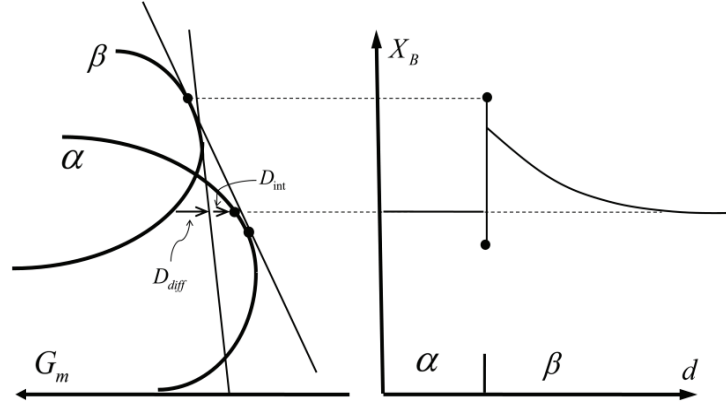


Figure 1-4. Schematic of concentration profile during a diffusionless transformation [4]

Practically, it is seldom possible to fully avoid diffusion during such diffusion-controlled transformations as ferrite precipitation from austenite. However, there are still situations where required partitioning of some alloying elements across the migrating interface is very small and as a result, precipitation of the new phase can be treated as a partitionless transformation.

1.3 *Theoretical analysis of growth of ferrite in austenite matrix*

Usually, ferrite precipitation (BCC structure) in steels at high temperatures, starts by nucleation of double spherical caps of ferrite at high angle grain boundaries of austenite (FCC structure) [7]. Detailed knowledge about structure of the interface between ferrite and austenite is a crucial factor in fully understanding and controlling this transformation. Unfortunately, transformation of austenite to martensite after quenching to room temperature makes it rather difficult to carefully analyze the interface structure. However,

obtained evidences suggest that interface structure is a mixture of coherent and incoherent regions [7][8].

In general, growth of ferrite involves both structural rearrangement (transition from FCC structure to BCC structure), and diffusional processes (e.g. partitioning of alloying elements due to compositional differences between ferrite and austenite). In other words, $\gamma \rightarrow \alpha$ transformation has a mixed nature and the available driving force for movement of the interface, $D_{\text{int}}^{\text{chem}} = -\Delta G^{\gamma \rightarrow \alpha}$, is consumed (dissipated) by both structural changes, which is called *friction*, and diffusional processes. However, for the sake of simplicity and depending upon which one of these two processes is the main source for dissipation of free energy, these transformations are usually categorized into either interface-controlled or diffusion-controlled. It means that, one may use either structural changes or diffusional processes to model the kinetics of the interface migration. Hutchinson *et.al* [6] mention that *“In principle, it does not matter which approach is taken since they must give the same interface velocity. However, in cases where it is thought that the majority of the free energy is dissipated by diffusional process in the bulk phases, the kinetics are usually cast in this light since our understanding of the nature of this diffusion far exceeds our current understanding of the atomic process occurring at the transformation interface”*.

1.3.1 ***Interface-controlled growth***

This is a rather general approach in which friction term (structural changes) is the main controlling processes that is taken into account.

As mentioned before, in solid state phase transformation one can use *eq.(1.22)* to calculate rate of a transformation. For example, in the case of interface migration:

$$J = M \cdot D$$

if J is expressed as the velocity of the interface, v , then [4]:

$$J \equiv v = M \cdot D$$

where, M is interface mobility ($1/M$ is usually regarded as the interface friction coefficient [2]) and D is the driving force for movement of the interface. In the case of ferrite precipitation, chemical potential difference between ferrite and austenite acts as the main source of energy to be consumed by different processes; *e.g.* the required driving force for overcoming the friction term is also provided from that source.

In a closed system at constant temperature and pressure, chemistry of the present phases at the interface may be used to evaluate D . Based on *eq.(1.14)*:

$$\int D d\xi = -\Delta G^{dissipated}$$

for steady state processes D is constant and as a result integration gives:

$$D \Delta\xi = -\Delta G^{dissipated}$$

For precipitation of 1 mole of ferrite, $\Delta\xi$ will be equal to unity and as a result:

$$D = \Delta G^m$$

$$v = M \cdot \Delta G^m \quad (1.33)$$

Here, it should be emphasized that ΔG^m is a portion of the total chemical force, D_{int}^{chem} that is used by the interface to overcome the friction of the lattice (to transform from FCC to BCC structure). This driving force is schematically presented in Figure 1-5a. In this figure, D_{int}^{chem} is the total chemical driving force moving the interface, ΔG^m is the driving force for overcoming the crystallographic barrier (friction) and ΔG^{diff} is the driving force required for diffusional processes [4]:

$$D_{int}^{chem} = \Delta G^{diff} + \Delta G^m \quad (1.34)$$

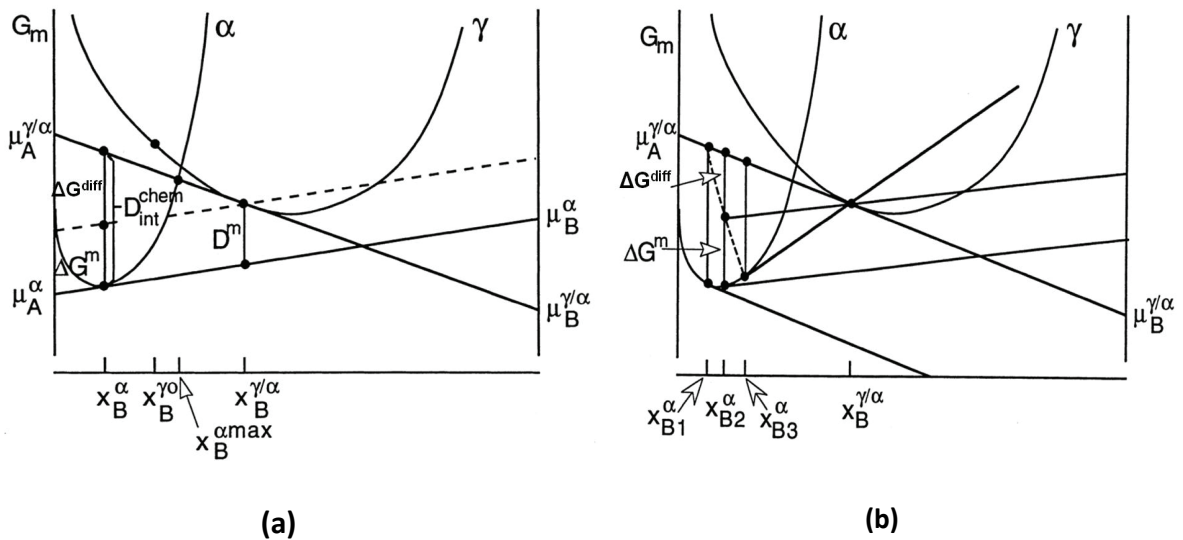


Figure 1-5. Schematic of Gibbs free energy diagram showing a) driving forces for diffusion and friction b) possible range of concentrations for a precipitate during massive transformation [4]

In Figure 1-5a, composition at the interface of the growing phase (ferrite), x_B^α , was chosen arbitrarily. However, it should be realized that there are lower and upper limits beyond which ferrite precipitation is not possible. The exact value of x_B^α is determined by

the balance between velocities predicted by interface-controlled and diffusion-controlled approaches as both approaches should yield the same velocity. x_{B1}^{α} and x_{B2}^{α} in Figure 1-5b are the lower and upper compositional limits at which nature of the transformation changes from a fully interface-controlled to a fully diffusion-controlled process, respectively.

In many cases, this modeling approach can be successfully employed to explain austenite decomposition. However, one should pay attention that there are many factors that may have significant impact on the mobility of the interface. For example, degree of coherency of the interface, pinning effects, build up of stresses or segregation of alloying element to the moving boundary in alloying steels are of phenomenon with a strong influence on the mobility of the interface. All these effects are usually united in a single mobility parameter and as a result the reported values for the interface mobility are “effective” values in which contribution of friction, segregation and *etc.* are included.

1.3.2 *Diffusion-controlled growth*

As an alternative, diffusional processes in the bulk can be employed for formulation of the kinetics of the interface migration. It is shown that [9][10], in theoretical treatment of ferrite growth at high temperatures (allotrimorphic α) it is reasonable to assume that dissipation of free energy due to structural rearrangements (friction) to be negligible, $\Delta G^m \approx 0$ [6].

It means that, the kinetics of the ferrite growth can be cast purely in terms of diffusion of different elements present in the transformation process *i.e.* all of the available chemical driving force is consumed by diffusion of participating atoms in the transformation.

1.3.2.1 *Binary systems (Fe-C)*

Carbon diffusion is usually considered as the governing factor in kinetics of isothermal growth of allotrimorph ferrite in Fe-C systems. In fact, carefully designed decarburizing experiments [10] have proven that application of the Zener's sharp interface treatment [1] and considering local equilibrium for carbon atoms across the interface ($\mu_C^\alpha = \mu_C^\gamma$), gives an adequate first order representation of the thickening kinetics. In this approach, the initial carbon concentrations at the interface at each temperature can be found from the equilibrium phase diagram. Some experimental observations obtained from decarburization process in Fe-0.57 wt% C alloy at different temperatures are presented in Figure 1-6. As seen, there is a perfect match between these experimental data points (circles) and theoretical calculations (solid line) using local equilibrium model proposed by Zener.

In other words, in the range of interface velocities usually encountered in decarburizing experiments (2×10^{-9} to 2×10^{-7} m/s), dissipation of free energy due to crystallographic changes can be neglected (infinite mobility, M , can be assumed for the interface).

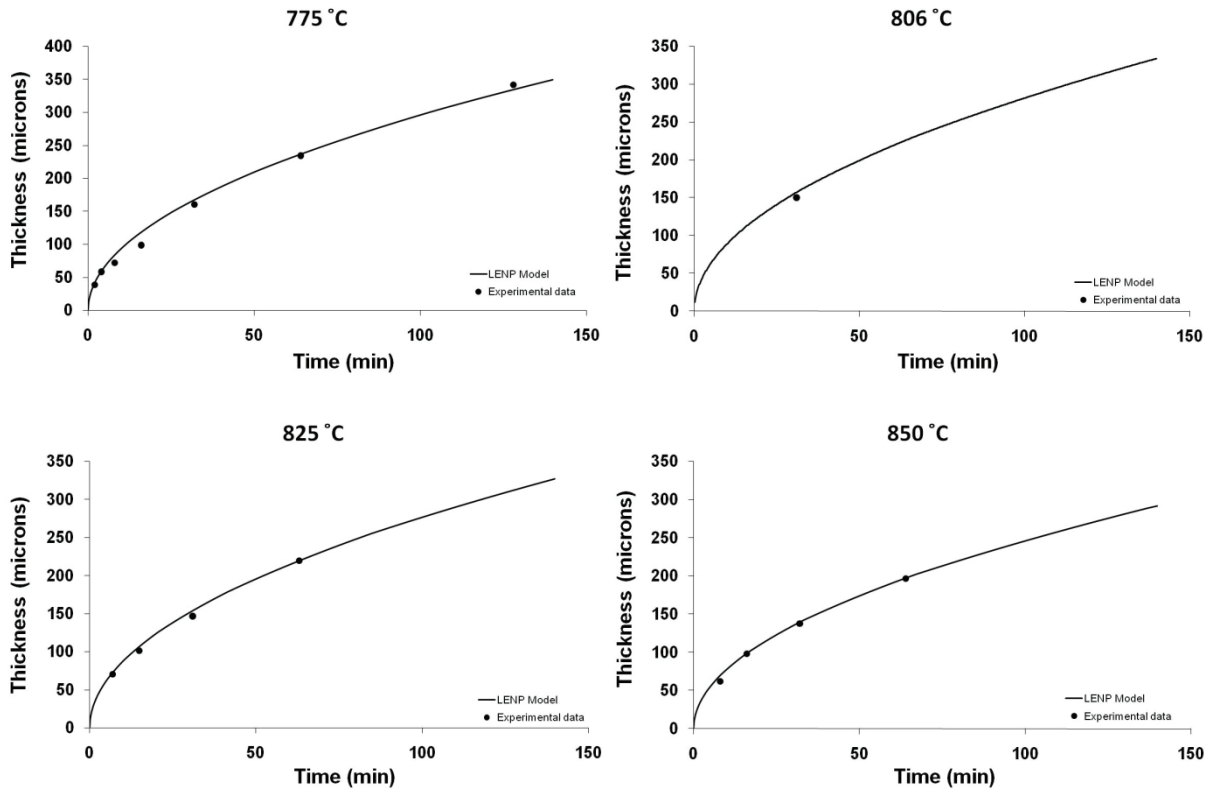


Figure 1-6. Growth of the ferrite layer during decarburization of binary Fe-0.57 wt% C system at different temperatures showing a perfect match with calculations considering local equilibrium at the interface [10]

Here, it must be insisted again that both the diffusion-controlled and the interface-controlled modes should be regarded as the extreme possibilities for explaining the kinetics of ferrite transformation. Some of the developed models [11], [12] for the mixed type of growth have shown that in the case of classical ferrite precipitation in Fe-C alloys, a mixed-mode model, in which contribution of both atomic rearrangements and bulk diffusion of carbon atoms are taken into account, can provide a better match with the experimental observations. A comparison of predicted kinetics under both diffusion controlled and mixed-mode assumption for thickening and lengthening of ferrite allotrimorphs in Fe-0.23 wt% C has been done by Krielaart *et.al.* in [11] (Figure 1-7).

Generally, in these models (mixed-mode), the carbon concentration profiles, which will be explained in detail later, are determined by both interface velocity and diffusion rate of carbon atoms.

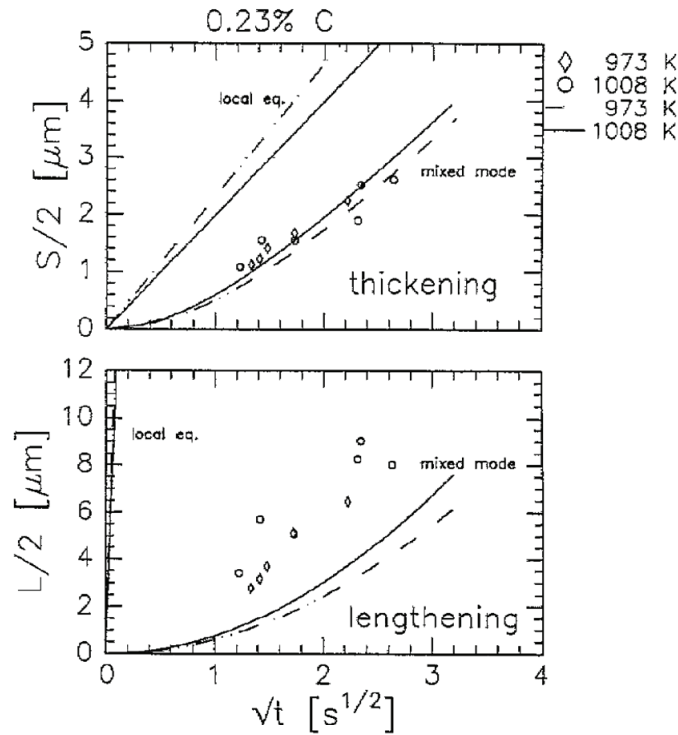


Figure 1-7: Comparison of the mixed-mode model (curved lines) with the diffusion-controlled model (the straight line). Calculated by Krielaart et.al. [11]

For example, during precipitation of ferrite (will be explained later) in Fe-C systems, as the interface advances the carbon atoms are constantly rejected from ferrite into the austenite (due to the low solubility of carbon in ferrite structure). As a result of this, a carbon flux is generated in the remaining austenite matrix and the interfacial carbon content grows toward the equilibrium composition. As was mentioned earlier, the initial carbon concentrations at the interface at each temperature can be found from the equilibrium phase diagram. However, in the diffusion-controlled mode the flux of carbon

atoms into the austenite is easily compensated by the relatively fast lattice transformation (infinite interface mobility) while in the mixed-mode growth the lattice transformation is not fast enough to compensate this flux. Consequently, in the diffusion-controlled mode austenite carbon concentration is pinned to its equilibrium value at all times but in the mixed-mode the carbon diffusion flux into the bulk austenite depletes the carbon at the interface and deviation from equilibrium value is expected [12].

Evolution of carbon profiles in different modes discussed so far, is schematically presented in Figure 1-8.

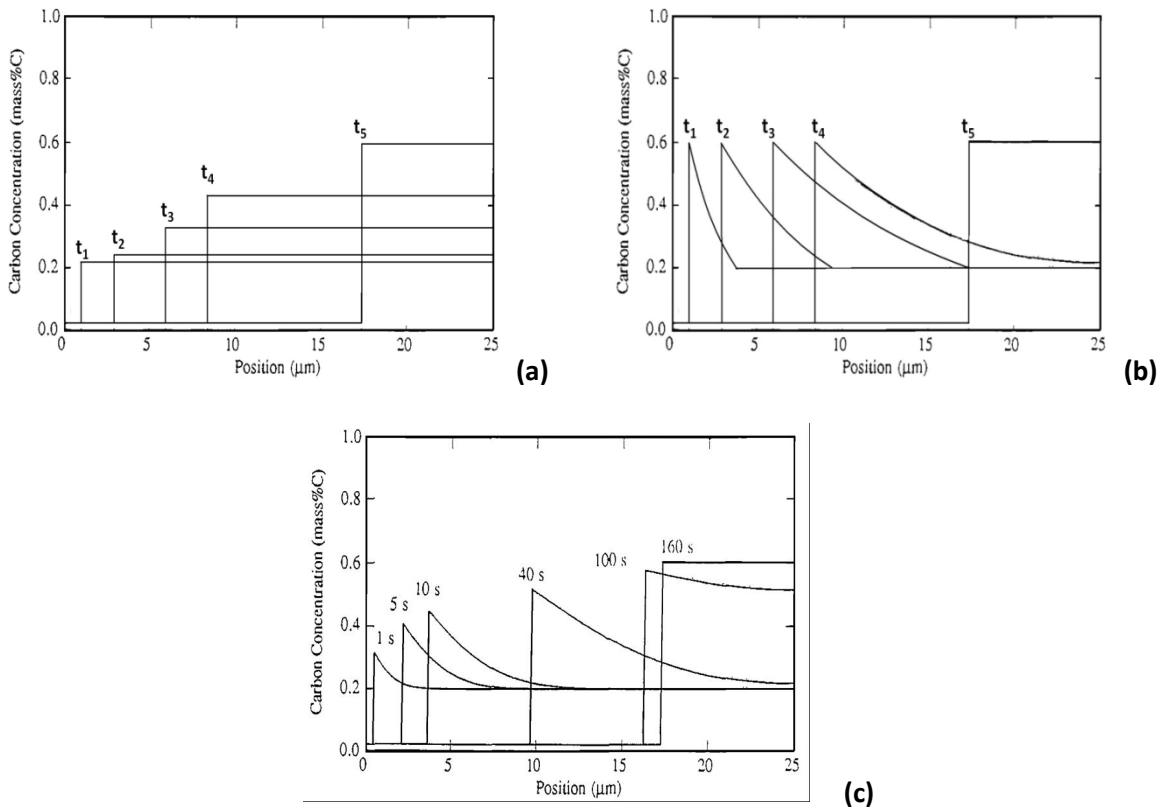


Figure 1-8: Comparison of evolution of carbon profiles in a) Interface-controlled model b) diffusion-controlled model and c) mixed-mode model [11] in a Fe-C alloy

a) Calculation of velocity in Fe-C system

Generally, it can be stated that in Fe-C systems having interfacial carbon compositions (to obtain concentration profiles) is a key parameter in finding the interface velocity during $\gamma \rightarrow \alpha$ transformation.

As the first step, neglecting the friction term (*i.e.* infinite mobility) and assuming local equilibrium at the interface one can write the following:

$$\mu_{Fe}^{\alpha} = \mu_{Fe}^{\gamma} \quad \text{and} \quad \mu_C^{\alpha} = \mu_C^{\gamma}$$

$$\Rightarrow D_{int}^{chem} = \Delta G_{int}^{diffusion} + \cancel{\Delta G_{int}^{friction}} = x_{Fe}^{\alpha} (\mu_{Fe}^{\alpha} - \mu_{Fe}^{\gamma}) + x_C^{\alpha} (\mu_C^{\alpha} - \mu_C^{\gamma}) = 0 \quad (1.35)$$

Using these conditions, the equilibrium interfacial concentrations can be calculated.

The second step will be determining a mathematic expression for carbon concentration profile in both ferrite and austenite.

From experimental point of view, there are two main techniques available for investigating the kinetics of the $\gamma \rightarrow \alpha$ phase transformation in steels:

1) the most common one is the classical precipitation technique which is of industrial relevance for microstructure evolution and has been studied for more than 50 years. In this case, a fully austenitized structure is cooled down into the two phase $\alpha + \gamma$ region where ferrite allotrimorphs start precipitating at the austenite grain boundaries.

2) the decarburizing technique which offers some advantages in terms of precision of growth kinetics data [10, 13-16]. In this technique, removal of the carbon from the surface of a fully austenitic structure at high temperatures, results in the formation of a ferrite layer at the surface.

A general picture of these two methods is presented in Figure 1-9.

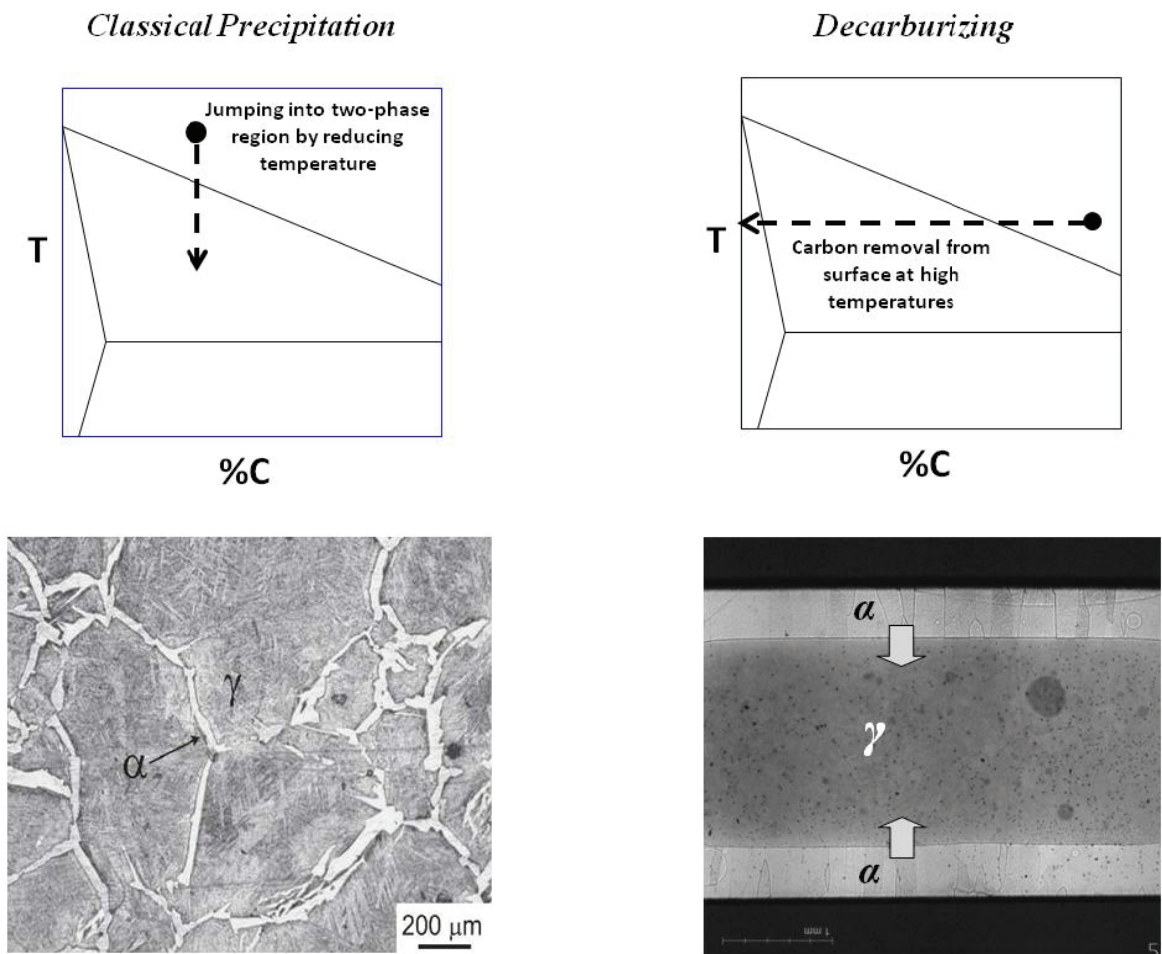


Figure 1-9. Schematic of general techniques for investigating ferrite growth in steels [17], [18]

1.3.2.1.a.1 Classical precipitation:

In the classical precipitation technique, excess carbon atoms are rejected from ferrite to the austenite side. As a result a carbon profile, similar to the one shown in Figure 1-10a, will be created in front of the migrating interface.

A general mathematical approach for finding carbon concentration profile in this case is explained below:

According to Fick's law one can write:

$$A dz(C^\gamma - C^\alpha) = -D^\gamma \left(\frac{dC^\gamma}{dz} \right) A dt \quad (1.36)$$

$$\Rightarrow v = \frac{dz}{dt} = - \frac{-D^\gamma \left(\frac{dC^\gamma}{dz} \right)_{Interface}}{C^\gamma - C^\alpha} = \frac{-D^\gamma \left(\frac{C_0 - C^\gamma}{L} \right)_{Interface}}{C^\gamma - C^\alpha} = \frac{D^\gamma (C^\gamma - C_0)}{L(C^\gamma - C^\alpha)} \quad (1.37)$$

where, L is width of the spike (carbon profile) in the bulk austenite, A is surface area of the moving interface, D^γ is carbon diffusivity in austenite, C_0 is bulk carbon concentration, $C^{\gamma-\alpha}$ is carbon concentration on the austenite side of the interface and $C^{\alpha-\gamma}$ is carbon concentration on the ferrite side of the interface.

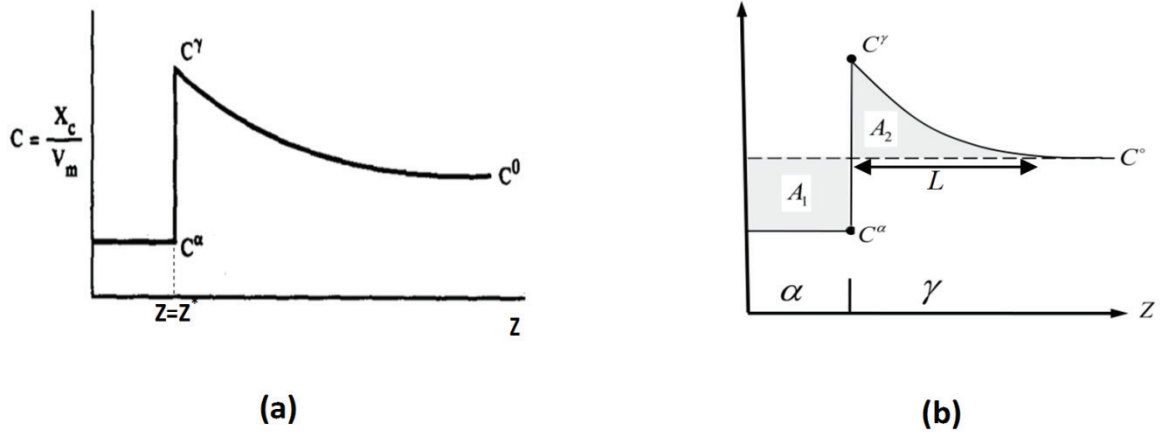


Figure 1-10 (a) Carbon concentration profile during classical precipitation (b) Areas to be considered in mass balance equation

Satisfying mass balance condition in areas A_1 and A_2 in Figure 1-10b, the following relation should be valid for L :

$$z(C_0 - C^\alpha) = \frac{1}{2}L(C^\gamma - C_0) \Rightarrow L = \frac{2z(C_0 - C^\alpha)}{(C^\gamma - C_0)}$$

$$\Rightarrow v = \frac{dz}{dt} = \frac{D^\gamma (C^\gamma - C_0)^2}{2z(C_0 - C^\alpha)(C^\gamma - C^\alpha)} \quad (1.38)$$

1.3.2.1.a.2 Decarburization

During decarburization technique situation is slightly different. Contrary to the classical precipitation where atoms are rejected from ferrite into the austenite, in the case of decarburization, carbon atoms are removed from ferrite into the atmosphere.

As seen in Figure 1-11, depending upon the temperature region in which decarburizing is happening, both ferrite and austenite may experience a flux of carbon atoms. Possible profiles at different temperatures are schematically presented in Figure 1-12 [19].

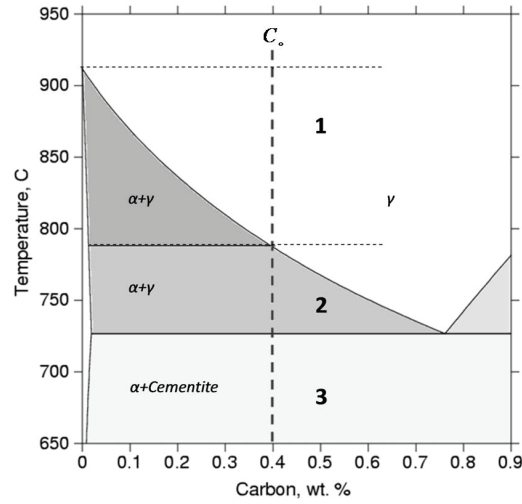


Figure 1-11. Fe-C phase diagram [19]

Depending upon region at which decarburizing is happening, Zener's sharp interface approach results in a different sets of equations for estimating the migration rate of the interface.

In regions 2 and 3 these profiles are identical and consequently, the general approach for finding the interface velocity will be the same. For instance, Carbon profile in region 3 is expressed as following [19], [20]:

$$C^\alpha(z,t) = C^{\alpha/\alpha+cem} \operatorname{erf}\left(\frac{z}{2\sqrt{D^\alpha t}}\right) / \operatorname{erf}\left(\frac{z^*}{2\sqrt{D^\alpha t}}\right) \quad (1.39)$$

and satisfying mass balance condition, one can write:

$$(C^{\alpha/\alpha+cem} - C_0) \times dz^* \times A = J^\alpha \times dt \times A$$

Where J is flux of carbon atoms (can be obtained using Fick's laws):

$$\Rightarrow \frac{dz^*}{dt} = \frac{D^\alpha \left(\frac{\partial C^\alpha(z,t)}{\partial z} \right)_{z=z^*}}{(C_0 - C^{\alpha/\alpha+cem})} \quad (1.40)$$

Here, D^α is carbon diffusivity in ferrite, $C^{\alpha/\alpha+cem}$ is carbon concentration at the ferrite-cementite interface and z^* is thickness of the decarburized layer (interface position).

Similarly, ferrite carbon profile in region 1 can be expressed by eq.(1.39) but, the following equation should be used for the austenite side [19], [20]:

$$C^\gamma(z,t) = \frac{-C_0 \operatorname{erf}\left(\frac{z^*}{2\sqrt{D^\gamma(t-t_0)}}\right)}{\operatorname{erfc}\left(\frac{z^*}{2\sqrt{D^\gamma(t-t_0)}}\right)} + (C_0 - C^{\alpha+\gamma/\gamma}) \frac{\operatorname{erf}\left(\frac{z}{2\sqrt{D^\gamma(t-t_0)}}\right)}{\operatorname{erfc}\left(\frac{z^*}{2\sqrt{D^\gamma(t-t_0)}}\right)} \quad (1.41)$$

finally, the interface velocity can be obtained by using mass balance equation:

$$(C^{\alpha/\alpha+\gamma} - C^{\alpha+\gamma/\gamma}) \times dz^* \times \cancel{A} = (J^\alpha - J^\gamma) \times \cancel{A} \times dt$$

$$v = \frac{dz^*}{dt} = \frac{(J^\alpha - J^\gamma)}{(C^{\alpha+\gamma/\gamma} - C^{\alpha/\alpha+\gamma})} = \frac{D^\alpha \left(\frac{\partial C^\alpha}{\partial z} \right)_{z=z^*} - D^\gamma \left(\frac{\partial C^\gamma}{\partial z} \right)_{z=z^*}}{(C^{\alpha+\gamma/\gamma} - C^{\alpha/\alpha+\gamma})} \quad (1.42)$$

Here, t_0 is the moment that diffusion in the austenite commences (incubation time during which carbon concentration decreases from bulk concentration to the Ac_3 line).

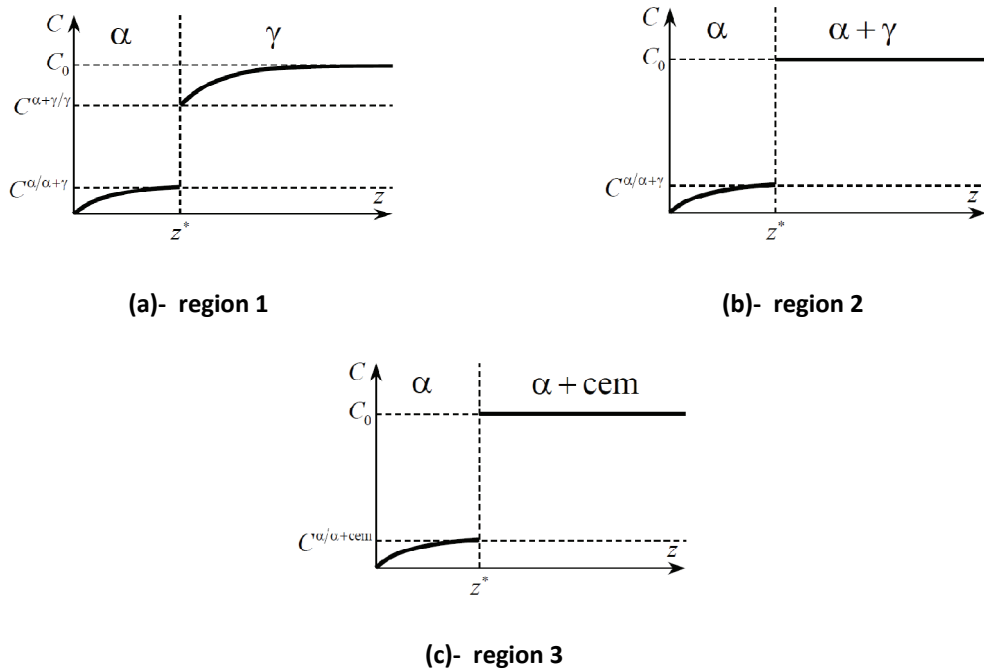


Figure 1-12. Carbon profile during decarburization process in different region 1 [19]

Interestingly, the migration rate in region 1 is proportional to the net-flux of carbon atoms, $(J^\alpha - J^\gamma)$ and depending upon sign of this expression, we can expect both positive and negative velocities during decarburization process *i.e.* the migrating interface can move both forward and backward.

It is worth insisting that, temperature dependency and effect of other alloying elements on diffusivity of carbon atoms should be always taken into account. In fact, presence of both interstitial (*e.g.* C and N) and substitutional elements can affect the carbon diffusivity by changing number of available sites for atomic jumps (*i.e.* interstitial site occupancy) and by positive and negative interaction with carbon atoms, respectively [21].

Karabelchtchikova [21] mentions that despite significant contribution of substitutional alloying elements, *“little theoretical and experimental knowledge is available to quantitatively describe the effect of alloying on carbon diffusivity. As a result, most applications assume carbon diffusivity to be either constant at fixed temperature or vary with carbon concentration only”*.

In this regard, one can point to the expression proposed by Agren [22] as one of the most popular expressions for carbon diffusivity in austenite:

$$D_C = 4.53 \cdot 10^{-7} \left[1 + y_c (1 - y_c) \frac{8339.9}{T} \right] \exp \left[- \left(\frac{1}{T} - 2.221 \cdot 10^{-4} \right) (17767 - y_c 26436) \right] \quad (1.43)$$

where y_c is $x_c / (1 - x_c)$ and x_c is mole fraction of carbon atoms.

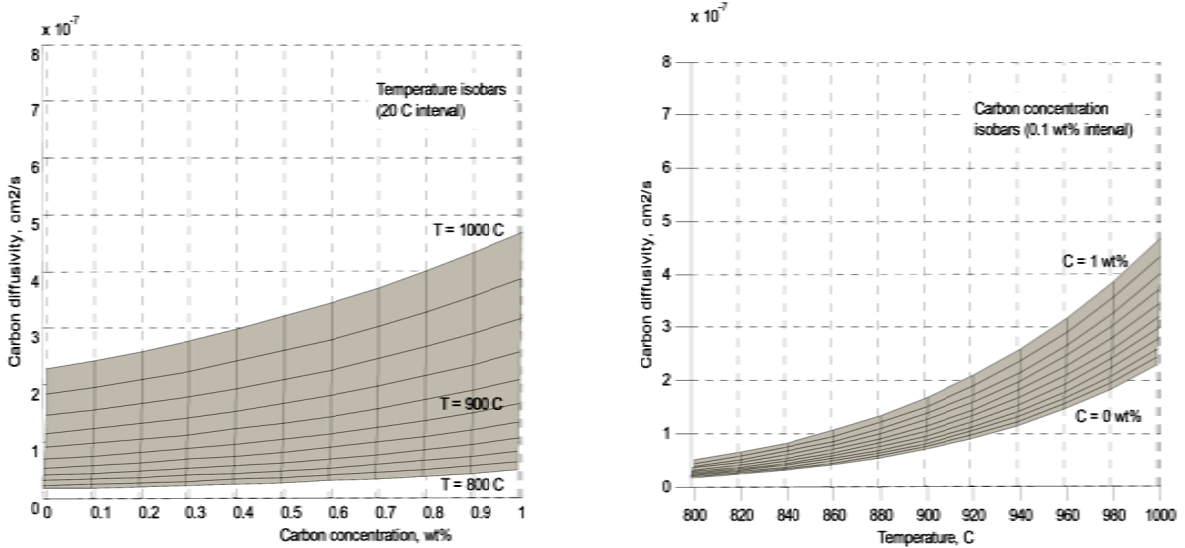


Figure 1-13. Variation of carbon diffusivity in austenite as a function of a) concentration and b) temperature [21]

Variation of austenite carbon diffusivity as a function of temperature and carbon concentration using eq.(1.43) is presented in Figure 1-13 [21].

1.3.2.2 *Ternary systems (Fe-C-X)*

Generally, effect of substitutional alloying elements on the kinetics of the interface migration during $\gamma \rightarrow \alpha$ transformation can be cast in terms of two major phenomena:

- 1) partitioning behaviour of the substitutional elements (X) during $\gamma \rightarrow \alpha$ transformation
and
- 2) segregation of substitutional atoms into the interface region.

It has been recognized for more than a half-century that the simple extension of the Zener model to the thickening of grain boundary ferrite allotrimorphs in ternary Fe-C-X, in which X is a substitutional alloying element (*e.g.* Ni, Mn, Mo, Cr, Si and *etc.*), and higher order iron alloys (*e.g.* AHSS steels) is not so straightforward.

The roots of the problem lie almost entirely in the differences in mobilities of the substitutional and interstitial solutes in steels (*e.g.* six orders of magnitude difference [23]). The instinctive choice of tie-line which includes the bulk composition does not yield a satisfactory solution, as the two solute mass balances cannot be simultaneously satisfied.

As a result, selection of an appropriate interfacial tie-line in ternary systems becomes a part of the solution of the growth problem, as pointed out, for example, by Kirkaldy [24] and Hillert [25], who examined solutions of the three-component diffusion equations under the assumption of full interfacial local equilibrium.

a) Local Equilibrium (LE and LENP)

Based on this approach, one should consider Local Equilibrium condition (LE) for all alloying elements across the γ - α interface:

$$\begin{cases} \mu_C^\alpha = \mu_C^\gamma \\ \mu_{Fe}^\alpha = \mu_{Fe}^\gamma \\ \mu_i^\alpha = \mu_i^\gamma \end{cases} \quad (1.44)$$

Simultaneously, satisfying the mass balance equations would yield to both the isothermal boundaries of γ + α two phase region and selection of an appropriate interfacial tie-line corresponding to a specific bulk composition.

In a conceptually similar approach, one can obtain bulk compositions corresponding to a specific tie-line in the ternary Fe-C-X phase diagram (IC contours in Figure 1-14a).

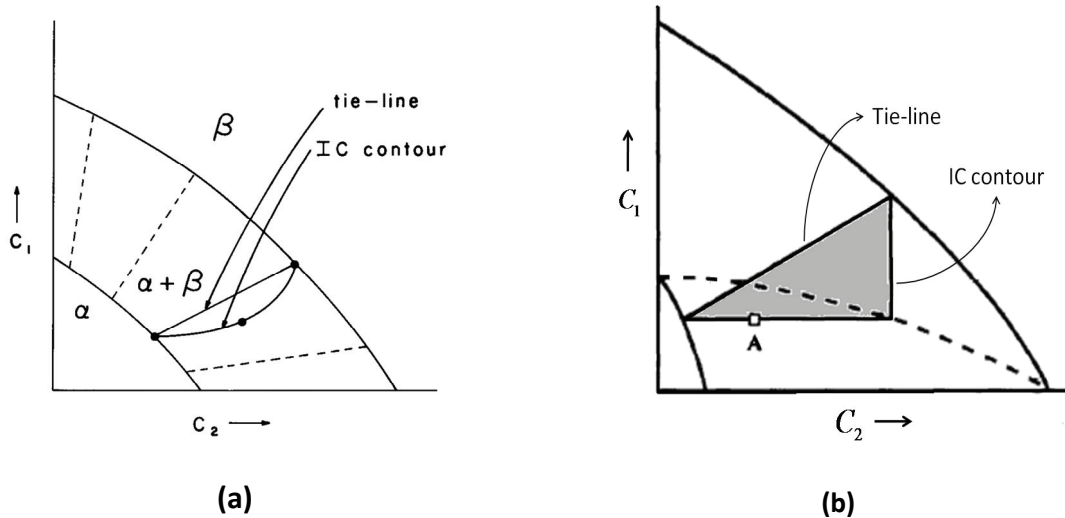


Figure 1-14. (a) IC contours for each tie-line [26] (b) envelope of zero partitioning [3]

In Fe-C-X systems, where carbon diffusivity (D_C) is several order of magnitudes larger than diffusivity of X (D_X), mass balance demands the IC contours to get a triangle shape (as shown in Figure 1-14b) [26][27][3]. The horizontal leg of this triangle represents a spectrum of bulk compositions, for which the interfacial tie-line is the one that permits negligible partitioning of the substitutional solute (X) and, as in Figure 1-15a, a thin “spike” forms ahead of the moving interface (high supersaturation region).

Under this condition, which is termed Local Equilibrium with Negligible Partitioning (LE-NP), mass balance requires the substitutional element in the thin spike to be balanced by depletion of that element in the ferrite. However, since this depletion is spread over a large volume of ferrite, its effect on the ferrite composition will be negligible as if a partitionless transformation is occurring. On this reasoning, one expects that ferrite growth will be fast, and limited mainly by the diffusion of carbon.

On the other hand, satisfying mass balance criteria for bulk compositions located on the vertical leg of the IC contours, requires the transformation product to be accompanied by a long-range redistribution of the substitutional solute (Figure 1-15b). Under this condition, which is termed Local Equilibrium with Partitioning (LE-P), the growth rate is mainly dictated by diffusion of substitutional atoms, *i.e.* very low transformation rate.

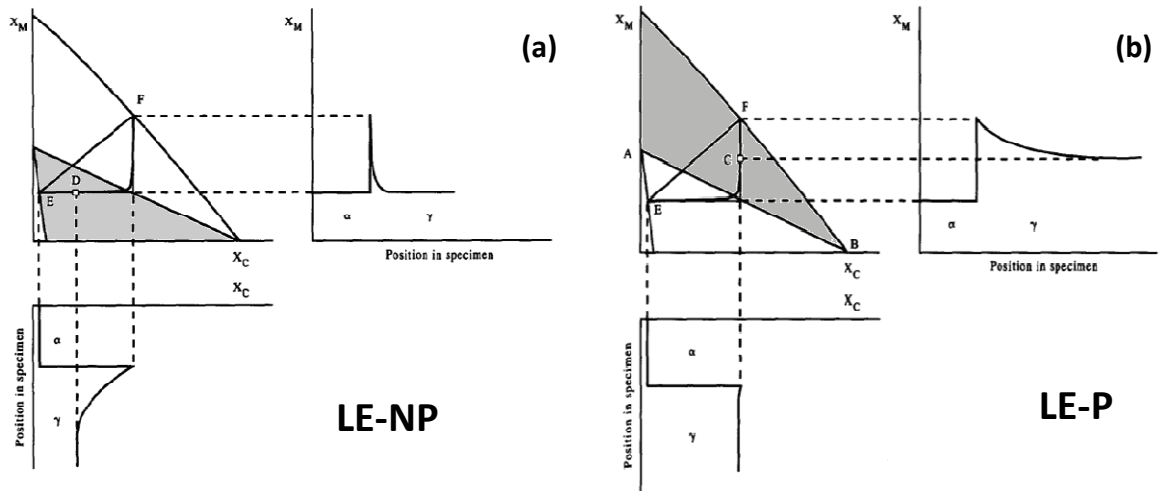


Figure 1-15. Schematic of a) Local Equilibrium with Negligible Partitioning, b) Local Equilibrium with full Partitioning

[3]

Repetition of such calculations for different tie-lines, leads to a set of triangle-shaped γ - α contour. As shown in Figure 1-14b, connecting right angled edges results in a curve which separates the γ - α region into two parts (low supersaturation and high supersaturation regions). This line is usually termed “the envelope of zero partitioning” or “Local Equilibrium Negligible Partition (LE-NP) boundary”. These arguments have been expressed in different language by Hillert [28], Purdy *et al.*[29], and Coates [26], [27].

For example, Hillert [28] has proposed a purely thermodynamic method for determining the LENP line. As seen in Figure 1-16, his proposal is based on finding the intersection of carbon iso-activity line (extrapolated from austenite side of the tie-line) with a horizontal line radiated from ferrite side of the tie-line.

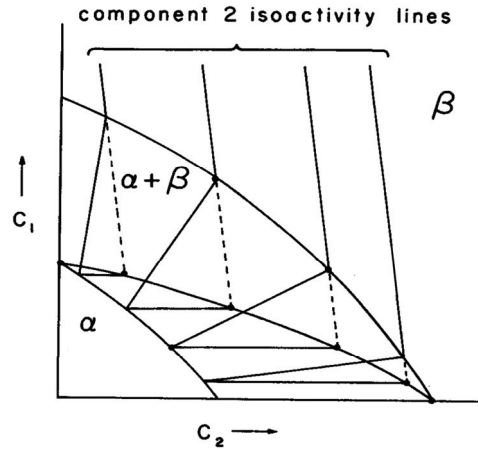


Figure 1-16. Hillert's thermodynamic approach for finding LEMP line in Fe-C-X systems [26]

b) Para Equilibrium (PE)

Calculation of the width of the alloying element diffusion spike ahead of the migrating interface reveals that width of the solute "spike" in some cases is less than austenite lattice parameter [30] which from physical point of view is not imaginable [31]:

$$w \sim D_X^\gamma / v \quad (1.45)$$

(where D_X^γ is diffusivity of the alloying element in the austenite and v is the growth rate)

For example, calculation of the spike width in Fe-0.51 at.pct C-3.1 at.pct Ni at 715 °C and Fe-0.56 at.pct C-3.1 at.pct Mn at 650 °C results in $w = 3 \times 10^{-9}$ cm and $w = 8 \times 10^{-9}$ cm, respectively [30].

These types of observations, which have their root in the low diffusivity of substitutional elements, have shed doubt on the validity of local equilibrium assumption.

As a result, an alternative treatment was first proposed by Hultgren [32] and later developed by Hillert [25]. In this conceptual state, which is called “Paraequilibrium” (PE), the substitutional component (X) is considered essentially inert and undisturbed by the passage of the interface (Fe/X ratio is always kept constant everywhere across the interface). The mobile interstitial component (C), however, is permitted to come to a constrained local equilibrium defined by the equality of chemical potentials:

$$\mu_C^\alpha = \mu_C^\gamma \quad (1.46)$$

while the substitutional solute (X) and the solvent (Fe) must suffer chemical potential differences across the moving interface [33]:

$$(\mu_{Fe}^\alpha - \mu_{Fe}^\gamma)x_{Fe} = (\mu_X^\gamma - \mu_X^\alpha)x_X \quad (1.47)$$

For the ternary case, these assumptions constrain the PE tie-lines to coincide with carbon component rays (lines radiating from the carbon corner of the ternary isotherm). This expression can be generalized to any number of interstitial and substitutional components (Figure 1-17).

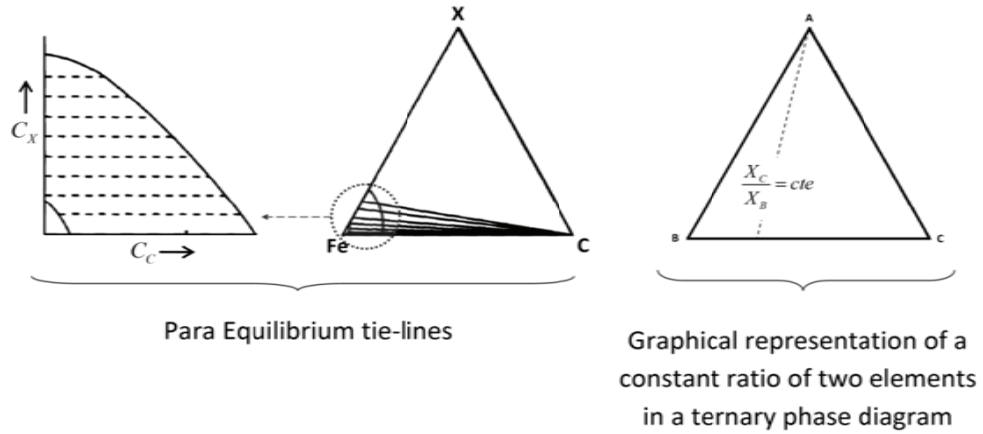


Figure 1-17. Para Equilibrium tie-lines [3]

Under paraequilibrium assumption, all substitutional elements “behave like a single component” and this makes the system “similar to a binary system”[34]. As a result, one can expect that the migration rate of the interface to be calculated similar to the diffusion controlled growth in binary Fe-C systems.

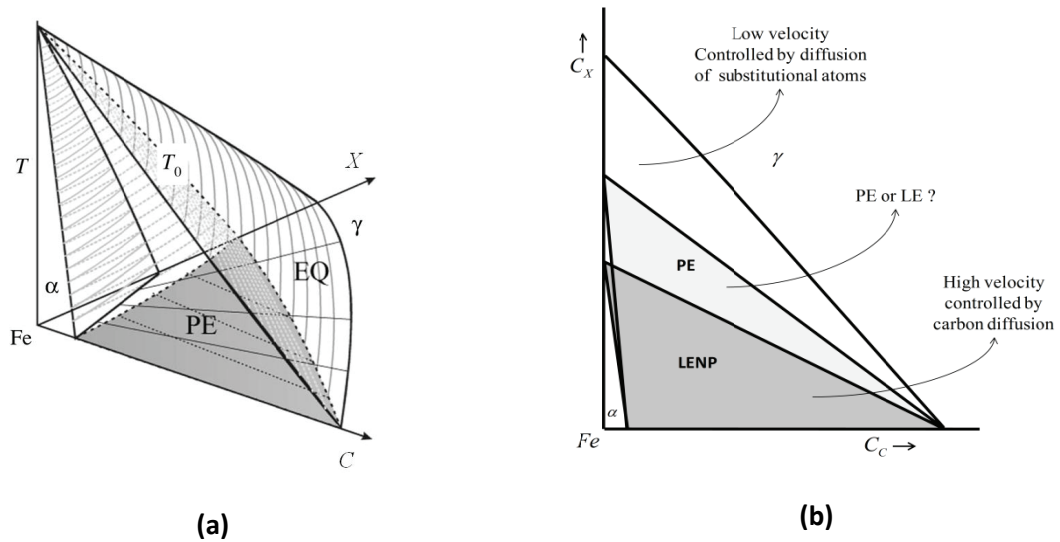


Figure 1-18. Schematic of Fe-C-X phase diagram showing the Para-Equilibrium phase boundaries [35], Isothermal section of the phase diagram

Both Local Equilibrium (LE) and Para Equilibrium (PE) boundaries are graphically presented in Figure 1-18b. As a rule, it has been proven [35] that the PE boundaries always fall within the LE (full equilibrium) phase boundaries.

Above the PE boundary both models are in agreement and predict a slow migration rate controlled by long range diffusion of substitutional element.

Similarly, below LE-NP line, both models predict a fast migration rate which is mainly controlled by carbon diffusion. However, it is worth mentioning that due to partitioning of substitutional element and formation of a thin spike in front of the interface under LE-NP condition, the growth kinetics predicted by PE is still faster than the one predicted under LE-NP condition.

As seen, the main controversy is in the middle part of the phase diagram (shown in light gray in Figure 1-18b) where each model predicts a very different growth rate for γ - α transformation.

Two comments are in order at this point. First, since the PE and LE-NP boundary conditions are computed from purely thermodynamic data, they represent cases which may or may not be realized in practice. They are not to be taken *a priori* as bases for models that purport to predict microstructure development in steels. Second, it has been demonstrated that kinetic transitions are possible. Indeed, several authors have presented evidence of a transition from PE kinetics at short times (high velocity) to LE-NP kinetics at long times (low velocity) [6][36].

Since in many cases (especially those involving austenite stabilizing elements like Ni and Mn) the PE and LE-NP limits are quite separate, and diagrams of the kind in Figure 1-18b are accessible to computation, they are useful aids in the design of critical experiments which could ultimately be used to develop and validate improved models of ferrite growth.

Finally, it is worth recalling that in reality all transformations dealing with both structural changes and solute partitioning, should be treated as a mixture of both interfacial and diffusional processes. However, in the kinetics models discussed above (PE and LE) it is assumed that all free energy of transformation is dissipated only by diffusional processes of solute elements in the bulk and contribution of interfacial processes (friction), capillary, stress effects and *etc.* are totally neglected.

c) Transition Models (PE to LENP)

In 1953 Hillert [12] introduced the idea of possible transition from PE to LENP interfacial condition. Since then there have been an ongoing discussion among researchers to develop a physically based model capable of predicting such a transition during $\gamma \rightarrow \alpha$ transformation.

One of the first models to predict a kinetic transition from PE to LE-NP interfacial contact conditions during the course of a grain boundary precipitation reaction was due to Odqvist *et al.* [37], [38] in 2002. These authors described the planar growth of proeutectoid ferrite in a Fe-C-Ni alloy, and showed the predicted trajectory of an

interfacial “tie-line” with time, beginning with a PE tie-line (parallel to a component ray) and ending with a full equilibrium tie-line. This model assumed a semi-infinite austenite grain size and incorporated energy dissipation due the interaction of solute with the interface and the buildup of the alloying element spike as per the model of Hillert and Sundman [39], which will be discussed later in detail. However, when the predicted evolution of the carbon conditions at the interface were coupled with a simple model for bulk C diffusion, the resulting ferrite growth kinetics were still much faster than those observed experimentally.

A second approach to the same problem was developed in 2004 by Hutchinson *et al.* [6] who used a discrete model for the atomic jumps at the interface instead of the continuum treatment used by Odqvist *et al.* [38]. The model of Hutchinson *et al.* [6] considered that a steady net flux of Ni across the interface would lead to the eventual build-up of a “spike” in the austenite and a consequent transition from initial PE to LE-NP conditions. This treatment worked well for the Fe-Ni-C system in spite of the fact that the dissipation associated with the flux of the substitutional element was not considered. This limitation precluded the application of the model to systems where a significant dissipation (solute drag effect) is expected.

As other recent approaches to the modeling of the transition problem one can point to the model due to Guo and Enomoto [40] who included a solute-drag term in their treatment of ferrite growth in Fe-C-Mn-Si alloys.

Even though, Odqvist's model [37], [38] was introduced before Hutchinson's approach [6], here for the sake of clarity, Hutchinson *et.al* model [6] is discussed first. After that, theories for solute drag and dissipation of free energy due to diffusional processes within the interface will be reviewed. At the end, the model developed by Odqvist *et.al.* [37], [38], will be discussed.

1.3.3 Model developed by Hutchinson *et.al.*

In 2004 Hutchinson *et.al* [6] conducted a series of classical precipitation experiments on Fe-C-Ni alloys containing 0.1 wt.pct Carbon and a range of Nickel concentration from 2.0 to 3.4 wt.pct at 700 °C. They realized that neither PE nor the LE boundary conditions could well describe the growth kinetics. They reported that in all cases growth kinetics at short times was in a better agreement with PE condition while after longer times the growth rates predicted by LE boundary condition could give a better match with the observation.

So, they proposed a discrete model in which, similar to the binary case, the interface velocity is controlled by net flux of carbon atoms across the interface. However, in this treatment, the chemical potential difference across the interface acts as a driving force for partitioning of Ni atoms and makes them to jump from ferrite side of the interface to the austenite side. This partitioning results in a gradual build-up of the spike and transition from PE to LE boundary condition.

Flux of Ni atoms in this approach can be written as:

$$J_{Ni}^{\alpha \rightarrow \gamma} = \frac{X_{Ni}^b \cdot M_{Ni}^{Trans-int}}{V_m} \cdot \frac{(\mu_{Ni}^\gamma - \mu_{Ni}^\alpha)}{\delta} \quad (1.48)$$

where δ is the thickness of the interface ($\delta = 1 \text{ nm}$), $M_{Ni}^{Trans-int}$ is the trans-interface mobility of Ni atoms, V_m is the molar volume, and X_M^b is the bulk content of the substitutional element (Ni). This expression can be obtained by using eq.(1.25) in a volume-fixed frame of reference.

Dealing with a moving interphase boundary, they also introduced a probability term, P , which conceptually is equivalent to the advective movement of atoms and controls net flux of Ni atoms across the interface. It depends on the ratio of the residence time of the moving interface (δ/v) to the diffusion time across the interface (δ^2/D_{Ni}):

$$P = 1 - \exp\left(\frac{-D_{Ni}^{Trans-int}}{v\delta}\right) \quad (1.49)$$

where, $D_{Ni}^{Trans-int}$ is the trans-interface diffusivity of Ni atoms and v is the interface velocity.

So the net flux of Ni atoms was written as the product of eq.(1.48) and eq.(1.49):

$$J_{Ni}^{\alpha \rightarrow \gamma} = \frac{X_{Ni}^b \cdot M_{Ni}^{Trans-int}}{V_m} \cdot \frac{(\mu_{Ni}^\gamma - \mu_{Ni}^\alpha)}{\delta} \left(1 - \exp\left(\frac{-D_{Ni}^{Trans-int}}{v\delta}\right)\right) \quad (1.50)$$

According to this expression, high interface velocity at the beginning of the ferrite growth leaves little chance for partitioning of substitutional alloying elements at the interface *i.e.*

distance passed by the interface is much larger than the corresponding distance can be passed by diffusion of Ni atoms. So, the transformation starts with no partitioning *i.e.* PE condition.

As the interface advances, its velocity slows down by time and substitutional atoms will find more opportunity to jump across the boundary. Eventually, at longer times the gradual build up of the alloying element spike in austenite leads to a continuous transition from PE to LENP contact conditions. As expected, depending upon the temperature and trans-interface diffusivity of the elements, $D_{Ni}^{Trans-int}$, the transition period may last for different times.

In the case of Fe-Ni-C at high temperatures, it is reasonable to assumed that all the chemical driving force for transformation, D_{int}^{chem} , is dissipated by volume diffusion in the bulk phases. In other words, negligible amount of energy is dissipated by structural rearrangements ($fcc \rightarrow bcc$), ΔG^m , and diffusional processes, ΔG^{diff} , within the interface:

$$D_{int}^{chem} = \underbrace{\Delta G^{diff}}_0 + \underbrace{\Delta G^m}_0$$

$$\Rightarrow D_{int}^{chem} = 0 \quad (1.51)$$

The total chemical driving force in this approach was chosen in a way to be expressed only in terms of the substitutional elements:

$$D_{\text{int}}^{\text{chem}} = -\Delta G_{\text{int}}^{\text{chem}} = \frac{(U_{\text{Ni}}^{\text{fcc}} + U_{\text{Ni}}^{\text{bcc}})}{2} \cdot (\mu_{\text{Ni}}^{\text{fcc}} - \mu_{\text{Ni}}^{\text{bcc}}) + \frac{(U_{\text{Fe}}^{\text{fcc}} + U_{\text{Fe}}^{\text{bcc}})}{2} \cdot (\mu_{\text{Fe}}^{\text{fcc}} - \mu_{\text{Fe}}^{\text{bcc}}) \quad (1.52)$$

where U_{Ni} and U_{Fe} are “u-fraction” of Ni and Fe atoms exactly at the ferrite and austenite side of the interface, *i.e.* the chemical driving force in this approach is calculated solely over the interface and spike region is not included in the calculations.

In general, *eq.*(1.52) is very similar to *eq.*(1.32):

$$\Delta G_m^\alpha = x_{\text{Ni}}^\alpha (\mu_{\text{Ni}}^\alpha - \mu_{\text{Ni}}^\gamma) + x_{\text{Fe}}^\alpha (\mu_{\text{Fe}}^\alpha - \mu_{\text{Fe}}^\gamma) \quad (1.34)$$

except for x_{Ni}^α and x_{Fe}^α which are replaced by average concentration of elements on ferrite and austenite side *i.e.* $(U_{\text{Ni}}^{\text{fcc}} + U_{\text{Ni}}^{\text{bcc}})/2$ and $(U_{\text{Fe}}^{\text{fcc}} + U_{\text{Fe}}^{\text{bcc}})/2$.

The implication is that, as the concentration of nickel on the austenite side starts changing, the interfacial carbon concentrations (X_C^γ and X_C^α) are also adjusted accordingly to satisfy *eq.*(1.51) and minimize the overall driving force acting over the interface. Similar to the binary Fe-C alloys, having interfacial carbon concentrations, the carbon profiles in bulk ferrite and austenite and consequently the interface velocity can be calculated.

The main difficulty in this approach is accurate estimation of the cross-interface mobility of nickel atoms (or any other substitutional alloying element) which is not available and has to be used as an adjustable parameter to fit the experimental data.

Hutchinson [6] states that “ *an important feature of this model is that it emphasizes only the variation in the boundary condition for C diffusion problem and assumes that the atomic rearrangements in the vicinity of the interface necessary to build the Ni spike and to maintain it during growth dissipate a negligible amount of free energy. This differentiates our approach from the recent approach of Odqvist et al. [38], which also considers a transition from PE to LENP during growth*”.

- ***Introduction of Capacity for the interface***

As expected, by increasing the transformation temperature, diffusion rate and as a result the partitioning rate of the solute elements will also increase. This means that, one may anticipate a faster transition from PE to LENP at higher temperatures.

Surprisingly, in a study conducted by Zurob *et al.* [17] on the kinetics of ferrite growth in Fe-C-Mn alloying system using controlled decarburization technique, unexpected kinetics transition was observed which could not be interpreted by any of the available models. This provided an evidence for existence of a missing physical parameter/s in previous calculations.

Zurob *et.al.* noticed that at intermediate temperatures, Local-Equilibrium with Negligible Partitioning (LENP) can be used to model the growth kinetics. Increasing the temperature, they noticed a transition manifested by extended PE state which precludes the build up of the alloying element spike. In fact, as shown in Figure 1-19, they reported a

long lasting intermediate mode (between PE and LENP) and finally a transition from LENP to PE kinetics by increasing the temperature.

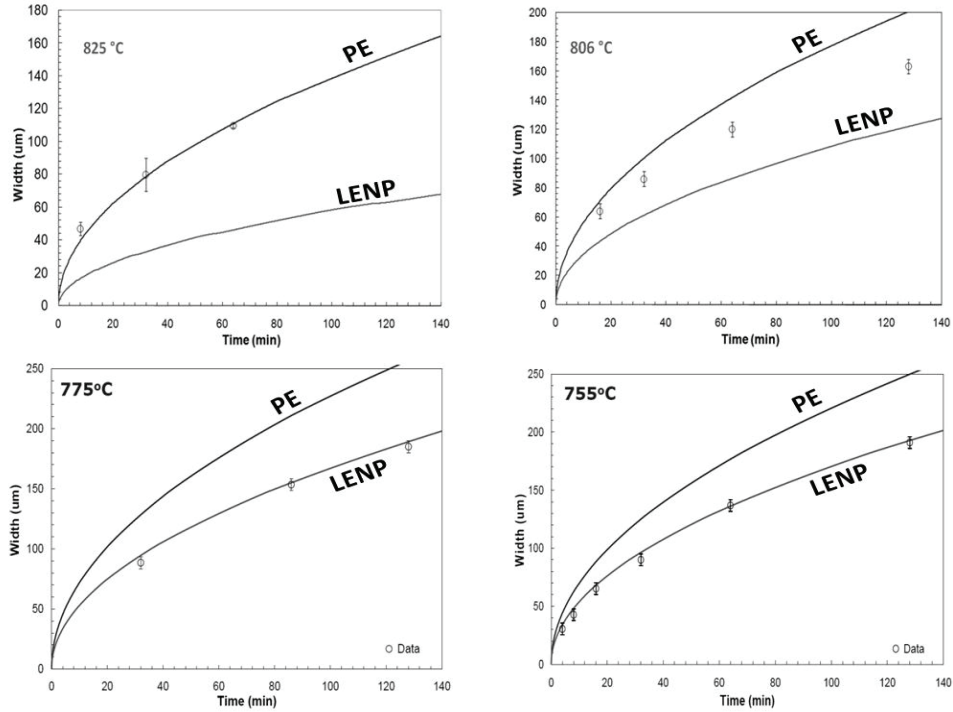


Figure 1-19. Kinetics of ferrite growth during decarburization of Fe-Mn-C at different temperatures [41]

To explain this behaviour, Zurob *et al.* [41] modified Hutchinson’s model by considering a thick interface region and creating an additional atomic flux for Mn inside the interface. They introduced a new parameter termed “interface capacity (X^*)”, which was a function of both temperature and solute content. In other words, the one-jump transition model of Hutchinson *et al.* [6] was converted to a two-jump process by considering a thick interface and extra atomic jump within the interface region which has a limited capacity for solute elements.

They [41] stated that, the new parameter (interface capacity) “modifies the interface capacity for Mn, making it possible to cap the accumulation of Mn inside the interface even in the presence of a thermodynamic driving force for accumulation. The introduction of this parameter is guided purely by the experimental data”.

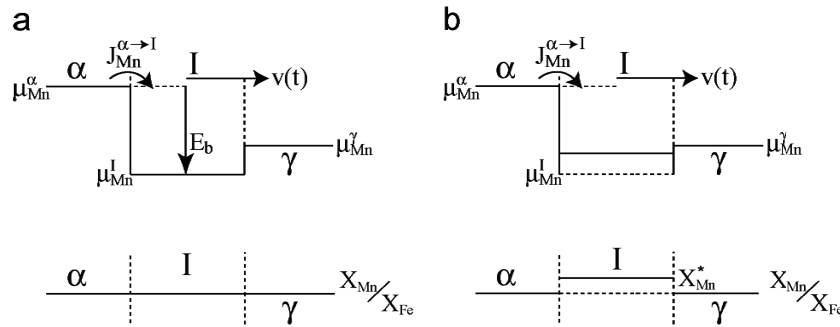


Figure 1-20. Schematic presentation of two-jump model by Zurob *et al.* [41]

Zurob *et al.* [41] showed that this new approach could be successfully used to explain the experimental observations in Fe-Mn-C alloys over a range of composition and temperature including the long lasting intermediate states and transition to PE kinetics at high temperatures.

The two jump approach is schematically presented in Figure 1-20.

The key equations describing the flux of solute elements, X , across the interface can be summarized as following:

$$J_X^{\alpha \rightarrow Int} = \frac{X_X^b \cdot M_X^{Trans-int}}{V_m} \cdot \frac{(\mu_X^{Int} - \mu_X^\alpha)}{\delta} \left(1 - \exp\left(\frac{-D_X^{Trans-int}}{v\delta}\right) \right) \left(1 - \frac{X_X^{Int}}{X_X^*} \right) \quad (1.53)$$

for the atomic flux from α into the interface and:

$$J_X^{Int \rightarrow \gamma} = \frac{X_X^{Int} \cdot M_X^{Trans-int}}{V_m} \cdot \frac{(\mu_X^\gamma - \mu_X^{Int})}{\delta} \left(1 - \exp\left(\frac{-D_X^{Trans-int}}{v\delta}\right) \right) \quad (1.54)$$

for the atomic flux from interface to γ .

In these equations, μ_X^{Int} is the chemical potential of X in the interface and is taken to be equal to $\mu_X^\alpha - E_b$, where E_b is the binding energy of X to the interface. The symbols X_X^{Int} and X_X^* refer to the actual solute concentration in the interface and the interface capacity, respectively. Equation (1.53) therefore implies that the probability of successful jumps of X atoms from ferrite into the interface is directly proportional to the available “capacity” of the interface, *i.e.* $(1 - X_X^{Int} / X_X^*)$. As it was mentioned before, a second key point of this approach concerns the temperature and concentration dependence of the interface capacity.

Zurob *et.al* argued that the binding energy of Mn atoms (E_b^{Mn}) is not very strong (around 5 KJ/mole) and as a result, the dissipation of free energy due to diffusion of substitutional elements inside the interface can be neglected in Fe-Mn-C system. However, in such alloying systems as Fe-Mo-C or Fe-Cr-C, where a strong binding energy for substitutional elements is expected, the free energy dissipation associated with the atomic flux within the interface will have a significant effect and some modification will be required.

1.3.4 Solute drag and dissipation of free energy

In the simplest form, the γ/α phase interface is treated as a sharp interface (Figure 1-21a) over which different properties are changed suddenly. However, despite usefulness of this model, in many cases it has been realized that considering a width for the interface, within which properties are changed, might be theoretically more acceptable. In fact, considering a width for the interface region will help to explain such physically important aspects as segregation and solute drag during phase transformation. Some common models for variation of thermodynamic properties within the interface region are schematically presented in Figure 1-21 [2].

Kinetically, there are two important effects associated with addition of substitutional element (X) to a $Fe-C$ system:

- 1) segregation and interaction of X with the potential well within the moving boundary and
- 2) interaction of X with carbon (C) atoms and spike build-up ahead of the interface.

One should pay attention that *“the segregation of solute towards the interface and the building up of the spike in austenite are of a different nature: the spike is to be seen as a concentration modification in the mother phase, reflecting the thermodynamic properties of the bulk phases, while segregation stems from the binding energy between the interface and the solute atoms”* [17].

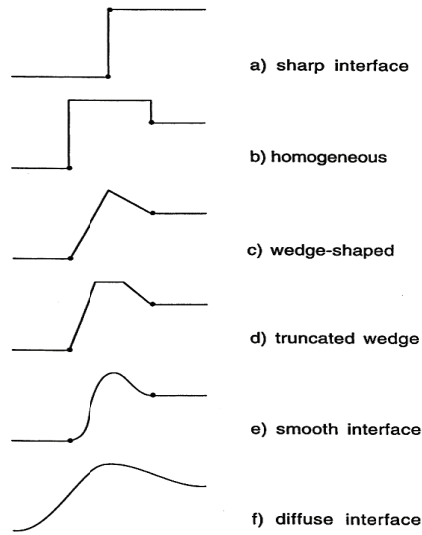


Figure 1-21. Schematic characterization of interface models [2]

Accordingly, a simple classification of common alloying elements in steels has been introduced by Hutchinson *et.al* [16] which is presented in Figure 1-22. In this classification, the interface interaction energy (E_b) is quantified based on atomic size of the solute element and the $X-C$ interaction, is categorized according to the dependence of C activity on solute content.

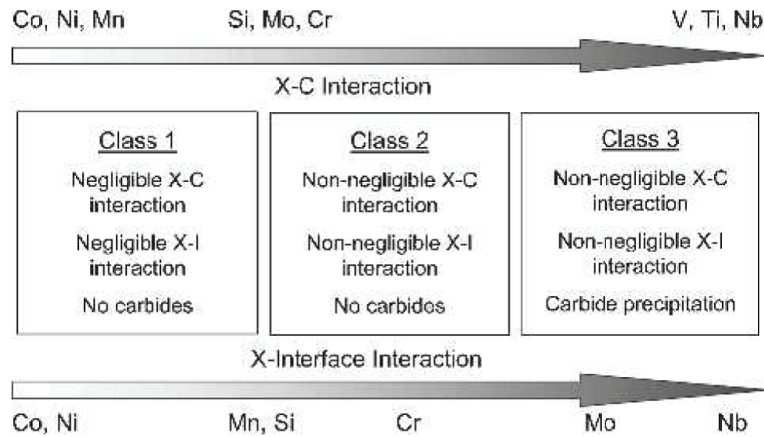


Figure 1-22. classification of the common alloying elements in steel [13]

Hutchinson *et al.* [16] state that “*it must be stressed that this classification refers both to the alloying elements and to the heat-treatment conditions adopted. For instance, the Fe-C-Mo system shifts from class II behaviour to class III behaviour as the transformation temperature is lowered and carbide precipitation occurs concurrently with the austenite-to-ferrite transformation*”.

As mentioned before, according to the theory of thermally activated growth, the relationship between migration rate of a boundary and driving force under non-equilibrium conditions can be expressed via equation (1.33):

$$v = M \cdot \Delta G^m \quad (1.35)$$

Where M is macroscopic mobility and ΔG^m is driving force for migration of the boundary.

In pure materials, M is called “intrinsic mobility” which is a thermally activated process and is usually expressed as:

$$M_{int} = M_0 \exp\left(-\frac{Q}{KT}\right) \quad (1.55)$$

Where M_0 is the temperature independent mobility (pre-exponential factor) and Q is the activation energy for atomic motion.

However, in order to take into account the effects associated with the presence of the extra components in alloying steels, some modifications to eq. (1.33) will be required:

For example, one can replace the intrinsic mobility, M_{int} , with the term “effective mobility (M_{eff}) [42]:

$$\frac{1}{M_{eff}} = \frac{1}{M_I} + \frac{1}{M_{II}} \quad (1.56)$$

where M_{II} is the extrinsic part of the mobility which is a function of both temperature and concentration. Here, the extrinsic contribution, M_{II} , originates from the fact that segregation of solute atoms to the boundary (due to the tendency of boundary for attracting the foreign atoms), decelerate the boundary movement. Depending on the nature of the solute atoms and velocity of the interface, this attraction may cause different amounts of deviation from kinetics behaviour observed in pure materials.

Alternatively, instead of changing the mobility term, the retarding effect of the solute segregation in equation (1.33), can be taken into account by reducing the available driving force [43]:

$$v = M_I \left(D_{int}^{chem} - P^{sd} V_m \right) \quad (1.57)$$

Where V_m is molar volume and P^{sd} is called “*solute drag force*” which should be calculated from available theoretical treatments.

So far, there have been two main methods to rationalize the solute drag effect:

The first approach, which was originally developed for calculation of solute drag during grain growth, is the one proposed by Cahn [44] and by Lucke and Stuwe [45]. They argued that in the presence of alloying elements, the defected structure at the boundary acts as a region with lower potential which attracts the foreign atoms toward that area. When a stationary boundary starts moving, clouds of these segregated atoms, despite their tendency for staying inside the boundary, are also forced to move. As the velocity of the boundary increases, due to low diffusivity of the segregated atoms, they cannot continue moving with the boundary and consequently start falling behind *i.e.* an extra attraction force should be exerted by the boundary to make them move faster and mutually a retarding mechanical force will be exerted on the moving boundary. This retarding force is called “*solute drag force*” in the literature.

Hillert [28] also proposed a more general treatment which is based on dissipation of free energy due to diffusion of foreign atoms inside the interface region.

The theoretical details of these methods will be discussed in the following sections.

1.3.4.1 ***Force-based models (Solute drag)***

Generally, foundation of this model lies in the concept proposed by Lucke and Detert [46] based on which, the boundary can either move with a cloud of foreign atoms attached to that (at low temperatures and small driving forces), or can break away from that solute atmosphere and move freely (at high temperature and large driving forces).

The basic idea is balance of forces acting over the interface [4], [47]. As schematically presented in Figure 1-23, the driving pressure for migration of the boundary, P^σ , should be balanced by such retarding forces as friction (atomic rearrangement), P^{fric} , and solute drag, P^{sd} :

$$P^\sigma = P^{fric} + P^{sd} \quad (1.58)$$

For example, in pure materials there is no solute drag and the driving pressure, P^σ , which is originated from surface energy of the curved boundary, should be only balanced by the friction term, P^{fric} :

$$P^\sigma = P^{fric}$$

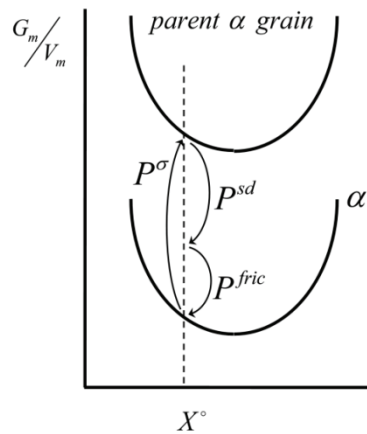


Figure 1-23. Balance of forces acting on the grain boundary during grain growth [47]

while, in the presence of other alloying elements, the pressure exerted by segregation of the foreign atoms to the boundary, P^{sd} , should also be taken into account.

To do so, both Cahn [42] and Lücke and Stüwe [45] considered a symmetric potential well around the boundary. This well, which is usually denoted by E or U , can be either positive (repulsive) or negative (attractive) in respect to the solute components and as shown in Figure 1-24, its tendency is a function of distance from centre of the boundary.

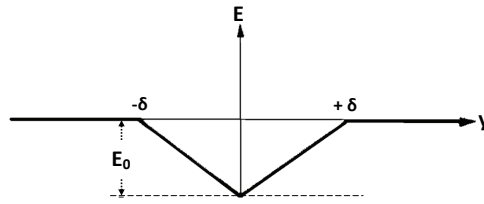


Figure 1-24. Attracting potential well around a boundary [19]

The associated solute profile around the boundary under steady state condition can be calculated using mass balance equations and equating the net flux of atoms at each point equal to zero:

$$J_X^{net} = J_X^{diff} + J_X^{conv} = 0 \quad (1.59)$$

where J_X^{diff} is the diffusive flux of the solute atoms due to the existing potential gradient at the boundary [44], [45]:

$$J_X^{diff} = -\frac{D_X C_X}{kT} \cdot \frac{\partial \mu}{\partial y} = -\left(D_X \frac{dC_X}{dy} + \frac{D_X C_X}{kT} \frac{dE}{dy} \right) \quad (1.60)$$

and J_X^{conv} is convective flux which arises from movement of the boundary:

$$J_X^{conv} = -v \cdot C_X(y) \quad (1.61)$$

In the second step, when the distribution of alloying elements around the boundary is determined, the solute drag force exerted by segregated atoms must be evaluated.

Both Lücke and Stüwe and Cahn suggested very similar but slightly different ways for evaluating the solute drag pressure, P^{sd} ,:

For a binary system (A-B) Lücke and Stüwe [45] suggested:

$$P^{sd}V_m = - \int_{-\infty}^{\infty} x_X \frac{dE}{dy} \cdot dy \quad (1.62)$$

where V_m is the molar volume and x_X is concentration of the solute at each point.

Cahn [44], [45]also used almost the similar equation and proposed the following:

$$P^{sd}V_m = - \int_{-\infty}^{\infty} (x_X - x_X^0) \frac{dE}{dy} \cdot dy \quad (1.63)$$

where x_X^0 is solute concentration in un-affected regions far from the potential well at the interface. In these equations $\left(-\frac{dE}{dy}\right)$ is the force exerted by one impurity atom.

As seen, the only difference between Cahn’s approach and the one suggested by Lücke and Stüwe is introduction of x_X^0 which was added only “for mathematical convenience without any physical argument” [48].

In the case of grain growth in one-phase materials, both equations yield the same results but, they give different results during phase transformation *i.e.* some further modifications will be required [48].

A schematic of composition profiles at different velocities and the associated solute drag as a function of the velocity is presented in Figure 1-25a and Figure 1-25b, respectively. As seen, under stationary state, there will be a symmetric distribution of foreign atoms and consequently, there will be a balance of forces on both side of the boundary *i.e.* no retarding effect. However, under non-stationary conditions the generated concentration asymmetry results in a retarding force (solute drag) acting against moving direction of the boundary.

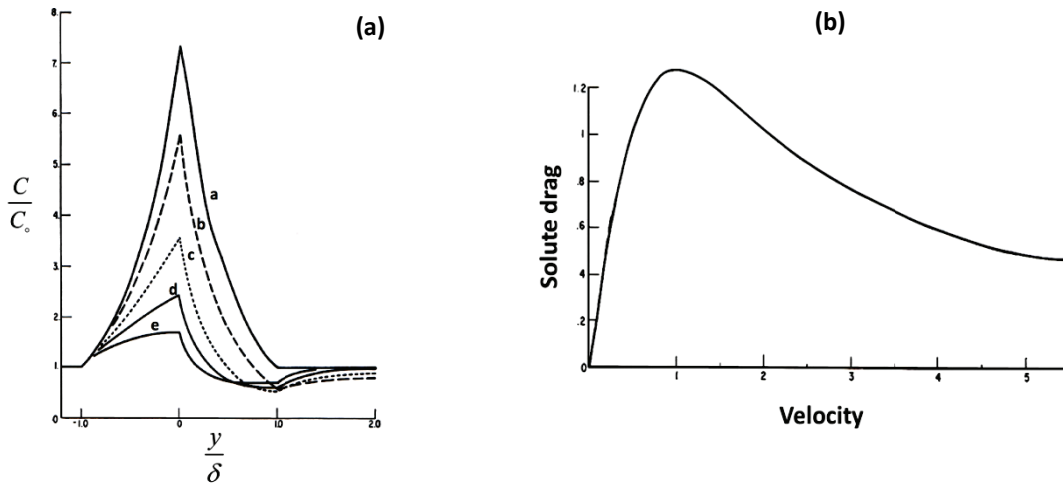


Figure 1-25. (a) Composition profiles for an attractive potential well at different interface velocities $V_a < V_b < V_c < V_d < V_e$ (b) impurity drag for various velocities [44]

It is worth mentioning that, from experimental point of view, both potential gradient, $E(x)$ and diffusion coefficient inside the boundary region, $D(x)$, are unknown and

calculation of solute drag in real cases is mainly based on some reasonable assumptions for $E(x)$ and $D(x)$.

Beside these continuum treatment for calculation of solute drag, Lücke and Stüwe [45] argued that if one assumes that the thickness of the boundary “is not bigger than about two atomic distances (because of short range of metallic bonding) such a continuum model is not really valid”. So, they suggested an atomistic approach in which atomic structure of the boundary is considered “in a very rough way” [45].

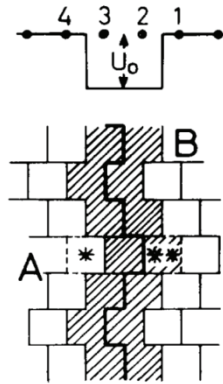


Figure 1-26. Schematic of atomistic treatment of solute drag proposed by Lucke and Stuew [45]

As schematically shown in Figure 1-26, they assumed a square potential well, U_0 , at the interface between phase A and B . During grain growth process, the foreign atoms passed by the interface experience a sudden potential change which makes them to move (to decrease their energy).

The drag exerted by these atoms at the interface can be evaluated through discrete version of eq.(1.62):

$$P^{sd} = \frac{1}{2}(C_3 - C_1 + C_4 - C_2)NU_0 \approx C_{eff}NU_0 \quad (1.64)$$

where C_m ($m=1,2,3,4$) is concentration of foreign atoms on each atomic plane and N is number of atoms per cm^3 . This drag force can affect the interface velocity through eq.(1.57):

$$v = M_I \left(D_{int}^{chem} - P^{sd} V_m \right) \quad (1.57)$$

Similar to the continuum treatment, the concentration profile at each velocity can be calculated assuming steady state condition ($J_X^{net} = J_X^{diff} + J_X^{conv} = 0$). The diffusive and convective fluxes from atomic plane m to atomic plane $m+1$ can be calculated by:

$$J^{conv} = Nv(C_m - C_0)$$

$$J^{diff} = \frac{ND}{b} \left[C_{m+1} \exp\left(\frac{-\Delta U}{2kT}\right) - C_m \exp\left(\frac{+\Delta U}{2kT}\right) \right]$$

As seen the diffusive flux, J^{diff} , is evaluated based on absolute reaction rate theory and net flux of atoms jumping to the right and left. Here b is distance between atomic planes, D is diffusivity of foreign atoms and C_0 is concentration of foreign atoms far from the interface.

1.3.4.2 *Free energy dissipation approach*

So far, the discussed models were based on forces acting over the boundary but, Hillert used another treatment for rationalizing the solute drag. He [39] *“argued that the work put into the movement of a boundary in order to overcome the solute drag, must dissipate by the diffusion of the solute taking place as a result of the boundary movement. It should thus be possible to evaluate P as $\Delta G_m/V_m$ where ΔG_m is the dissipation of free energy due to diffusion when boundary passes through a volume containing one mole of atoms”*.

He stated that the available chemical driving force for movement of the interface, $D_{\text{int}}^{\text{chem}}$, *“must be equal to the sum of sinks of Gibbs energy”* [48]. Under steady state condition one can write:

$$\underbrace{D_{\text{int}}^{\text{chem}} + P^\sigma V_m}_{D^{\text{eff}}} = \Delta G^{\text{diff}} + \Delta G^{\text{fric}} \quad (1.65)$$

where ΔG^{diff} is the dissipation of free energy due to diffusion of solute atoms, ΔG^{fric} is dissipation due to structural changes during transformation and $P^\sigma V_m$ is dissipation associated with curvature of the interfaces ($\Delta G_m^\sigma/V_m = P^\sigma$).

A schematic of balance of forces at the boundary during grain growth is presented in Figure 1-27.

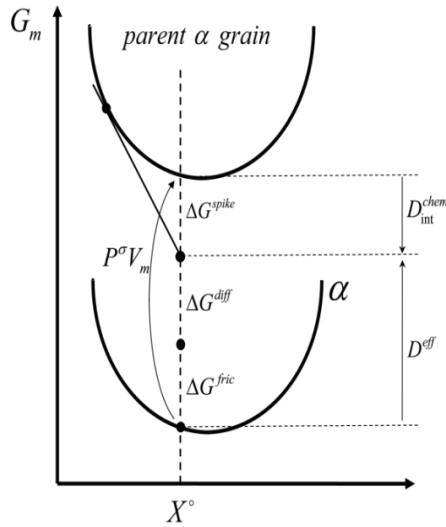


Figure 1-27. Energy balance at the boundary during grain growth [47]

During grain growth, both phases have the same composition and as a result, there is no chemical driving force acting on the boundary *i.e.* the main source of energy for movement is surface energy of the curved boundary. However, segregation of solute elements into the potential well can create a negative spike just ahead of the moving boundary. The associated dissipation of free energy due to diffusion of elements down the spike results in a negative chemical driving force which is presented by ΔG^{spike} in Figure 1-27.

As mentioned in section 1.2.1, rate of dissipation of Gibbs energy in a process, \dot{G}_i , can be expressed by eq.(1.16):

$$-\dot{G}_i = J_i D_i \quad (1.16)$$

Accordingly, Hillert used the same argument for calculating dissipation associated with the flux of atoms (due to a potential well at the interface) and stated that rate of free energy dissipation in a binary A-B system can be given as:

$$\frac{dG}{dt} = -\int_V J_B \cdot \frac{d(G_B - G_A)}{dy} \cdot dy \quad (1.66)$$

Knowing that $\Delta t = \frac{V_m}{Av}$ and $dV = A dy$, the final equation for dissipated energy due to

the diffusional flux (*e.g.* inside the boundary or spike) is expressed as:

$$G_m = \left(\frac{dG}{dt} \right) \cdot \Delta t \quad \rightarrow \quad G_m = -\frac{V_m}{v} \int_{-\infty}^{\infty} J_B \cdot \frac{d(G_B - G_A)}{dy} \cdot dy \quad (1.67)$$

Similar to the force-based approaches, the concentration profile within the boundary at different velocities can be evaluated using the steady state assumption:

$$J_X^{net} = J_X^{diff} + J_X^{conv} = 0$$

where J_X^{diff} in a binary $A-B$ alloy is evaluated based on eq.(1.26):

$$-J_A^{diff} = J_B^{diff} = -\frac{D}{RTV_m} x_A x_B \frac{d(G_B - G_A)}{dy} \quad (1.68)$$

and J_X^{conv} is

$$-J_A^{conv} = J_B^{conv} = \frac{v}{V_m} (x_B - x_B^{tr}) = -\frac{v}{V_m} (x_A - x_A^{tr}) \quad (1.69)$$

x_i^{tr} is the net composition of material passed by the interface [49].

Here, it is interesting to know that, Cahn, Lucke and Stuwe both assumed a wedge-shaped function for potential well at the interface but, Hillert had to use a square-shaped or truncated wedged-shaped functions in his approach to see the similar behaviour.

Hillert then mentions that [39] “one should take into account the atomistic nature of the system and ... thus obtain the same type of variation with velocity for square well function that Cahn and Lucke and Stuwe had found for the wedge-shaped function without considering the atomic nature”.

1.3.4.3 Solute drag and free energy dissipation during phase transformation

As mentioned before, both the forced-based approach by Cahn, Lucke and Stuwe and the thermodynamic approach (dissipation of free energy) by Hillert are initially developed for grain growth problems. However, “there is no reason why both models should not apply to migration of grain boundaries as well as phase interfaces” [4].

In line with such efforts to expand these concepts to phase transformations, one can point to the paper published in 1989 by Liu and Agren [50] who used the thermodynamic approach for calculating free energy dissipation inside the interface in Fe-X-C alloys. In general, Liu and Agren [50] assumed that the total driving force for transformation is dissipated by interfacial energy, finite interface mobility, atomic diffusion within the interface and diffusion in the matrix ahead of the interface. This model was later used

with minor modifications for simulation of solute drag effect in different systems. For example, in 1996 and 1998 Suehiro *et.al* applied Liu and Agren’s model for analyzing the effect of Niobium on massive transformation in steels [51] and recrystallization (moving grain boundary) in Al-Mg alloys [52]. In their approach the interface was divided into three regions (Figure 1-28a) while in another application in 1997 by Liu [53] for analyzing effect of Mo on bay formation in TTT diagrams, the interface region was divided into two zones (Figure 1-28b).

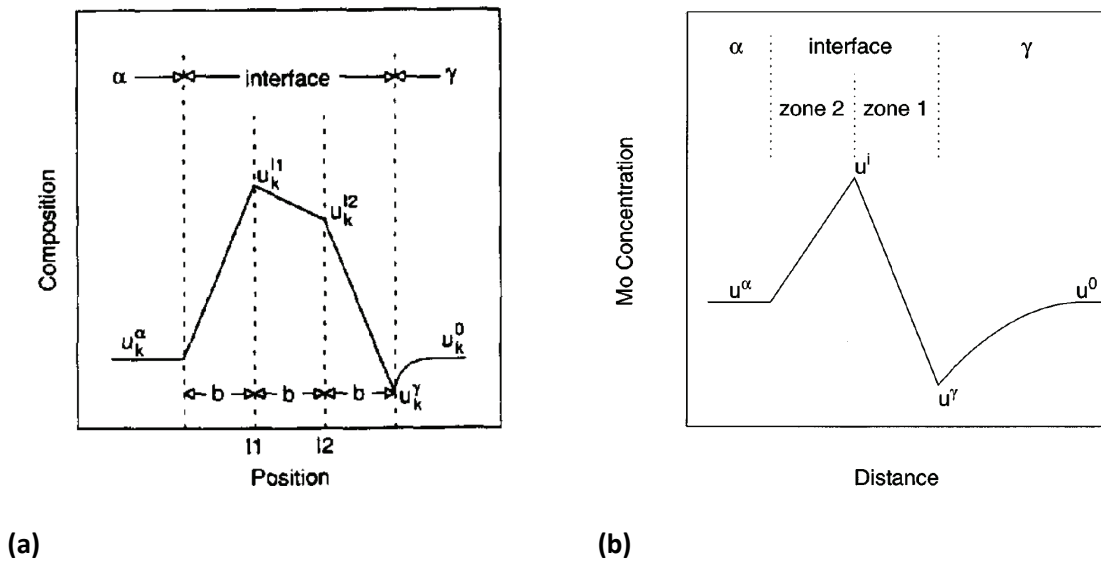


Figure 1-28: Schematic of concentration profile across the phase interface in the thermodynamic approach developed by Liu *et.al* [50] a) three-zone model used for analyzing the effect of Niobium on massive transformation [51] and b) two zones model used for analyzing effect of Mo on bay formation in TTT diagrams [53].

In another attempt, Purdy and Brechet [31] in 1995 tried to extend the solute drag treatment (force-based approach) to phase transformations. Purdy and Brechet assumed a wedged-shape potential well at the interface (Figure 1-29) and employed eq.(1.63) proposed by Cahn to evaluate the drag force exerted by segregated atoms into the

inter-phase region. Later in 1999, with reference to the model by Purdy and Brechet Enomoto [54] analysed the solute drag effect in Fe-Mn-C systems.

In general, to perform such calculations (*i.e.* solute drag treatment in phase transformation), as the first step, it is necessary to find a relationship between binding energy of atoms to the interface, E , and chemical potential difference, $\Delta\mu_i$ (thermodynamic driving force). However, “there are no physical grounds for introducing the chemical driving force into the solute drag treatment” [48] and this, has in fact, introduced puzzling results when it comes to comparison between predictions by the two approaches for phase transformation problems.

For example, Purdy and Brechet used difference in molar Gibbs energies of solute elements across the interface region (at $+\delta$ and $-\delta$ in Figure 1-29) but, in some cases they noticed that using this condition would “*lead to very different conclusions*” from those predicted by the dissipation approach by Hillert.

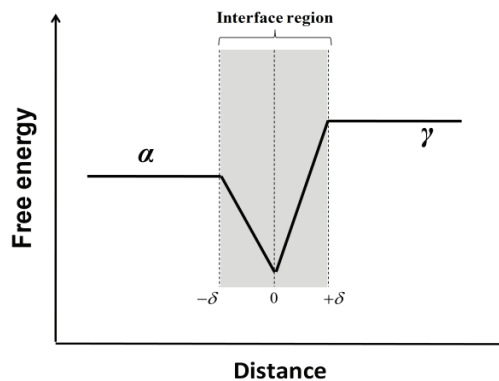


Figure 1-29. Suggested potential well at the interface used by Purdy and Brechet [31] for calculating solute drag during phase transformation

Introducing $E = \Delta\mu_B - \Delta\mu_A$, Hillert [55] later showed that in order to get similar results in both approaches, one should include the spike ahead of the interface into the calculation of chemical driving force in the dissipation approach. In other words, the retarding force predicted by Cahn's equation within the interface region is equivalent to the free energy dissipated in both interface region and spike ahead of the interface. This, in fact, "*was a puzzling result*" and showed that, solute drag within the interface should be compared with the dissipating processes acting over that whole region (interface + spike) [55].

Later, using $E = \Delta\mu_B - \Delta\mu_A$, Hillert showed in [48] that:

On one hand, Cahn's model is symmetric with respect to all elements in the structure and treats both solute and solvent atoms similarly but, the problem is that, based on this model only $(x_B - x_B^0)$ of atoms are interacting with the interface while physically, contribution of all atoms should be considered. So, Cahn's relation may work well for grain growth and single phase materials but, it cannot satisfactorily be used for phase transformation [48].

On the other hand, in the case of Lucke-Stuwe's model, Hillert [48] criticized that it only takes into account the solute elements and does not show a symmetric behaviour with respect to all element. Again, it might not be important for grain growth problems but, cannot be used for phase transformation.

1.3.5 *Model developed by Odqvist et.al.*

Here it is worth paying attention to the model proposed by Odqvist *et al.* [37][38] in 2002 which is one the first continuum models capable of predicting PE to LEMP transition at the interface. This model is an older but more advanced approach compare to the one developed by Hutchinson et.al [6].

In this treatment, similar to the Hutchinson's model [6], the interface velocity is controlled by flux of carbon atoms in ferrite and austenite. Moreover, in this approach, not only partitioning of substitutional elements, but also segregation of these elements to the boundary and structural changes (friction) are taken into account.

In other words, Odqvist's model is based on local energy balance between the total chemical driving forces, $D_{\text{int}}^{\text{chem}}$, and total dissipation of Gibbs free energy due to the friction, ΔG^m , and diffusional processes, ΔG^{diff} , (*e.g.* diffusion of substitutional element within the interface and spike ahead of the migrating interface):

$$D_{\text{int}}^{\text{chem}} = \Delta G^{\text{diff}} + \Delta G^m$$

The expression used for the total chemical driving force is:

$$D_{\text{int}}^{\text{Chem}} = U_{\text{Fe}}^0 \left[\mu_{\text{Fe}}^{\gamma} (U_X^0, a_C^{\alpha}) - \mu_{\text{Fe}}^{\alpha} (U_X^0, a_C^{\alpha}) \right] + U_X^0 \left[\mu_X^{\gamma} (U_X^0, a_C^{\alpha}) - \mu_X^{\alpha} (U_X^0, a_C^{\alpha}) \right] \quad (1.70)$$

which is similar to *eq.*(1.32) and written per mole of substitutional atoms in the substitutional lattice. In this equation U_{Fe}^0 and U_X^0 are initial contents of substitutional

elements (Fe and X respectively) and a_C^α is carbon activity which is assumed to be the same everywhere.

In order to describe the interaction of solute atoms with the moving boundary, Odqvist *et al.* [37][38] considered a thick interface region between ferrite and austenite within which thermodynamic “properties of the interface vary continuously from those of ferrite to those of the austenite”[56] (Figure 1-30a).

As a result, a chemical potential gradient and consequently, an atomic flux of solute elements will be expected within the interface. Dissipation of free energy associated with the flux of solute elements is then calculated as per the model of Hillert and Sundman [39]:

$$\psi_i = T \cdot (J_i Z_i) = J_i D_i \quad (1.16)$$

This expression yields the following for dissipated energy under steady state assumption:

$$\Delta G_X^{Diff} = - \int (U_X - U_X^0) \left[d(\mu_X - \mu_{Fe}) / dy \right] dy \quad (1.71)$$

Here, it should be emphasized that in this approach the total driving force, eq.(1.70), was calculated over both interface region and spike region ahead of the interface *i.e.* consequently, eq.(1.71) was also integrated over the same area (Figure 1-30b)

Dealing with a moving interface, under steady state condition one can write the following for solute concentration (X=Ni,Mn,...) at each point:

$$\frac{v}{V_m}(U_X - U_X^\alpha) = J_X \quad (1.72)$$

where U_X is u-fraction of component X , J_X is atomic flux, V_m is molar volume per substitutional atom and v is velocity of the interface.

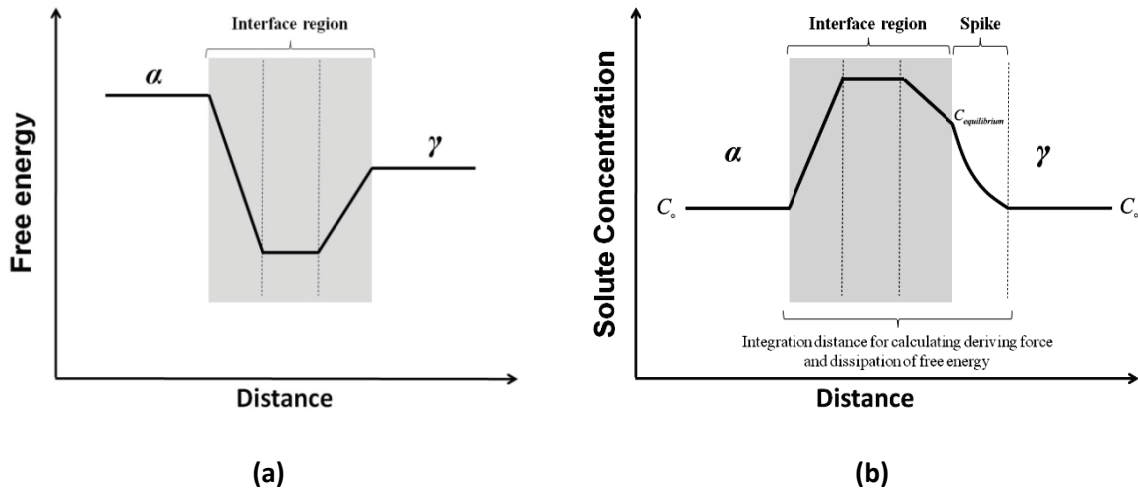


Figure 1-30. Schematic presentation of a) the variation thermodynamic properties and b) concentration gradient in Odqvist's model

Carrying out a series of such calculation at different velocities, Odqvist et al. [37] reported a possible path for transition from PE boundary condition at high velocities to LENP at low velocities (Figure 1-31). However, when the predicted evolution of the carbon conditions at the interface were coupled with a simple model for bulk C diffusion in a semi-infinite austenite grain size, the resulting ferrite growth kinetics were still much faster than those observed experimentally.

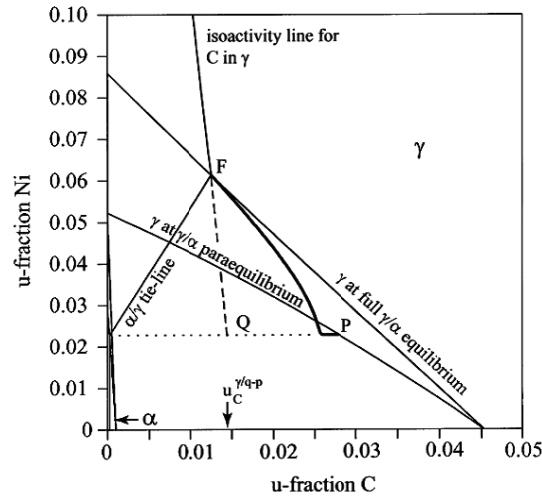


Figure 1-31. $\alpha+\gamma$ phase field in Fe-C-Ni phase diagram at 973 K (700 °C). PF line is showing the possible transition path from PE to LENP growth condition [37][38]

1.4 *Experimental observations on $\gamma \rightarrow \alpha$ transformation kinetics*

A quick look at the available literature in this area shows that most of the practitioner's interest has been focused on understanding effect of both temperature and composition on kinetics of the interface migration.

As explained in section 1.3.2.1, classical precipitation and controlled decarburization are two major techniques which are usually used for analyzing the ferrite growth.

Decarburization provides a very accurate method of measuring ferrite growth kinetics with minimal complications due to nucleation, crystallography or impingement of the carbon diffusion profiles. This method, which was used in the past by a number of investigators [11-13], consists of reheating the specimen into the austenite one phase region in an atmosphere of wet-H₂. The oxygen potential of this atmosphere is high enough to remove carbon from the specimen but too low to oxidize iron. The removal of

carbon from the specimen is controlled by diffusion in the solid. If the specimen is sufficiently thick, overlap of the carbon diffusion profiles does not take place and the diffusion problem can be simulated with a simple 1-D model. If the decarburization experiment is carried out at a suitable temperature, as shown in Figure 1-9, a planar ferrite layer will grow from the surface into the austenite. The growing ferrite grains traverse many crystals of the parent austenite, thus eliminating any strong interfacial structural effects. The effect of nucleation on the transformation kinetics is often minimal because the nucleation times (2 to 4 min) are typically small compared to the total decarburization times (8 to 300 min).

However, one should notice that the range of interface velocities encountered in decarburizing experiments is at least an order of magnitude slower than those encountered in precipitation experiments [57]. As explained in the previous section, both theoretical calculations by Hillert, Cahn, Lucke and Stuwe on solute drag and experimental observations [58] suggest that the interface velocity may play an important role in kinetics of the transformation and PE to LENP transition paths.

1.4.1 *Classical precipitation experiments*

There have been numerous investigations in the literature designed based on this technique. Among them, traditional precipitation data on the Ni and Mn containing systems obtained by Oi *et al* [59] and Hutchinson *et.al.* [6] are of relevance.

Oi *et al* [59], investigations in Fe-Mn-C and Fe-Ni-C systems using classical precipitation at different temperatures and compositions revealed that experimentally obtained boundary (shaded lines in Figure 1-32) for transition from fast growth (unpartitioned) to slow growth rate (partitioned) is located between theoretically calculated PE and LENP boundaries. These observations, which were consistent with similar results [60] reported by other researchers, were attributed to the solute drag effect.

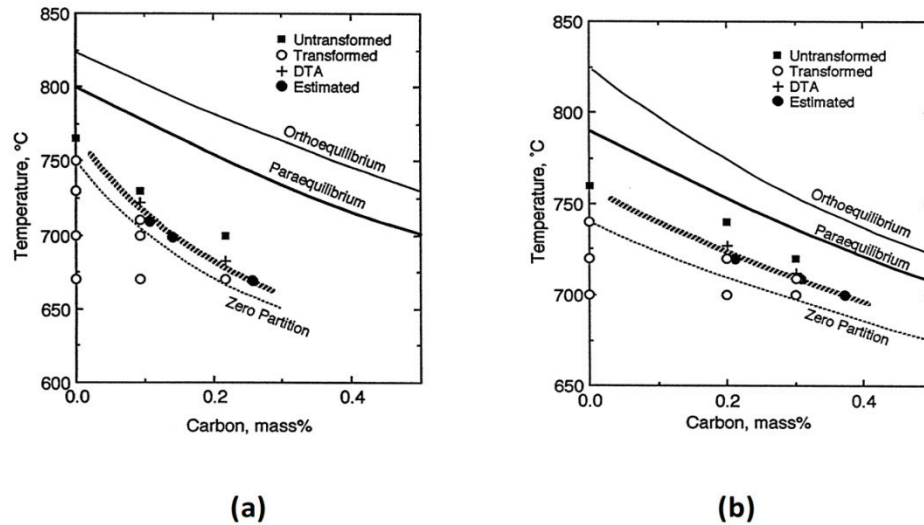


Figure 1-32. Experimentally obtained boundary for transition from fast growth rate to slow growth rate obtained using classical precipitation technique a) isopleth for alloy containing 2 wt% Mn b) isopleth for alloy containing 2.5 wt% Ni [59]

In agreement with Oi *et al* [59] results, Hutchinson *et.al.* [6] also reported fast ferrite formation above LENP boundary in Fe-Ni-C alloys. In fact, for concentrations located between theoretical PE and LENP limits, they observed a fast transition at early times followed by a very slow growth rate at longer times. They noticed that neither PE nor LENP boundary conditions can be used to explain the whole transformation kinetics. They

developed a model (described in section 1.3.2.2c) which suggested that PE boundary condition at short times is gradually changed to LNEP condition at longer times.

1.4.2 *Controlled decarburization experiments*

Systematic decarburizing investigations on Fe-C [23] alloys at different temperatures have shown that kinetics of the transformation can be fully explained by considering LNEP condition at the interface.

However, the same type of experiments on Fe-X-C systems, in which X is a substitutional element, have revealed different kinetic behaviors depending upon nature of the substitutional element (X). For example, in Fe-Ni-C [10], in which Ni has negligible tendency for segregation to the interface, LNEP boundary condition prevails at all conditions whereas subsequent reports on such systems as Fe-Mo-C and Fe-Cr-C, in which Mo and Cr have a strong bonding energy for jumping into the interface, have shown a meaningful deviation from LNEP boundary condition (Figure 1-33).

Amount of the deviation, which is usually attributed to the interaction of Mo and Cr atoms with the moving interface, can be approximately quantified in terms of the required energy (ΔG) which should be added or subtracted from Gibbs free energy curves of either ferrite or austenite to match the experimental observations with the LNEP or PE models. The table presented in Figure 1-33 shows an example of such calculations performed by Hutchinson *et.al* [16]

Treatment Temperature (°C)	Estimated Dissipation (J/mol)
825	8
806	10
775	43

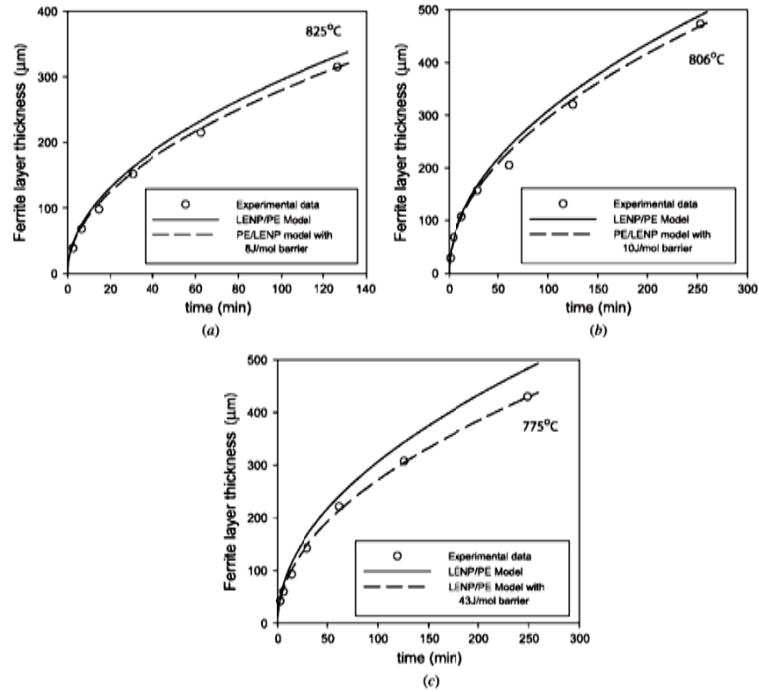


Figure 1-33. Kinetics of ferrite layer growth in decarburizing experiments on Fe-0.54 wt% C-0.51 wt% Mo alloy, by Hutchinson *et.al* [16]

As seen, surprisingly a constant value can be used at each temperature to fit all the experimental data *i.e.* a velocity independent solute drag which is in contrast with the theory of solute drag where a solute drag is a function of velocity (Figure 1-25b).

Similar type of deviation has also been reported [18] for Fe-Si-C systems at different temperatures.

As mentioned in section 1.3.2.2, Fe-Mn-C alloy is another interesting system in which an unexpected kinetics behavior during decarburization has been reported [17].

Usually, one may expect to see PE condition at low temperatures and a transition to LENP by increasing the temperatures (as partitioning becomes easier at higher temperatures). Contrary to the modeling suggestions, no experimental evidence of such transition has been reported during decarburizing experiment in this system. Instead, decarburizing experiments on Fe-Mn-C systems have revealed LENP boundary condition at intermediate temperatures and surprisingly, a transition from LENP to PE by increasing the temperatures. Here, it is worth mentioning that, recently classical precipitation experiments by Capdevila *et.al.* [61] in medium carbon Fe-Mn-C steels at low temperatures revealed a PE to LENP transition which was in agreement with expectations.

1.4.3 *Evidences on boundary segregation and spike build-up*

Obtaining experimental data on segregation of alloying elements into the boundary under different conditions has always been one of the challenging objectives for researchers. As Purdy [57] mentions "*the complexity of the structure of the ferrite austenite interface and its dependence on several degrees of freedom (orientation relationship, interface plane, as well as nanometere-scale displacements) militates against an easy description of its equilibrium and dynamic properties*". Nevertheless, significant technological advancements in different areas during last 20-30 years have opened new opportunities

for practitioners for unique observations which were not possible in the past. Some recent experimental studies are relevant here:

For example, STEM investigations on segregation of molybdenum atoms to the interface during classical ferrite precipitation have shown that the Mo accumulation at the interface is a function of both reaction time and temperature [62]. Moreover, as seen in Figure 1-34, the extensive scatter in data at each transformation time can be attributed to the existing crystallographic differences between different interfaces in samples. The same type of observation using STEM is also reported by Enomoto *et al.* [63] in a Fe-Mo-C alloys.

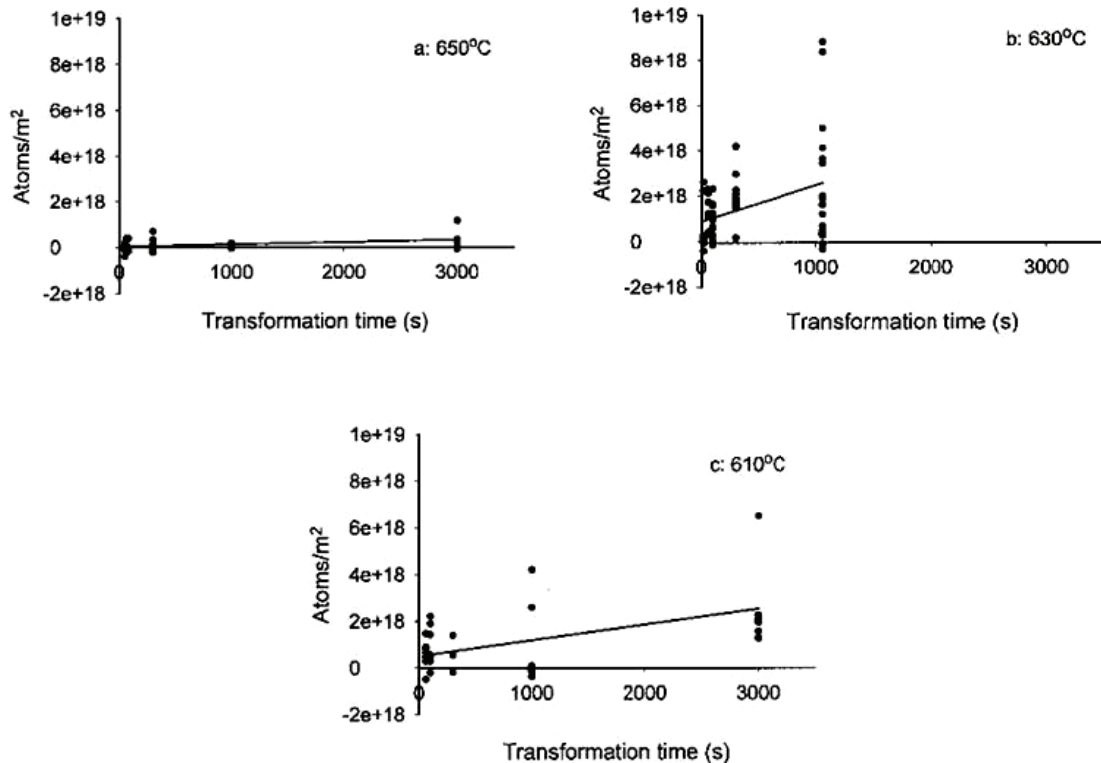


Figure 1-34. STEM results on Mo accumulation at γ/α interphase boundaries of precipitation experiments on Fe-0.24 wt pct C-0.93 wt pct Mo alloy at different times and temperatures (each point is an average of different measurements on a single boundary) [62]

In line with efforts for observing alloying element spike ahead of the migrating interface, one can point to a paper by Guo *et al.* [36] who employed high-resolution microanalysis (STEM) to demonstrate the existence of Mn enrichment at quenched ferrite-austenite interfaces after isothermal transformation for as little as 600 sec. at 750 °C. They reported well-developed Mn profiles in both ferrite and austenite after cessation of fast ferrite growth. In other words, their observations showed that the unpartitioned ferrite growth at short transformation times, where interface velocity is high, is replaced by partitioned growth at longer times, where interface velocity drops significantly.

Recently, Chen and van der Zwaag [64], [65], [66] have also used an elegant thermal cycling method to demonstrate the presence of "buried Mn spikes", planted in austenite by previous thermal cycles, via their kinetic interaction with moving transformation interfaces.

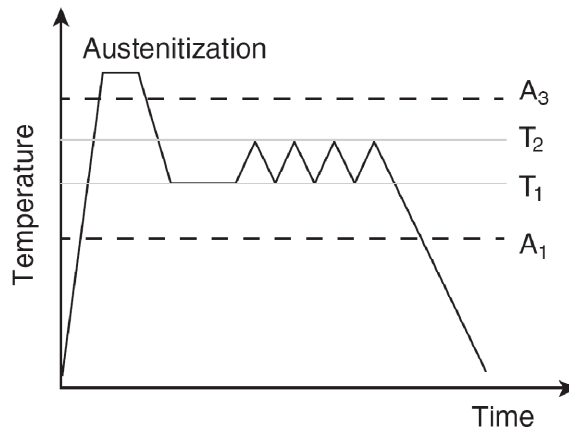


Figure 1-35: The heat treatment procedures used by Chen *et.al* [64] for their experiment

In this technique, “the material is thermally cycled in the two phase region with both phases present at all time”. Employing a sensitive dilatometer, this procedure allows one to follow the volume changes occurring in the sample as a function of temperature. Generally, it is shown [64], [65], [66] that these type of experiments reveal more features than normal transformation processes and provide a unique opportunity for investigating such kinetic parameters as the interface mobility.

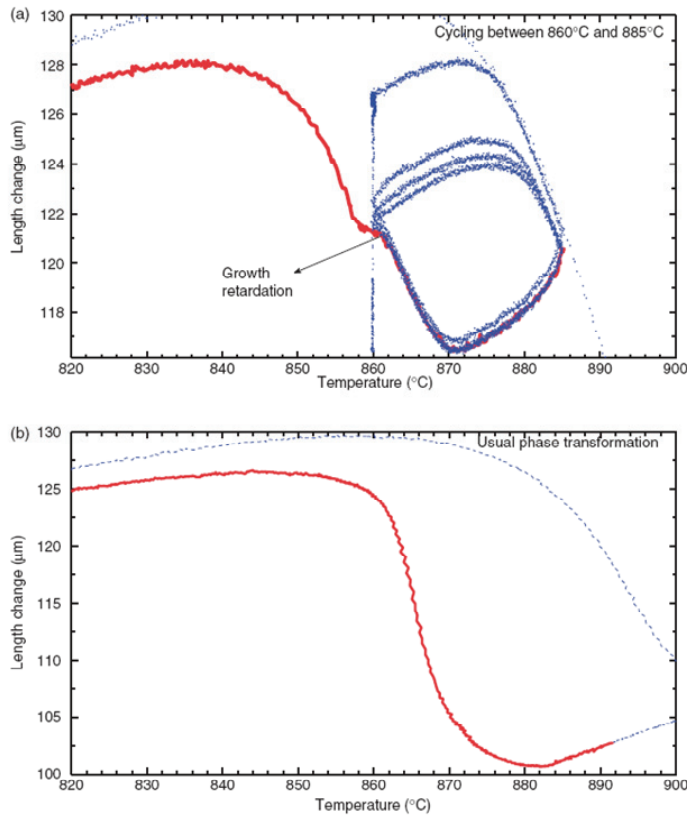


Figure 1-36: The dilation results by Chen *et.al* [64] in Fe-0.17Mn-0.023C alloy as a function of temperature (a) the cyclic procedure between 860 °C and 885 °C. The growth retardation is observed during the final stage cooling step (in solid and red line) and (b) the usual $\gamma \rightarrow \alpha$ transformation in which no growth retardation is observed during cooling (in solid and red line).

As an example, a cyclic treatment applied by Chen *et.al* [64] on a Fe-Mn-C alloy between 860 °C (T_1) and 885 °C (T_2) is schematically presented in Figure 1-35. Behaviour of the

system during thermal cycling process and during normal cooling from 885 °C to room temperature are shown in Figure 1-36a and Figure 1-36b respectively. A special growth retardation between 861 °C to 856 °C at the final stage of the thermal cycling procedure (*i.e.* during cooling down from 885 °C to room temperature) is indicated in Figure 1-36a. Surprisingly, such retardation is not observed in the case of normal γ to α transformation process with no thermal cycling.

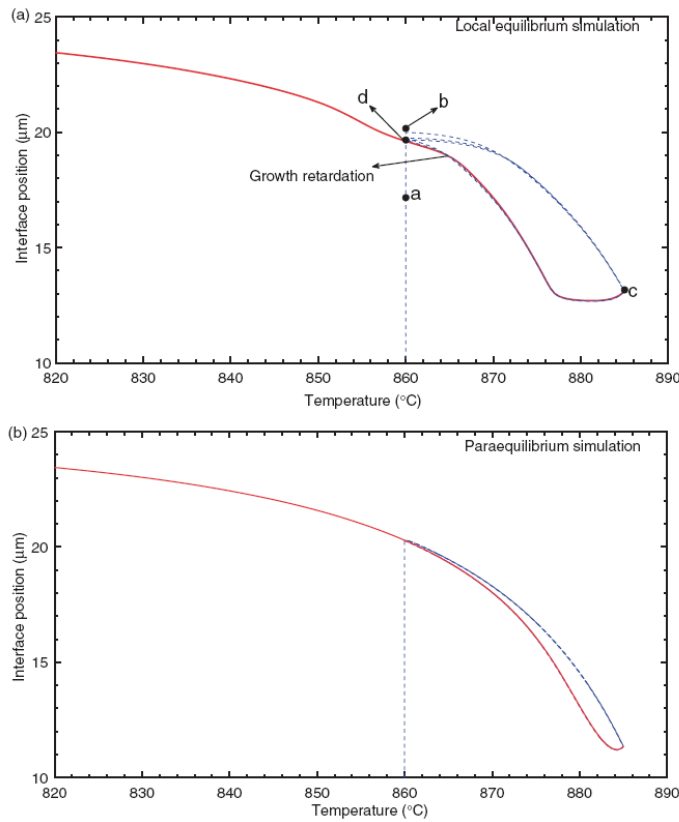


Figure 1-37: γ/α interface position simulated by Chen *et.al* [64] in Fe-0.17Mn-0.023C alloy under (a) local equilibrium conditions and (b) paraequilibrium conditions as a function of temperature after the cyclic phase transformations between 860 °C and 885 °C.

Theoretical calculations by Chen *et.al* [64] for simulating the interface position as a function of temperature during this thermal cycling procedure under local equilibrium (LE)

boundary conditions, showed the same type of retardation at the final cooling down step (Figure 1-37a). Interestingly, no retardation was observed during calculations under para-equilibrium (PE) condition (Figure 1-37b). As a result, Chen *et.al* [64] concluded that this retardation, which is “*qualitatively comparable to the experimental observations*”, can be related to the passage of the moving interface through the “residual Mn spike” planted during previous cycles of the thermal cycling procedure. The evolution of Mn profile ahead of the moving interface during the cyclic phase transformation based on the LE boundary condition is schematically presented in Figure 1-38.

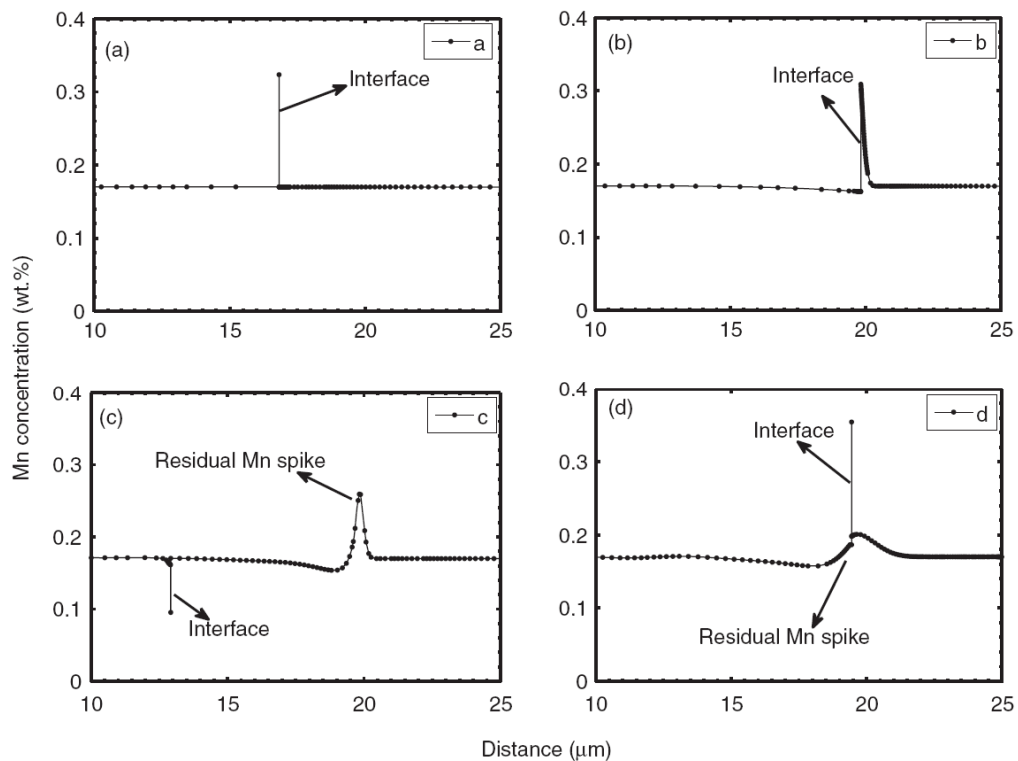


Figure 1-38: The evolution of Mn profiles by local equilibrium model during the cyclic phase transformation (by Chen *et.al* [64]). It shows how the γ/α interface encounters the buried Mn spike in the matrix (inherited from previous thermal cycles) during the final cooling down step. The plots (a)–(d) correspond to the points marked a, b, c, d in Figure 1-37.

2. Model Development

As mentioned in chapter 1, so far, austenite to ferrite transformation has been one of the most popular research areas in materials science which has been investigated from different aspects by different researchers. As a result, currently there is a very good wealth of experimental data available in the literature on the kinetics of this transformation. However, despite all effort so far to develop a self consistent model for ferrite growth, yet there has been no reliable model capable of predicting ferrite transformation in different compositions and temperatures.

Development of a physically based model to predict the evolution of alloying elements at the migrating interface has been set as the main objective in the present contribution.

It is clear that further advances in modeling are required to account, quantitatively and self-consistently, for:

- Solute drag (here interpreted as trans-interfacial diffusional dissipation);
- Austenite grain size effects;
- Near cessation of ferrite growth at non-equilibrium fractions (“stasis”); and
- The relaxation times for transitions from initial PE contact conditions.

Consequently, collecting critical experimental data in order to check the validity of the model will be an inevitable part of the research. As the first step, some of the available experimental data in the literature can be employed. Reasonable match between the experimental data point and modeling results in such systems as Fe-Ni-C, Fe-Mn-C and

Fe-Mo-C, in which rather different behaviors for substitutional elements are expected, can be considered as a good sign for overall health of the model.

Moreover, designing a critical experiment with unique conditions at the migrating interface and comparing the modeling predictions with the obtained results, is another challenge which has been tried to be addressed in this contribution.

2.1 Self-Consistent Model for Ferrite growth

2.1.1 Key Physical Processes:

In order to model the kinetics of ferrite growth, it is necessary to develop a description for the following processes:

- Alloying element diffusion across the interface and the dissipation associated with it.
- Evolution of the corresponding carbon concentrations at the interface.
- Carbon diffusion in the bulk phases.
- Ferrite growth as dictated by the carbon mass balance at the interface.

Each of these processes is described in detail in the following sections:

2.1.2 Alloying Element Diffusion:

It is generally assumed that initial ferrite growth occurs under PE conditions due to the high initial interface velocity. The PE condition is not a long-lived state because a chemical potential difference for the substitutional solutes will generally be present across the

interface and this will drive the diffusion of the alloying element across the interface and change the interfacial conditions.

In addition to diffusional jumps that are driven by the chemical potential difference between ferrite and austenite, it is also possible to have diffusion within the interface due to the presence of a potential well which is associated with the interaction of the alloying element with the interface. Figure 2-1a shows the most general case, in which, there is a difference between the chemical potentials of the substitutional element in ferrite and austenite, as well as a potential well at the interface.

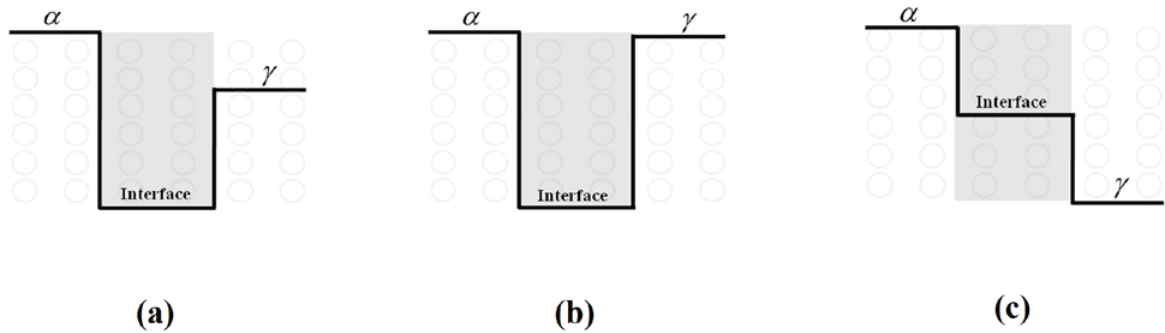


Figure 2-1. Schematic of X chemical potential profiles across the interface:
a) general case, b) Fe-Mo c)Fe-Ni

Two limiting cases are worth emphasizing; in the Fe-Mo-C system it is possible to choose combinations of temperature and composition which will lead to the same chemical potential of Mo in ferrite and austenite. The interaction of Mo with the interface leads to a potential well as shown in Figure 2-1b. This profile resembles the potential well often used for modeling interfacial dissipation during grain-growth or recrystallization. The other extreme is that shown in Figure 2-1c, where the interaction of the alloying element

with the interface is weak and the dominant driving force for diffusion of the alloying element is the difference between the chemical potentials of ferrite and austenite. This is exemplified by the Fe-Ni-C and Fe-Mn-C systems. .

As mentioned in the previous chapter, most treatments of diffusion within the interface are continuum treatments [27,35,42,43] that predict sharp concentration gradients within the interface. We have adopted a discrete-jump model for diffusion across the interface (in the spirit of Hutchinson *et al.* [6]), because the existence of concentration gradients over distances of the order of the atomic spacing is questionable.

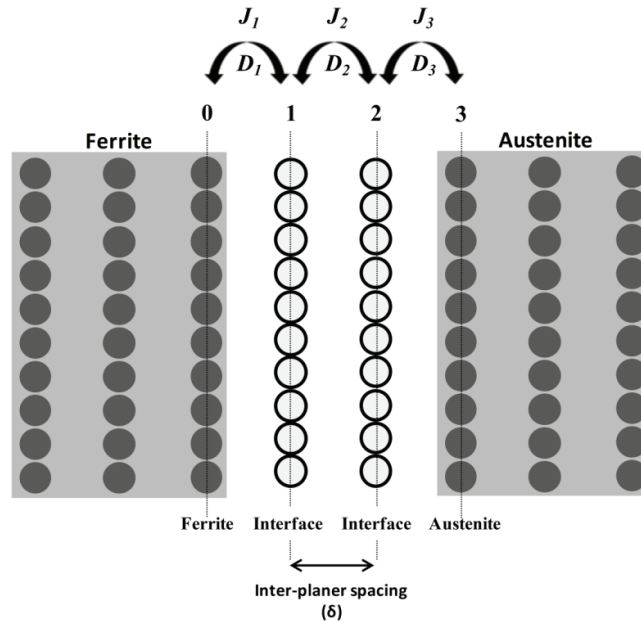


Figure 2-2. Interface model in terms of atomic planes (0,1,2,3) and definition of the various diffusivities (D_1, D_2, D_3), jumps and fluxes (J_1, J_2, J_3)

The model is, in fact, similar to that of Lucke and Stuwe [45]; the interface is assumed to consist of two atomic layers, as shown in Figure 2-2, and diffusion from one side of the

interface to the other involves 3 jumps; one jump from ferrite into the interface, another jump within the interface and finally a jump from the interface to austenite (it should be noted that the "square" chemical potential profiles in Figure 2-1 are intended to show schematically the relative levels at the different atomic planes, and are not to be interpreted as continuum).

The jumps in Figure 2-2 are assumed to occur with diffusion coefficients of D_1 , D_2 and D_3 , respectively. The evolution of the alloying element concentration on plane 'i', dx_X^i , as a result of both atomic jumps and movement of the boundary can be expressed as:

$$dx_X^i \cdot \frac{\delta}{dt} = \underbrace{J_X^i - J_X^{i+1}}_{\text{due to diffusion}} + \underbrace{v(x_X^{i+1} - x_X^i)}_{\text{due to movement of the boundary}} \quad (2.1)$$

where the flux term from plane 'i-1' to plane 'i', J_X^i , is given by using Eq.(1.25) in volume-fixed frame of reference which yields:

$$J = -M_{AB} x_A \cdot x_B \nabla(\mu_A - \mu_B)$$

$$\Rightarrow J_X^i = -\frac{D_X^i}{RT} x_{Fe}^{i-1} x_X^{i-1} \cdot \frac{(\mu_X^i - \mu_X^{i-1}) - (\mu_{Fe}^i - \mu_{Fe}^{i-1})}{\delta} \quad (2.2)$$

In these equations, D_X^i are the diffusion coefficients of the substitutional element (X) as defined in Figure 2-2, R is the gas constant, dt is the time increment used in the calculations, δ is the distance between atomic planes, and v is the interface velocity.

The interface velocity will evolve during ferrite growth leading to non-steady-state conditions. However, for a sufficiently small time increment, dt , it is reasonable to assume steady-state and the left hand side of Eq.(2.1) tends to zero. As a result, for a given interface velocity, and assuming that the transformation is non-partitioning, *i.e.* $x_X^0 = \text{constant}$, one can calculate the concentration of X at each atomic plane. The dissipation associated with diffusion across the interface (solute drag) can then be calculated using a discrete jump version of Eq.(1.67) proposed by Hillert and Sundman [39] :

$$\Delta G^{dissipated} = -\frac{V_m}{v} \int_{-\delta}^{+\delta} J_M \cdot \frac{d(\mu_M - \mu_{Fe})}{dy} \cdot dy \quad (1.67)$$

$$\Delta G^{dissipated} = \sum_{i=1}^{i=3} -\frac{V_m}{v} \cdot J_X^i \cdot \left[(\mu_X^i - \mu_X^{i-1}) - (\mu_{Fe}^i - \mu_{Fe}^{i-1}) \right] \quad (2.3)$$

The concentration of the alloying element across the interface and the associated dissipation can thus be expressed as a function of velocity. The associated carbon concentrations can then be calculated using the procedure described in the next section.

2.1.3 Evolution of Carbon Concentrations at the Interface:

Given the fast diffusivity of carbon, it is reasonable to assume that the carbon chemical potential is constant across the interface. In order to determine the value of the carbon chemical potential we employ a simple energy balance across the interface:

$$D_{\text{int}}^{\text{chem}} + \Delta G^{\text{friction}} + \Delta G^{\text{diff}} = 0 \quad (2.4)$$

where $D_{\text{int}}^{\text{chem}}$ is the chemical driving force given by the following expression introduced by Hutchinson *et.al* [6]:

$$D_{\text{int}}^{\text{chem}} = \frac{(U_X^{\text{fcc}} + U_X^{\text{bcc}})}{2} \cdot (\mu_X^{\text{fcc}} - \mu_X^{\text{bcc}}) + \frac{(U_{\text{Fe}}^{\text{fcc}} + U_{\text{Fe}}^{\text{bcc}})}{2} \cdot (\mu_{\text{Fe}}^{\text{fcc}} - \mu_{\text{Fe}}^{\text{bcc}}) \quad (2.5)$$

where U_X and U_{Fe} are the mole fraction of 'X' and 'Fe', respectively, on the substitutional lattices (U-fraction) at the interface boundaries with adjacent phases *i.e.* austenite and ferrite. As expected, the driving force expressed by Eq.(2.5), is zero for the limiting cases of PE and LE-NP.

Under most conditions of interest in the present work, the friction term (dissipation due to the structural rearrangement at the interface) is negligible and Eq.(2.4) reduces to:

$$D_{\text{int}}^{\text{chem}} + \Delta G^{\text{diff}} = 0 \quad (2.6)$$

This equation along with the assumption of constant carbon chemical potential is sufficient to determine the carbon concentrations on the ferrite and austenite sides of the interface as well as the carbon concentrations within the interface.

Here, it is worth insisting that, similar to Agren *et.al* [50], the total driving force for interface migration ($D_{\text{int}}^{\text{chem}}$) in this process is calculated over the interface region only and this means that, the dissipation of free energy should consequently be calculated over the

same area *i.e.* free energy dissipation due to diffusion of atoms in the spike ahead of the interface should not be taken into account.

When this calculation is performed as a function of velocity it is possible to trace, on the ternary isotherm, the interfacial compositions that the system will sample as it evolves from PE to LENP. Two examples are shown in Figure 2-3. The first is for Fe-Ni-C at 1048 K (775 °C) (Figure 2-3a) and the second is for Fe-Mo-C (Figure 2-3b) at the same temperature. In this calculation, the diffusion coefficients for the various jumps within the interface were assumed to be equal to the bulk diffusion coefficient in ferrite for the first jump, D_1 , equal to the bulk diffusion coefficient in austenite for the third jump, D_3 , and equal to the geometric average of D_1 and D_3 for the second jump, D_2

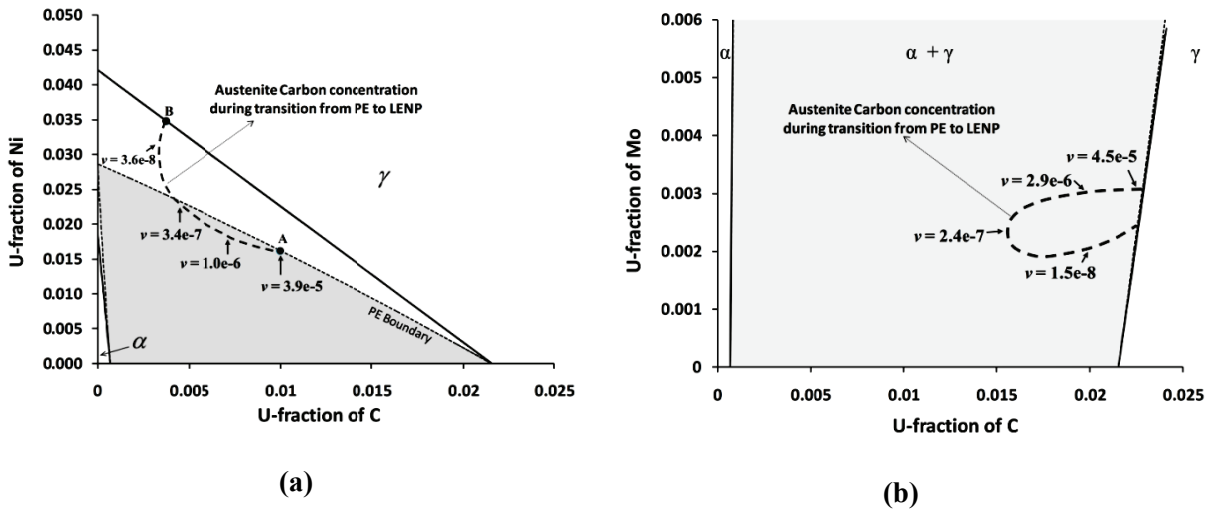


Figure 2-3. : Isothermal sections for a) Fe-Ni-C and b) Fe-Mo-C at 775 °C, plotted as U_x vs. U_c . Path taken by the system is shown along with arrows indicating interface velocity (v)

It is clear from Figure 2-3 that the path from PE to LENP can be complicated due to the effect of dissipation on the interfacial carbon concentration. This point, which is important

for understanding the evolution of the system and the overall growth, will be discussed in detail in Section 3.

2.1.4 Carbon Diffusion in the Bulk-phases:

Sections 2.1.2 and 2.1.3 described the evolution of interfacial conditions as a function of velocity. In order to derive the actual kinetics as a function of time, it is necessary to incorporate carbon diffusion in the bulk phases. Two cases are considered in this contribution; ferrite precipitation at austenite grain boundaries and ferrite growth during a controlled surface decarburization treatments.

The first situation is the case that is of industrial relevance for microstructure evolution in steels which has been studied for more than 50 years. Here, it is sufficient to model only carbon diffusion in the austenite phase.

The case of decarburization, which offers some advantages in terms of precision of growth kinetic data, requires the calculation of the carbon profiles in both austenite and ferrite. In both cases, carbon diffusion is modeled using a Murry-Landis explicit finite-difference method [67] that includes the carbon dependence of the carbon diffusivity in austenite.

In the case of decarburization, the specimens are large enough that they can be assumed semi-infinite and overlap of the carbon diffusion profiles in the austenite does not take place (Figure 2-4a).

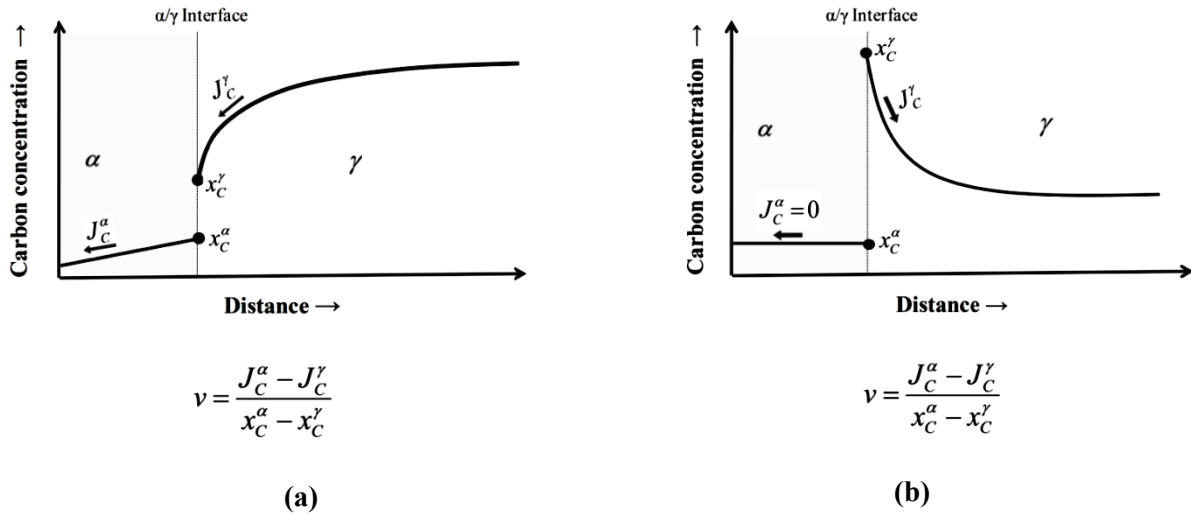


Figure 2-4. Schematics of C profiles in a) decarburization and b) precipitation; along with velocity equations for the two different cases

In contrast, the overlap of the carbon diffusion profiles in the austenite is critical for capturing the kinetics of ferrite growth in classical precipitation (Figure 2-4b). In order to capture the kinetics accurately in the case of ferrite precipitation, and to estimate the ferrite volume fraction, a spherical geometry was assumed and the diameter of the sphere was set equal to the experimentally determined grain size.

2.1.5 Growth Rate:

As explained in the previous chapter, the instantaneous growth rate of the ferrite layer can be calculated from the mass balance at the interface. In the case of ferrite precipitation, the mass balance leads to Eq.(1.37):

$$v = -\frac{J_C^\gamma}{x_C^\alpha - x_C^\gamma} \quad (1.37)$$

For decarbuization, calculation of the interface velocity requires consideration of the carbon flux in both ferrite and austenite. The velocity is then given by Eq.(1.42):

$$v = \frac{J_C^\alpha - J_C^\gamma}{x_C^\alpha - x_C^\gamma} \quad (1.42)$$

2.2 Model Parameters:

In order to implement the above model it is essential to have reliable thermodynamic and kinetic data. The thermodynamic description of the bulk ferrite and austenite phases in the Fe-Ni-C and Fe-Mo-C systems was obtained from the TCFE2 database which was accessed using the TQ interface of the ThermoCalc Software Package [68]. In the case of the Fe-Mn-C system, the TCFE2 description appears to systematically underestimate the solubility of Mn in ferrite. For this reason we have developed a modified description which is described in Appendix 1. As for the kinetic data, the bulk diffusion coefficients of the substitutional elements were extracted from the Mob2 database, which is also available from ThermoCalc. The carbon diffusion coefficient in austenite was obtained from Eq.(1.43) proposed by Agren [22], while the carbon diffusion coefficient in ferrite was measured experimentally from decarburization experiments on binary Fe-C alloys [23]

A key challenge is to develop a thermodynamic description of the interface and to estimate the diffusion coefficients for transport across the interface. We have employed the approach of defining an interface-phase as proposed by Hillert [69]. For simplicity, the

Gibbs energy expression of this phase was developed by modifying that of the bulk austenite phase in the following manner:

- 1- The reference state for the free energy was shifted by 3.5 KJ/mol in order to capture an interfacial energy of the order of 0.5 J/m^2 .
- 2- The Fe-X interaction term in the substitutional sublattice was decreased in order to favour the segregation of the alloying element to the interface or increased in order to favour desegregation. While accurate values of the interaction parameter are not available, reasonable estimates could be made based on the measured binding energies of alloying elements to grain boundaries.

In the literature many different values for the cross-interface diffusivities have been used and these vary over many orders of magnitude [63–66]. For this reason, the three diffusion coefficients, D_1 , D_2 and D_3 were initially used as adjustable parameters. However, it quickly became apparent that in order to capture the experimental trends, it was necessary to use values of the cross-interface diffusion coefficient that are of same order of magnitude as those in the bulk phases. This is consistent with the conclusions of recent applications of solute drag theory to recrystallization [70]. Therefore, except Fe-Si-C and Fe-Cr-C alloys, in which D_2 and D_3 were equated to the bulk austenite diffusion coefficient, all other results presented in subsequent sections were obtained using the bulk ferrite diffusion coefficient for D_1 , the bulk austenite diffusion coefficient for D_3 and the geometric average of the two for D_2 . In addition to providing an excellent description of the experimental data, the present approach effectively removes three adjustable parameters from the

model. From the mechanistic point of view, the use of these values is attractive because one would expect that jumps to-and-from ferrite would be dominated by attachment kinetics in ferrite and thus would have similar diffusion coefficient as bulk diffusion in ferrite. Similarly, jumps to-and-from austenite would occur at a similar rate to jumps within the bulk austenite. It is worth pointing out that atomistic simulations seem to confirm that diffusion across the interface occurs at a rate comparable to bulk diffusion [67, 68].

Based on the above discussion, the only fitting parameter in the model is the interaction parameter of Fe and X within the interface. As will be shown in 2.3, excellent agreement with the experimental data is obtained by estimating this parameter from grain-boundary binding energies.

2.3 Application of the model

The evolution of contact conditions during growth is dominated by the alloying element diffusion within, and across, the interface. In this regard, different situations can be identified:

- a) a situation where the interaction of the alloying element with the interface itself is weak (*i.e.* the binding energy of the solute to the boundary is small compared to the chemical potential difference between ferrite and austenite). This case is exemplified by the Fe-Ni-C and Fe-Mn-C systems.

- b) The second extreme is exemplified by Mo at temperatures in the range of 775-850 °C. In this temperature range the chemical potentials of Mo in ferrite and austenite are almost identical. The dominant effect is due to Mo interaction with the interface, much like the interaction of solutes with grain boundaries.
- c) Other alloying systems may lie between the two extremes mentioned above. In these general cases both types of interactions are important. Free energy dissipation due to solute diffusion may arise from contribution of both the interaction with the boundary (driven by the potential well within the interface) and diffusion across the boundary driven by solute partitioning tendencies between the bulk phases. This case is exemplified by the Fe-Cr-C and Fe-Cu-C and Fe-Si-C systems.

These systems are discussed in detail in the following Sections.

2.3.1 Fe-Ni-C and Fe-Mn-C

In order to validate the model, it is necessary to identify discriminating experimental data that provides a critical test of the model.

The key weakness of experimental data on ferrite formation during classical precipitation, is that there is a large scatter in the reported allotrimorph half-widths due to nucleation, crystallography, stereology and variations in the grain size. For this reason, In the case of precipitation experiments, we have avoided direct comparison of the measured and predicted allotrimorph width. Instead, we have focused on the measured ferrite volume

fraction at long holding times and the critical compositions and temperatures for partitionless ferrite growth.

We have therefore modeled the results of Oi *et al.* [59] in which the critical temperature for the cessation of ferrite growth was measured (Figure 2-5a and Figure 2-5c) and the data of Hutchinson *et al.* [16] for which the critical composition for ferrite growth stasis at 700 °C was measured (Figure 2-5b).

The best fit of the effective cessation of ferrite growth was obtained by adjusting the interaction parameter between Fe and Ni in the interface such that the initial chemical potential of Ni in the interface is 1.5 kJ/mol greater than the average of the initial chemical potentials of Ni in ferrite and austenite. The choice of this value is based on the weak interaction of Ni with the interface along with the tendency for C to repel Ni from the interface. As shown in Table 2-1, the model accurately predicts the temperature at which ferrite growth stops for the Fe-2.66%Ni-0.196%C and 2.42%Ni-0.293%C alloys employed by Oi *et al.* [59]. Similarly, the model predicts that the volume fraction of ferrite formed at 700 °C will dramatically decrease between 2.76%Ni and 3.14%Ni in agreement with the experimental data of Hutchinson *et al.*[6].

Similarly, in the case of the Fe-Mn-C system, the experimental trends could be captured by setting the initial chemical potential of Mn in the interface to a value which is 2.5 kJ/mol lower than the average of initial chemical potentials of ferrite and austenite.

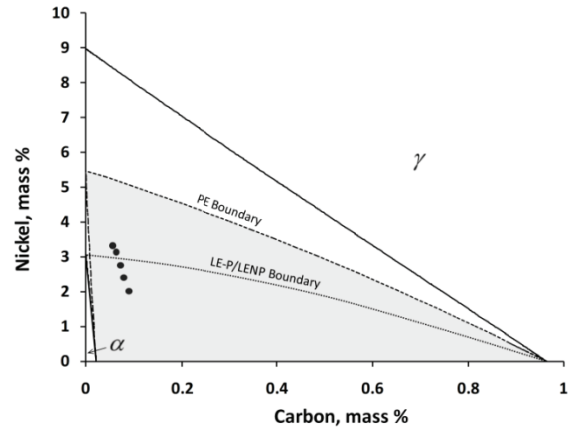
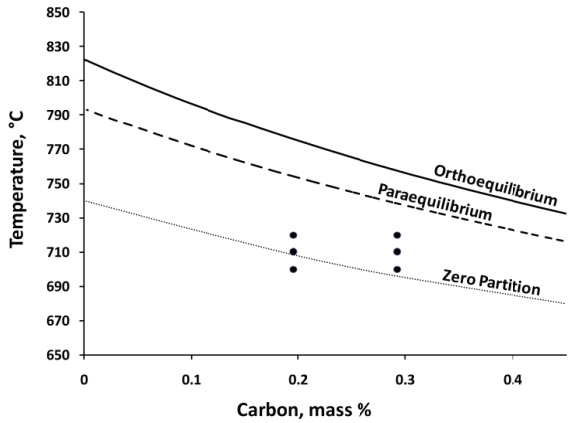
Once again, the model accurately captures the critical temperatures for the arrest of ferrite growth as shown in Table 2-1.

It should be pointed out that the quantitative agreement between the measured and calculated volume fractions can be improved by varying the values of the diffusion coefficients and binding energies for each alloy and temperature. However, we prefer to maintain constant values of these parameters in order to focus on the physical picture. In addition, one should not expect perfect agreement given the inherent simplifications in the model as well as the uncertainties associated with cross-interface diffusivities and binding energies and bulk carbon diffusion coefficient.

In order to obtain a greater insight into the mechanisms responsible for the cessation of ferrite growth, the interfacial carbon concentration on the austenite side of the interface and the carbon flux in austenite are plotted in Figure 2-6, as a function of time for two cases, Fe-2.41%Ni-0.078%C and Fe-2.08%Mn-0.095%C, both at 700 °C. For the sake of clarity, Figure 2-6 was constructed for a grain-size of 500 μm in order to postpone the overlap of the carbon diffusion profiles in austenite. Both compositions lie inside the envelope of no partition.

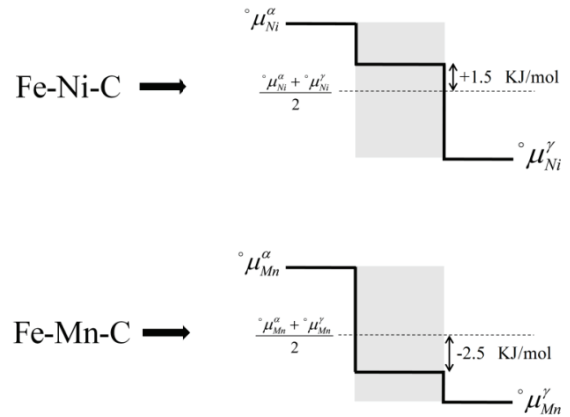
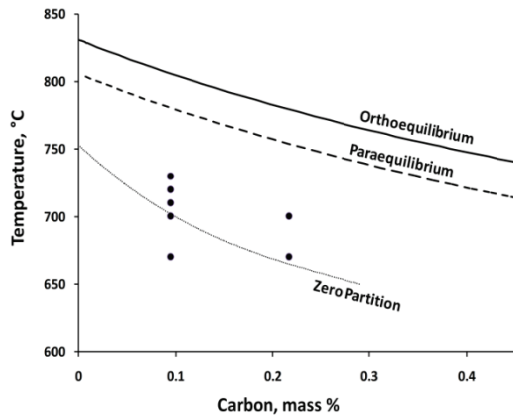
In both cases, the interface stops because the carbon concentration at the interface drops below the carbon concentration ahead of the interface. The drop in carbon concentration at the interface is a result of the build-up of the alloying element spike in austenite as well as the dissipation of energy which requires an increase in the supersaturation for growth

to continue. The relative contributions of these two effects will be the subject of further analysis in Chapter [3].



(a)

(b)



(c)

(d)

Figure 2-5. a) 2.5 wt% Ni isopleth with alloy compositions (black circles) examined by Oi, Lux and Purdy [59], b) Isothermal section of Fe-Ni-C phase diagram at 700 °C with five alloy compositions examined by Hutchinson *et al.* [6], c) 2.0 wt% Mn isopleths with different alloy compositions examined by Oi, Lux and Purdy [59] d) Schematic of the initial chemical potential profiles used for calculations in Fe-Ni-C and Fe-Mn-C systems

In both of the above cases, the bulk composition was within the envelope of no partitioning, therefore the interface could, in principle, continue moving forward once the carbon diffusion profile in austenite has sufficiently relaxed. In such a case, ferrite growth

will resume and the volume fraction would increase beyond the predicted values shown in Table 2-1. This resumption of growth may in fact be responsible for the discrepancy between the calculated and measured volume fractions just below the LENP limit (*e.g.* 34% vs. 47% for the 2.66% Ni alloy at 700 °C). On the other, in an alloy whose bulk composition is outside the envelope, one would expect the interface to stop and further growth to occur very slowly under full-partitioning conditions.

Table 2-1. Experimentally obtained ferrite volume fraction and new model predictions for different Fe-Ni-C and Fe-Mn-C alloys at different temperatures

Alloy	Temperature K (°C)	Measured, V_f	Calculated, V_f
2.66%Ni-0.196%C	973 (700)	47%	34%
	983 (710)	n/a	20%
	992 (720)	3%	0%
2.42%Ni-0.293%C	973 (700)	21%	18%
	983 (710)	<1%	0%
	993 (720)	0%	0%
2.02%Ni-0.088%C	973 (700)	82%	81%
2.41%Ni-0.078%C		77%	79%
2.76%Ni-0.071%C		66%	76%
3.14%Ni-0.062%C		<10%	26%
3.33%Ni-0.055%C		<10%	22%
2.08%Mn-0.095%C	943 (670)	67%	35%
	973 (700)	23%	32%
	983 (710)	3%	4%
	993 (720)	n/a	0%
	1003 (730)	0%	0%
2.17%Mn-0.217%C	943 (670)	18%	6%
	973 (700)	0%	0%

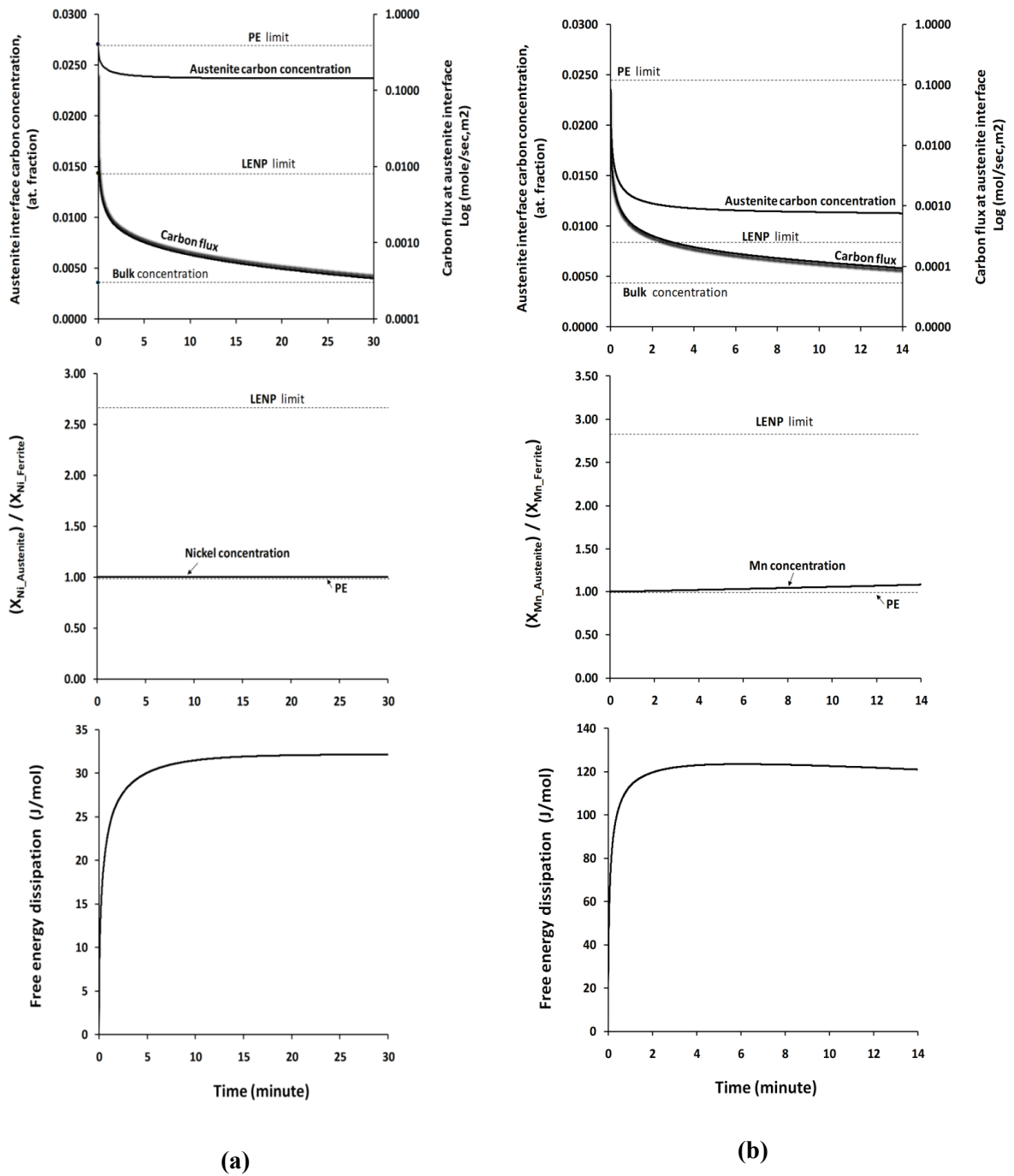


Figure 2-6. Evolution of carbon concentration, carbon flux, and substitutional alloying element concentration on the austenite side of the interface as a function of time in a) 3.14% Ni-0.062% C alloy, b) Fe-2.08%Mn-0.095%C alloy, evolution of the free energy dissipation for each alloy as function of time is also presented in the last row

As mentioned earlier, a limitation of ferrite precipitation data is that the reported measurements show a large scatter and this is not ideal for critical tests of ferrite growth

models. An alternative is to use the kinetics of ferrite growth under decarburization conditions where the kinetics can be measured with high precision.

In the case of Fe-Ni-C system, a ternary alloy of composition Fe-0.74C-1.46Ni (mass %) was arc melted from high purity stocks of Fe, Ni and C. In order to break down the as-cast structure, the alloy was cold-rolled to a reduction of 50%, sealed under high vacuum and annealed for 72 hrs at 1100 °C. Small samples of approximate dimensions of 3x4x8 mm³ were then sectioned from the alloy. The surfaces of the samples were then polished using SiC paper down to a 4000 grit. Samples were electroplated with a layer of pure Fe (5 to 10 μm) prior to decarburization. The electroplating was made in a distilled water based solution containing 2.3 mol/l FeCl₂ and 1 mol/l NaCl using a 25 to 30 mA current applied from a counter electrode (pure iron) to the working electrode (samples) for 10 minutes at 80 °C to 85 °C. The reason for the deposition is to avoid preferential Ni oxidation at the surface of the material during decarburization that may influence the ease of C removal from the surface during the decarburization process.

The decarburization treatment involved spot welding the samples to a holder which was then inserted through an O-ring seal into the tube-furnace, under a flow of a non-decarburizing gas (argon or dry-hydrogen). A heating time of 5 minutes, allowed the samples to austenitize and reach to the desired decarburization temperature. Water-saturated hydrogen (at room temperature) was then used to decarburize the samples for the desired period of time.

The decarburization experiment was terminated by stopping the flow of wet-hydrogen, purging the work-tube with Ar for 2 to 3 minutes and finally quenching the samples in water. Blank samples, with no flow of wet-hydrogen, were used to verify that the austenitizing and purging steps resulted in no ferrite formation. Overall, the temperature was controlled to within less than ± 2 °C and quenching times were generally less than 5 seconds. Decarburization treatments were carried out at 735, 755, 775°C for times ranging from 2 to 128 minutes.

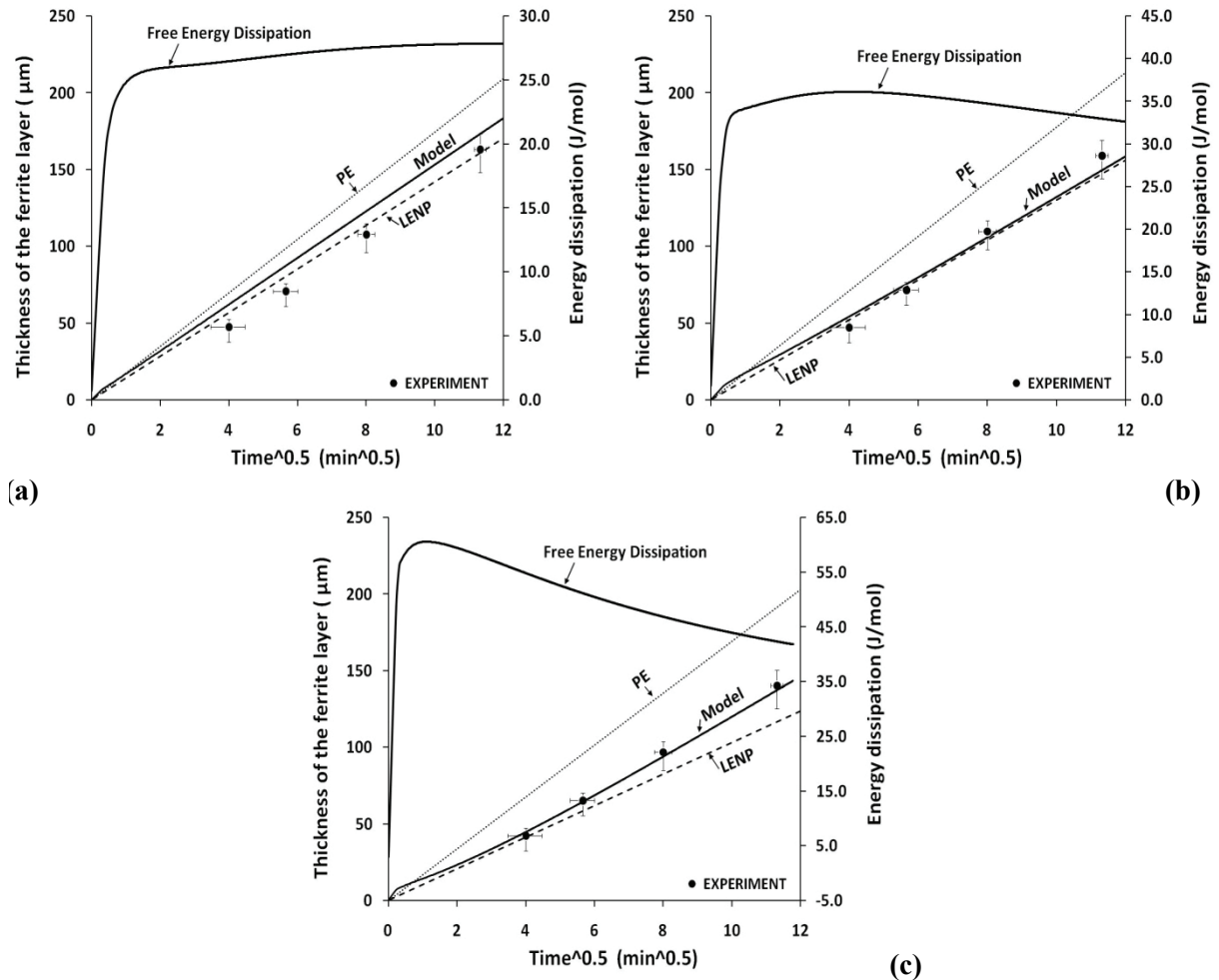


Figure 2-7: Ferrite layer growth kinetics during decarburization of Fe-1.46 Ni-0.74C alloy : a) 735 C, b) 755 C, c) 775 C. Comparisons with the PE, LEMP and the developed model are shown in each case as well as the free energy dissipation during reaction,

Results are presented in Figure 2-7. As seen using the same cross-interface diffusion coefficients and interface binding energies used for ferrite precipitation in Fe-Ni-C alloys, yield a good match with the experimental data.

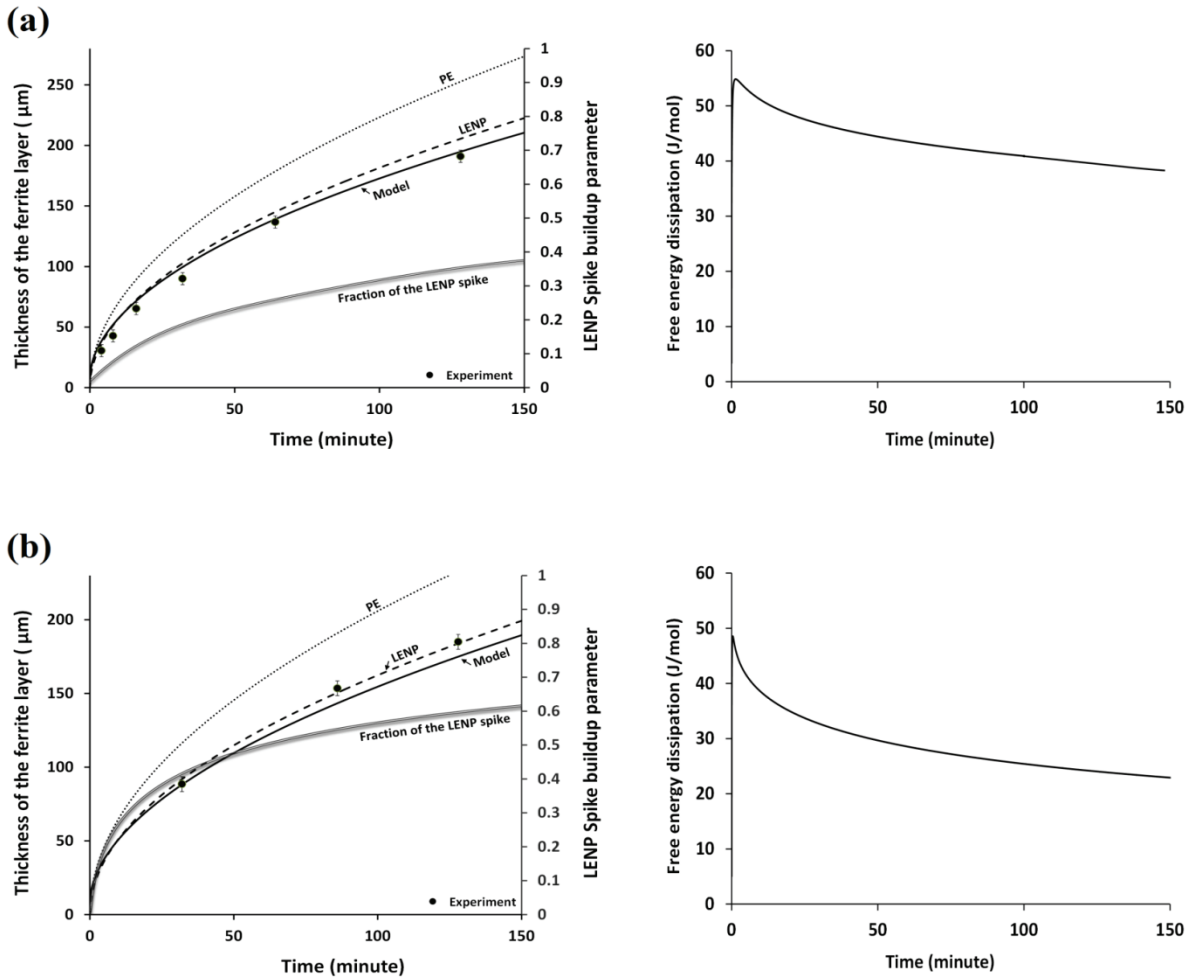


Figure 2-8. Kinetics of decarburization (left) and evolution of free energy dissipation (right) in Fe-0.94%Mn-0.57%C alloy at a) 755 °C b) 775 °C, the secondary axis in the left column is presenting the LENP spike buildup parameter (P_{Spike}) which is defined in the text and varies from 0 in the case of PE to 1 in the case of LENP.

Taking advantage of the available experimental results, already reported by Zurob *et.al.* [38, 54], the kinetics of decarburization in the Fe-Mn-C system was also examined in detail for a range of Mn contents (0.5-2%Mn) and temperatures (725-874 °C). Using the same cross-interface diffusion coefficients and interface binding energies described above for

ferrite precipitation, the model shows excellent agreement with the experimental kinetics measurements as shown for selected conditions in Figure 2-8 and Figure 2-9. In order to aid subsequent discussions, Figure 2-8 and Figure 2-9 also include the energy dissipation and height of the alloying element spike for each of the conditions considered.

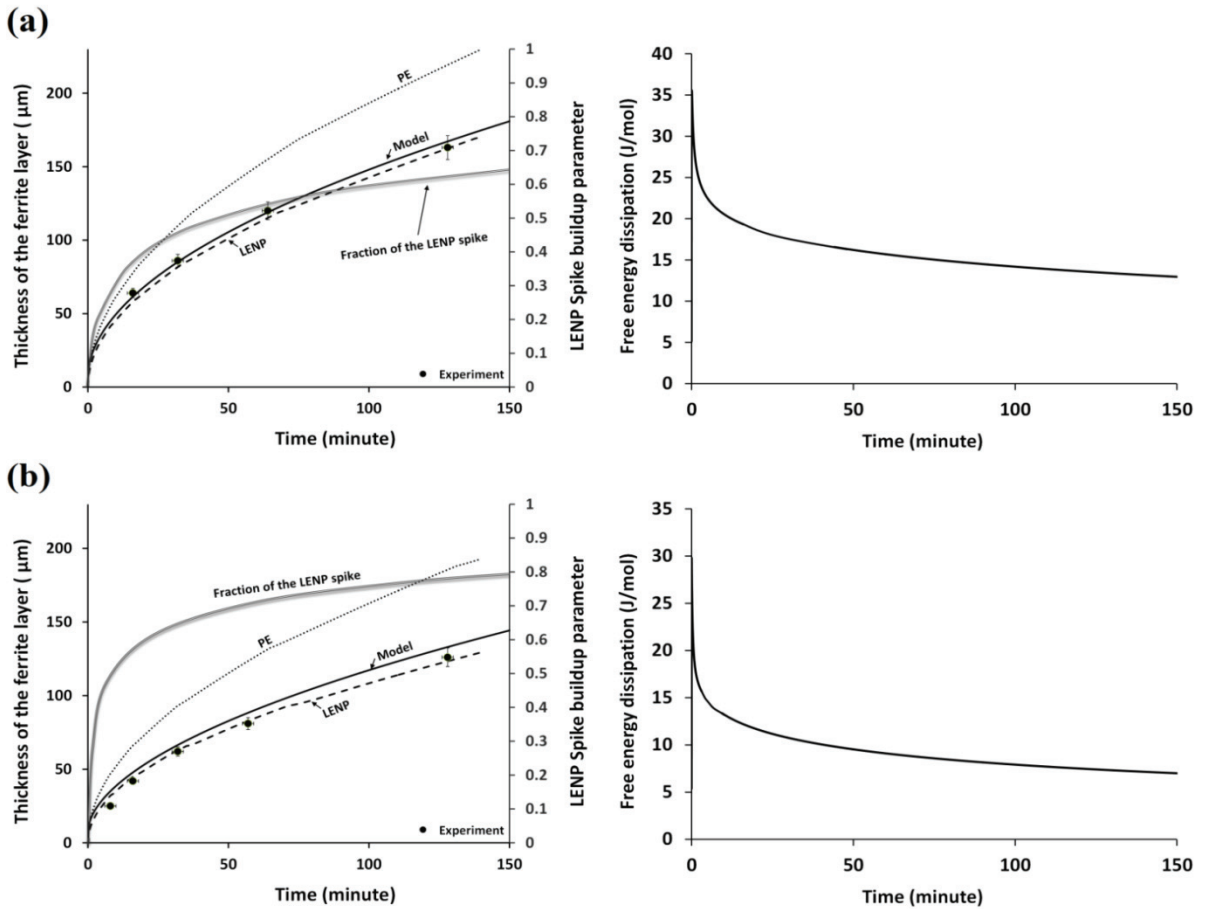
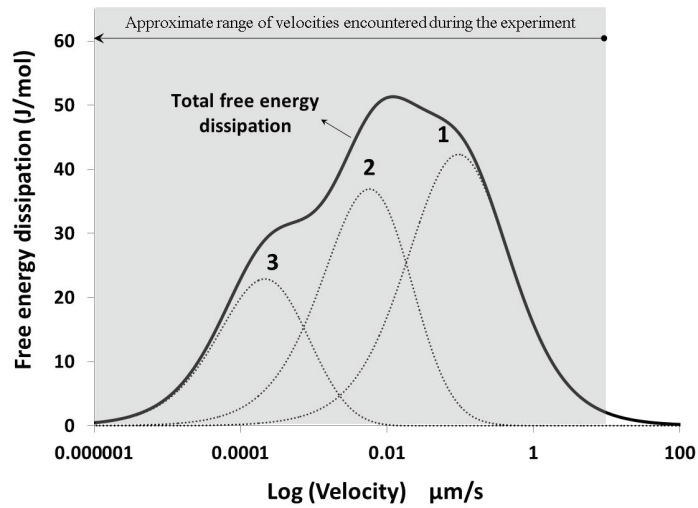


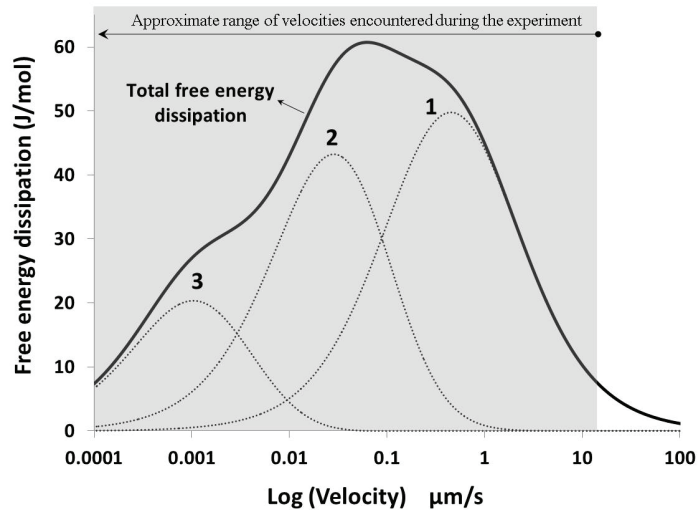
Figure 2-9. Kinetics of decarburization (left) and evolution of free energy dissipation (right) in Fe-0.94%Mn-0.57%C alloy at a) 806 °C b) 825 °C, the secondary axis in the left column is presenting the LENP spike buildup parameter (P_{Spike}) which is defined in the text and varies from 0 in the case of PE to 1 in the case of LENP.

Here, it might be interesting to pay attention to the fact that the free energy dissipation presented in all of these calculations (at a certain time/velocity) is, in fact, a total value

which is originated from contribution of different atomic jumps within the interface. For example, contribution of each atomic jump and range of the velocities encountered (the shaded area) during the decarburizing of Fe-1.46Ni-0.74C alloy at 735 °C and 775 °C are presented in Figure 2-10.



(a)



(b)

Figure 2-10: Free energy dissipation associated with atomic jumps from ferrite into the interface ,1, within the interface ,2, and from austenite into the interface, 3, during interface migration in Fe-1.46Ni-0.74C alloy at (a) 735 °C and (b) 775 °C. The shaded area is representing the range of the velocities encountered during the decarburizing experiments of this alloy.

2.3.2 *Fe-Mo-C system*

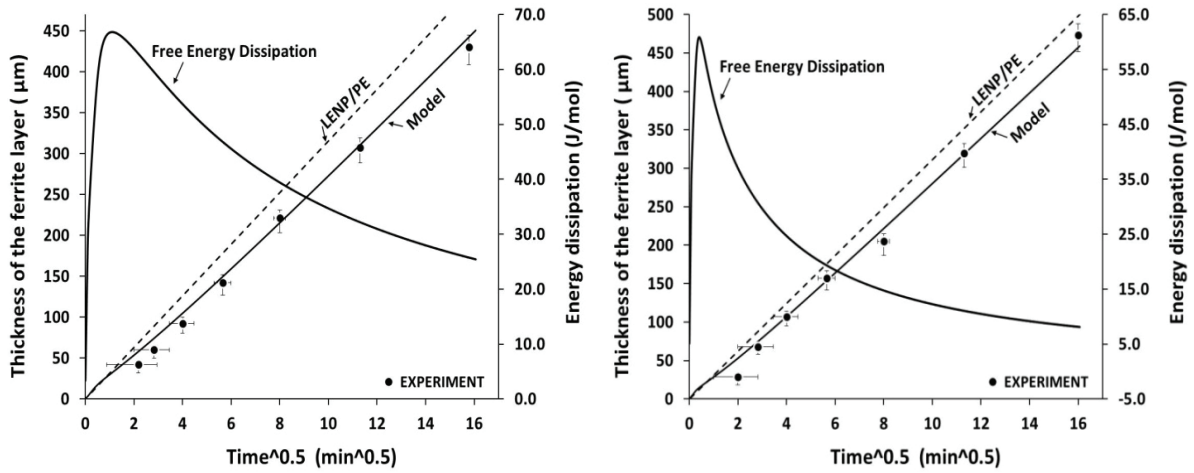
The Fe-Mo-C system offers an excellent opportunity to test models that include the effects of energy dissipation due to cross-interface diffusion. The reason is that compositions and temperatures can be chosen where the chemical potentials of Mo in the ferrite and austenite of bulk composition are the same. As a result, there is no spike and the consequential changes in contact conditions can be ignored *i.e.* the dominate interaction is that of Mo with the potential well at the interface.

In order to test the model, kinetics of ferrite growth under decarburization conditions in Fe-0.51%Mo-0.54%C alloy [16] was examined. The cross-interface diffusion coefficients, D_1 , D_2 and D_3 were assumed to be equal to the ferrite, geometric average and austenite diffusion coefficients, respectively. An interaction coefficient of Fe and Mo in the interface was varied such that the initial chemical potential of Mo in the interface is 15 kJ/mole lower than the average initial chemical potentials of ferrite and austenite.

The results of the calculations are compared with experimental measurements in Figure 2-11 for temperatures of 775 °C, 806 °C and 825 °C. The agreement is excellent in all cases. It is particularly interesting to point out that the experimental kinetics appeared to be parabolic, which suggests that the interfacial conditions were not changing.

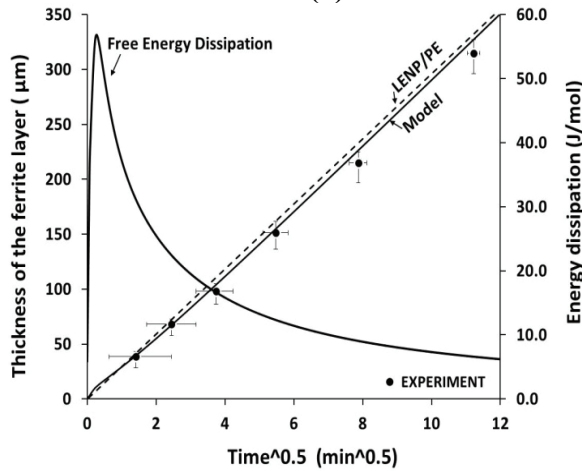
As mentioned in previous chapter, in the past [16], this type of behaviour has led researchers to conclude that the energy dissipation was constant, which is inconsistent with solute drag theories where a velocity-dependent drag is expected. However, as

shown in Figure 2-11, calculations using the new model suggest that the dissipation is decreasing only slowly with time and this gives kinetics that are close to parabolic over the times investigated here.



(a)

(b)



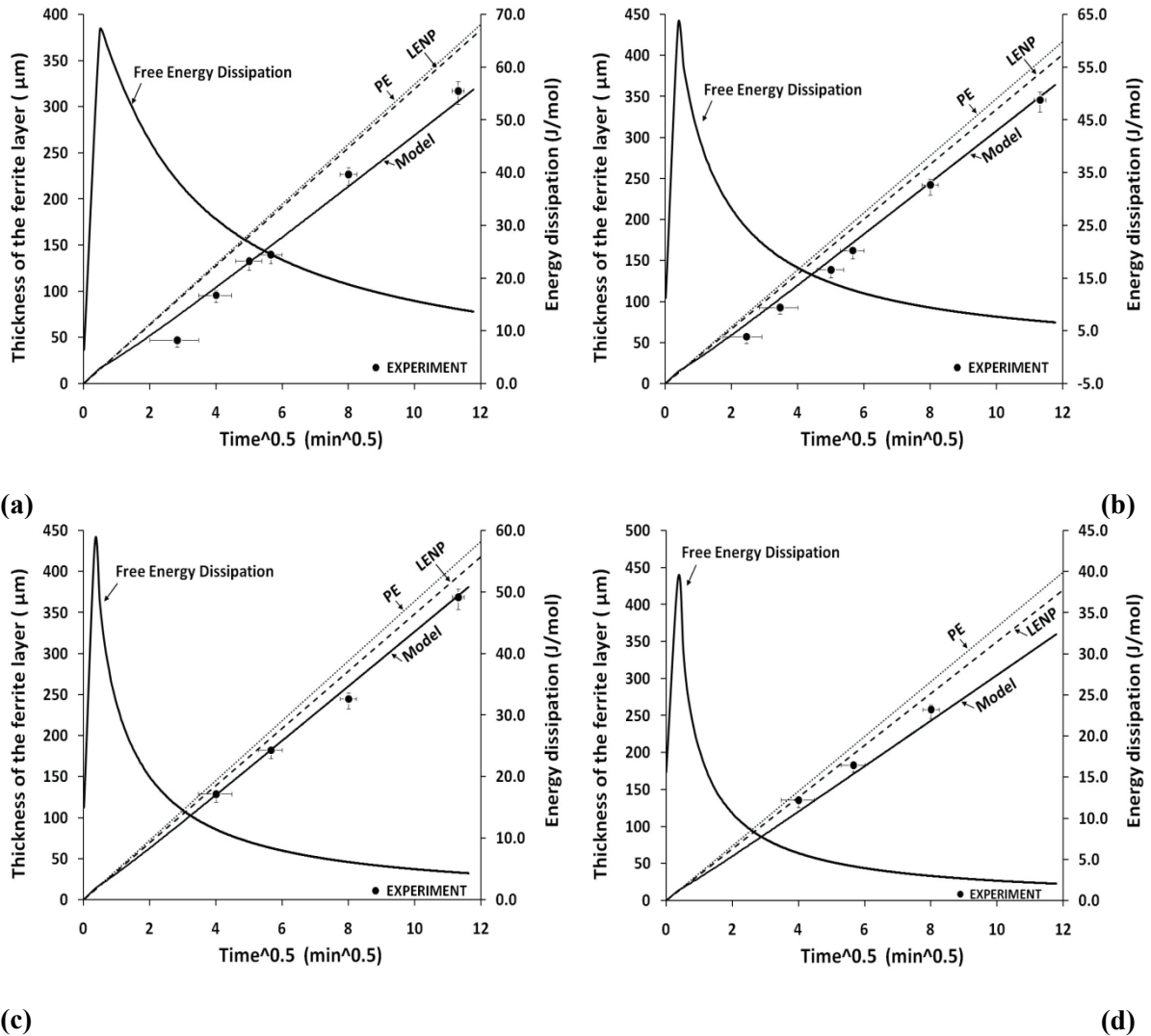
(c)

Figure 2-11. Kinetics of decarburization and evolution of free energy dissipation in Fe-0.51%Mo-0.54%Co alloy at a) 775 °C b) 806 °C and c) 825 °C.

2.3.3 General cases (*Fe-Si-C, Fe-Cr-C and Fe-Cu-C*)

Other alloying systems usually lie between the two extremes discussed above. In these systems, the total free energy dissipation may arise from both solute interactions with the

boundary (due to the existing potential well at the boundary) and diffusion across the boundary driven by solute partitioning tendencies between the bulk phases.



(a) **(b)** **(c)** **(d)**
Figure 2-12: Experimental ferrite layer growth kinetics measurements from Fe-0.88 Si-0.58C alloy examined by Zurob et.al [18]: a) 775 °C, b) 806 °C, c) 825 °C d) 850 °C . Comparisons with the PE, LENP and the developed model are shown in each case as well as the free energy dissipation during reaction.

Depending on the temperature dependence of the partitioning behaviour of the solute it is conceivable that situations may exist where the overall solute drag effect even increases with increasing temperature, *i.e.* the opposite dependency that would be predicted by extrapolating from grain boundaries.

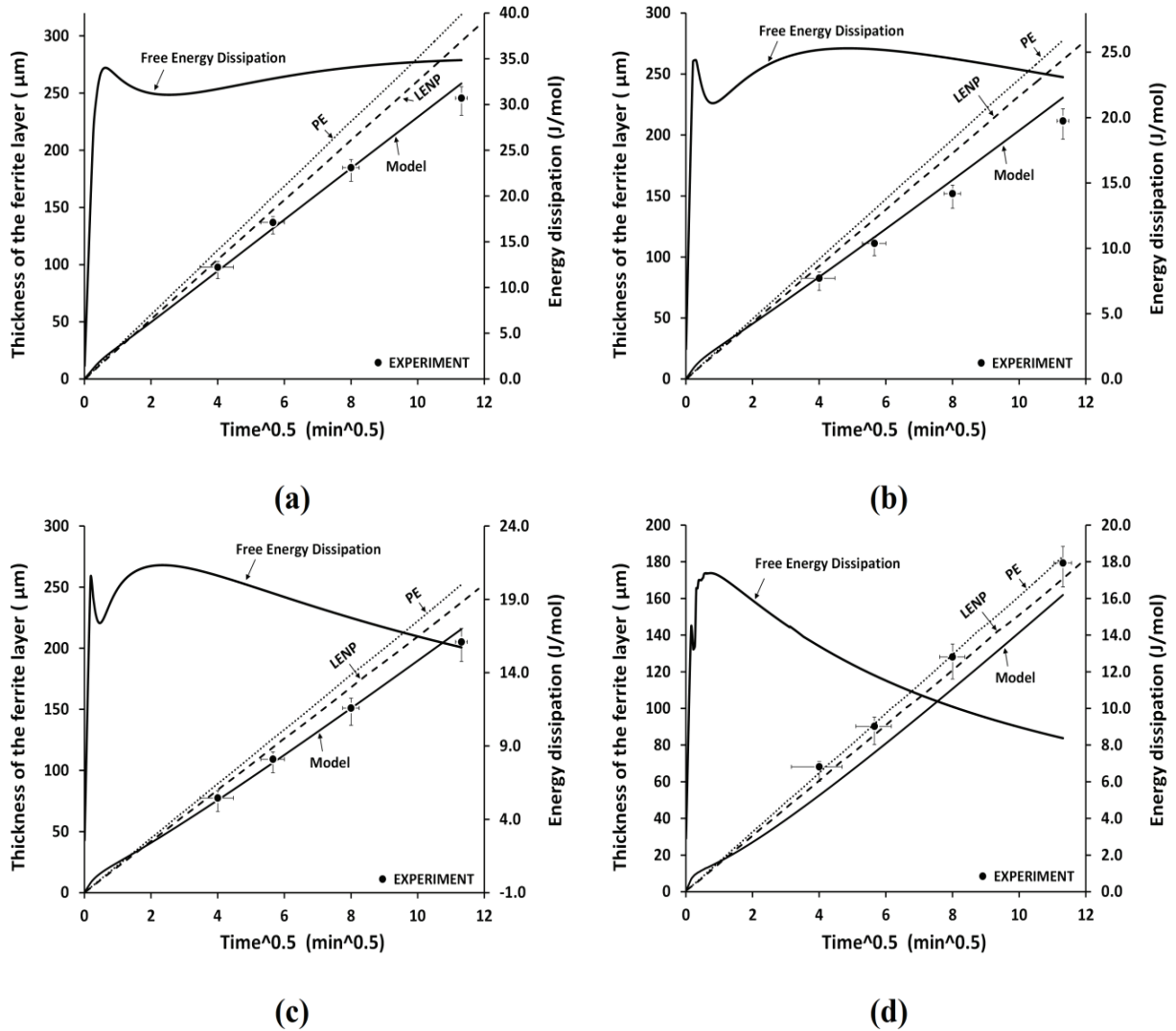


Figure 2-13: Experimental ferrite layer growth kinetics measurements from Fe-2.00Cr-0.58C alloy examined by Beche *et.al* [23] : a) 775 °C, b) 806 °C, c) 825 °C, d) 850 °C. Comparisons with the PE, LENP and the developed model are shown in each case as well as the free energy dissipation during reaction.

In line with such investigations, taking advantage of the available experimental results already reported by Zurob *et.al.*, the kinetics of decarburization in Fe-Si-C [18], Fe-Cr-C [23] and Fe-Cu-C [75] systems were examined.

In these systems, Si, for example, is a ferrite stabilizer and hence during growth there will be a positive driving force for partitioning of Si from the austenite to the ferrite.

Moreover, interaction of Si with the potential well at the interface may be a non-negligible contribution to the total energy dissipated during transformation which should be considered.

Copper (Cu), on the other hand, is an austenite stabilizer and hence there will be a positive driving force for partitioning of Cu from ferrite to the austenite during growth.

In order to run the model, similar to the previous cases, the thermodynamic description of the interface was based on that of the FCC phase with reference states of the end components shifted to simulate an interfacial energy of 0.5 J/m² and the interaction parameter between the solute element (*i.e.* Si, Cr and Cu) and Fe in the interface was varied to produce initial chemical potentials of 9 kJ/mol, 1.5 kJ/mol and 1.15 kJ/mol lower than the average of the initial chemical potentials of Si, Cr and Cu in bulk phases, respectively.

Results of the calculations are compared with experimental measurements at different temperatures in Figure 2-12, Figure 2-13 and Figure 2-14. As seen, in the case of Si and Cr generally there is an excellent agreement between the calculations and the experimental data points (except in the case of the Cr alloy at 850 °C, the experimental kinetic is a little faster than the model predictions). However, it should be pointed that this satisfying match was obtained assuming the diffusivity of Cr and Si within the interface to be equal to the ferrite diffusivity (instead of the geometric average which is usually used).

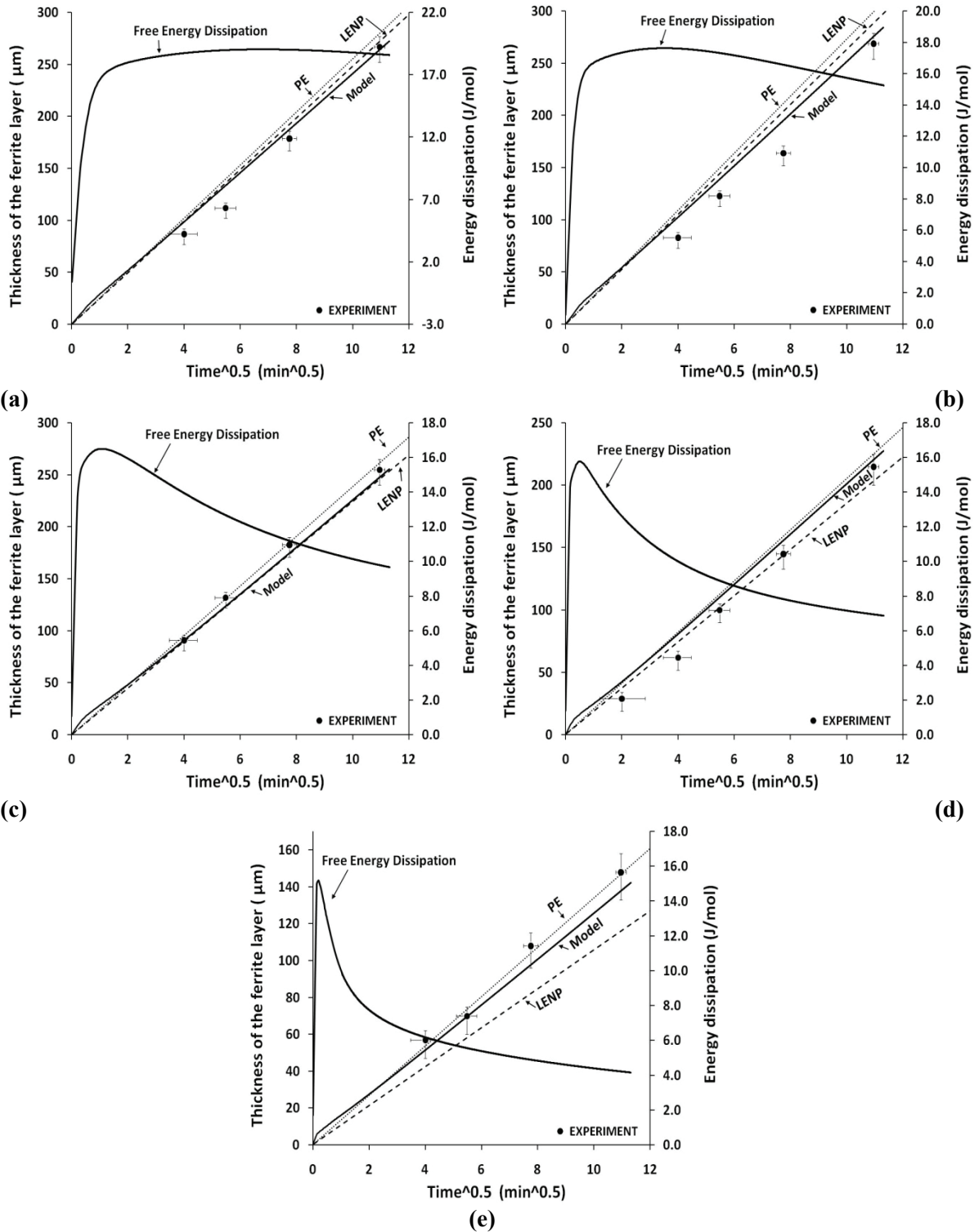


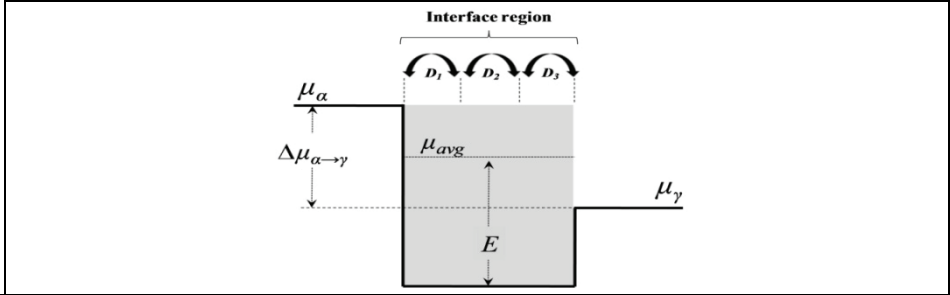
Figure 2-14: Experimental ferrite layer growth kinetics measurements from Fe-0.97 Cu-0.56C alloy [75]: a) 755 °C, b) 775 °C, c) 806 °C d) 830 °C e) 855 °C. Comparisons with the PE, LENP and the developed model are shown in each case as well as the free energy dissipation during reaction.

In the Fe-Cu-C alloy, there also is an acceptable agreement between the modelling predictions and the experimental observations. Here, it should be mentioned that the small deviation seen at each temperature can be adjusted by applying minor changes in the value of the segregation energies used for the calculations.

A summary of the all parameters used for the calculations in different systems, mentioned above, is presented in Table 2-2. Moreover, for the sake of clarity, activity coefficients of different alloying elements, which is directly related to the interaction tendency (through their interaction parameter) of elements with Fe atoms in bulk ferrite and bulk austenite (extracted from TCFE6 thermodynamic database), are also presented in Table 2-3. In general, this parameter can be used as characteristic of solubility and chemical interaction between like and unlike atoms. A negative $\varepsilon_{(X-X)}$ value is an indication for clustering tendency of X atoms in the Fe matrix *i.e.* deviation from a random distribution of the number of contacts between X and Fe atoms. These distribution tendencies may affect the amount of alloying element segregation to the migrating interfaces during phase transformation.

In the case of Mo and Cr, big negative values of $\varepsilon_{(X-C)}$ are indications of high desire of these atoms for carbide formation. Moreover, approximately close values of $\varepsilon_{(X-X)}$ shows that the main difference in the bonding energies of Mo and Cr within the interface region is, in fact, due to their atomic size differences. As another example, analysing $\varepsilon_{(X-C)}$ values shows that Si has a strong tendency for distribution among Fe atoms in both ferrite and austenite while Cu atoms attract each other and have a rather strong tendency for clustering.

Table 2-2: Summary of the parameters used for modelling of the interface migration in different systems



	T (°C)	μ_α (KJ/mol)	μ_γ (KJ/mol)	μ_{avg} (KJ/mol)	$\Delta\mu_{\alpha\rightarrow\gamma}$ (KJ/mol)	E (KJ/mol)	D_1 (m ² /s)	D_2 (m ² /s)	D_3 (m ² /s)
2.66Ni-0.196C	700	-68.0	-74.9	-71.5	- 7.0	+1.5	1.1e-17	3.9e-19	1.4e-20
	710	-69.1	-76.1	-72.6	- 7.0	+1.5	1.6e-17	5.6e-19	2.0e-20
	720	-70.2	-77.2	-73.7	- 7.0	+1.5	2.4e-17	8.3e-19	2.9e-20
2.42Ni-0.293C	700	-68.7	-75.6	-72.2	- 7.0	+1.5	1.1e-17	3.9e-19	1.4e-20
	710	-69.9	-76.8	-73.3	- 7.0	+1.5	1.6e-17	5.6e-19	2.0e-20
	720	-70.1	-77.9	-74.4	- 7.0	+1.5	2.4e-17	8.3e-19	2.9e-20
1.46Ni-0.74C	735	-76.9	-83.3	-80.1	- 6.5	+1.5	4.5e-17	1.3e-18	4.0e-20
	755	-79.2	-85.6	-82.4	- 6.4	+1.5	1.1e-16	2.7e-18	9.5e-20
	775	-81.5	-87.9	-84.7	- 6.3	+1.5	2.2e-16	6.3e-18	1.8e-19
2.08Mn-0.095C	670	-67.0	-78.6	-72.8	- 11.5	-2.5	2.8e-18	3.2e-19	3.6e-20
	700	-71.0	-81.1	-76.0	- 10.1	-2.5	2.1e-17	1.8e-18	1.5e-19
	710	-72.3	-82.0	-77.2	- 9.6	-2.5	4.2e-17	3.1e18	2.3e-19
	720	-73.7	-82.9	-78.3	- 9.2	-2.5	6.2e-17	4.4e-18	3.1e-19
2.17Mn-0.21C	730	-75.1	-83.8	-79.5	-8.7	-2.5	7.0e-17	5.2e-18	3.8e-19
	670	-66.8	-78.2	-72.5	- 11.5	-2.5	2.8e-18	3.2e-19	3.6e-20
0.94Mn-0.57C	700	-70.7	-80.7	-75.7	- 10.0	-2.5	2.1e-17	1.8e-18	1.5e-19
	755	-84.8	-93.4	-89.1	- 8.6	-2.5	1.5e-16	1.0-17	7.2e-19
	775	-87.5	-95.4	-91.5	- 7.8	-2.5	3.9e-16	2.4e-17	1.5e-18
	806	-91.7	-98.6	-95.1	- 6.9	-2.5	8.4e-16	5.1e-17	3.0e-18
0.51Mo-0.54C	825	-94.2	-100.6	-97.4	- 6.4	-2.5	1.7e-15	9.9e-17	5.8e-18
	775	-74.0	-71.9	-73.0	+ 2.2	-15.0	3.5e-16	3.7e-17	4.0e-18
	806	-78.0	-75.1	-76.5	+ 2.8	-15.0	7.3e-16	7.5e-18	7.6e-18
0.88Si-0.58C	825	-80.4	-77.2	-78.8	+ 3.2	-15.0	1.4e-15	1.4e-16	1.4e-17
	775	-174.7	-169.7	-172.2	+ 5.0	-9.0	3.9e-16	5.3e-17	7.2e-18
	806	-176.8	-172.4	-174.6	+ 4.4	-9.0	1.2e-15	1.4e-16	1.6e-17
	825	-178.1	-174.0	-176.0	+ 4.1	-9.0	2.0e-15	2.2e-16	2.5e-17
2.00Cr-0.58C	850	-179.8	-176.0	-177.9	+ 3.8	-9.0	4.3e-15	4.4e-16	4.5e-17
	775	-62.3	-65.6	-64.0	- 3.3	-1.5	1.5e-16	1.1e-17	8.5e-19
	806	-65.5	-68.0	-66.7	- 2.4	-1.5	4.4e-16	3.2e-17	2.2e-18
	825	-67.4	-69.4	-68.4	- 2.0	-1.5	8.0e-16	5.5e-17	3.8e-18
0.94Cu-0.56C	850	-70.0	-71.5	-70.8	- 1.5	-1.5	1.6e-15	1.1e-16	7.7e-18
	775	-48.5	-50.5	-49.5	- 2.0	-1.15	6.5e-17	3.1e-18	1.5e-19
	775	-51.1	-53.0	-52.0	- 1.9	-1.15	1.7e-16	6.7e-18	2.7e-19
	806	-55.0	-56.8	-55.9	- 1.9	-1.15	4.5e-16	1.8e-17	7.4e-19
	830	-58.0	-59.8	-58.9	- 1.8	-1.15	9.0e-16	3.6e-17	1.5e-18
	855	-61.0	-62.8	-61.9	- 1.8	-1.15	1.7e-15	7.4e-17	3.2e-18

Table 2-3: Activity coefficient of the investigated element in austenite and ferrite matrix of Fe-X-C alloys at different temperatures

	$T (^{\circ}C)$	Austenite		Ferrite	
		$\epsilon_{(X-X)}$	$\epsilon_{(X-C)}$	$\epsilon_{(X-X)}$	$\epsilon_{(X-C)}$
Fe-Ni-C	700	-1.92	4.81	-0.042	7.66
	710	-1.87	4.77	-0.045	7.59
	720	-1.83	4.74	-0.053	7.51
	735	-1.77	4.68	-0.062	7.46
	755	-1.68	4.61	-0.082	7.35
	775	-1.61	4.55	0.12	7.25
Fe-Mn-C	670	1.25	-5.17	-4.83	-7.06
	700	1.18	-4.98	-5.35	-6.68
	755	1.07	-4.67	-6.67	-6.03
	775	1.03	-4.56	-4.85	-5.82
	806	0.97	-4.40	-3.73	-5.50
	825	0.94	-4.31	-3.23	-5.31
Fe-Mo-C	775	-2.25	-11.91	-0.486	-21.84
	806	-2.06	-11.48	-0.47	-20.38
	825	-1.95	-11.23	-0.44	-19.52
Fe-Si-C	775	13.94	10.18	16.52	6.58
	806	13.25	9.89	15.71	6.26
	825	12.85	9.73	15.23	6.07
	850	12.35	9.51	14.62	5.83
Fe-Cr-C	775	0.28	-12.39	-2.64	-20.88
	806	0.33	-11.94	-2.46	-19.59
	825	0.35	-11.68	-2.35	-18.83
	850	0.38	-11.34	-2.23	-17.88
Fe-Cu-C	755	-6.81	8.08	-11.73	0.37
	775	-6.71	7.93	-10.66	0.45
	806	-6.57	7.72	-9.82	0.55
	830	-6.44	7.53	-9.32	0.63
	855	-6.36	7.41	-8.88	0.71

It is also interesting to pay attention to the $\epsilon_{(Mn-Mn)}$ in bulk ferrite. As seen, in contrast to other elements, in which $\epsilon_{(X-X)}$ either decreases or increases as a function of temperature, in this case the clustering tendency of Mn atoms first increases up to around 775 °C and then changes its trend and starts decreasing by increasing temperature.

2.3.4 *Temperature-Jump experiments:*

In addition to the classical precipitation and decarburizing experiment mentioned above, changing temperature during decarburization process provides new opportunities for further investigations.

For example, due to grain boundary ferrite precipitation at low temperatures (*e.g.* 600 °C), investigation of the solute drag effect in Fe-Mo-C systems by decarburization is not straightforward. In these cases, the decarburizing process can be initiated at higher temperatures (*e.g.* 850 °C) to form a ferrite layer at the surface. Then, taking advantage of the incubation time for ferrite precipitation around the bay formation region of TTT diagram, samples can be quickly transferred to the low temperature and continue the decarburization process (*i.e.* growth of the ferrite layer) at that temperature region.

This type of temperature change is usually followed by some important events which should not be overlooked in analysing the experimental observations. For example, immediately after the temperature change, system undergoes a transient situation at the interface which may have a big effect on the kinetics of the phase transformation. Based on equilibrium thermodynamics, imposing a big temperature change requires a big change in concentration of alloying elements (*i.e.* Carbon) at the interface. As a result, considering diffusion rate of different alloying elements, one may want to know whether the system is capable of pumping the required amount of atoms to or away from the interface in a very

short time to satisfy the equilibrium condition or not? or how fast can the system reach to the steady state conditions and *etc.*

So, in general, this technique can be employed as a useful method for better understanding of evolution of the interfacial compositions and behaviour of the alloying systems during austenite to ferrite transformation.

In the present study, as the first step in line with such experiments, a binary Fe-C system was imposed to a sudden change in decarburizing temperature to analyse carbon behaviour immediately after this jump.

After that, a similar test was performed on a Fe-Mo-C alloy which, in fact, offered an excellent opportunity to test possible effects of the free energy dissipation on interface migration during such a sudden temperature variation. These experiments are explained in detailed bellow.

2.3.4.1 *Temperature jump in Binary system (Fe-C)*

A binary alloy of composition Fe-0.57C (mass %) was arc melted from high purity stocks of Fe and C. In order to break down the as-cast structure, the alloy was cold-rolled to a reduction of 50%, sealed under high vacuum and annealed for 72 hrs at 1100 °C. Small samples of approximate dimensions of 3x4x8 mm³ were then sectioned from the alloy. The surfaces of the samples were then polished using SiC paper down to a 4000 grit.

The decarburization treatment involved spot welding the samples to a holder which was then inserted through an O-ring seal into the tube-furnace, under a flow on a non-decarburizing gas (argon or dry-hydrogen). A heating time of 5 minutes, allowed the samples to austenitize and to reach to the desired decarburization temperature. Water-saturated hydrogen (at room temperature) was then used to decarburize the samples for the desired period of time. Decarburization treatments were initiated in the first tube furnace at 850 °C for 20 minutes and then, continuing purging wet-H₂, sample was pushed through the work tube into the second furnace at 750 °C. Samples were hold at the second temperature for different times ranging from 2 to 70 minutes. A schematic of the decarburizing setup is presented in Figure 2-15 .

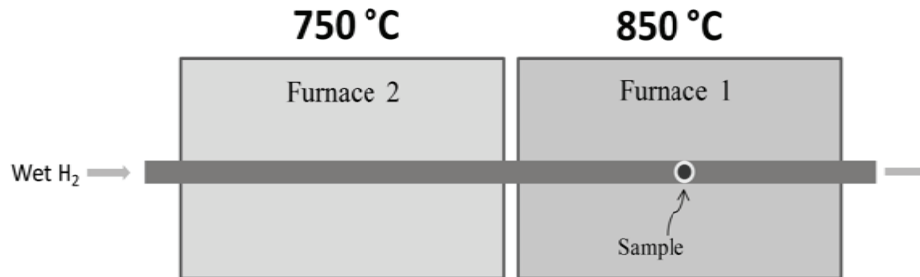


Figure 2-15: Decarburizing setup for temperature-jump experiments in Fe-C system

The decarburization experiment was terminated by stopping the flow of wet-hydrogen, purging the work-tube with Ar for 2 to 3 minutes and finally quenching the samples in water. Blank samples, with no flow of wet-hydrogen, were used to verify that the austenitizing and purging steps resulted in no ferrite formation. Overall, the temperature was controlled to within less than ± 2 °C and quenching times were generally less than 5 seconds.

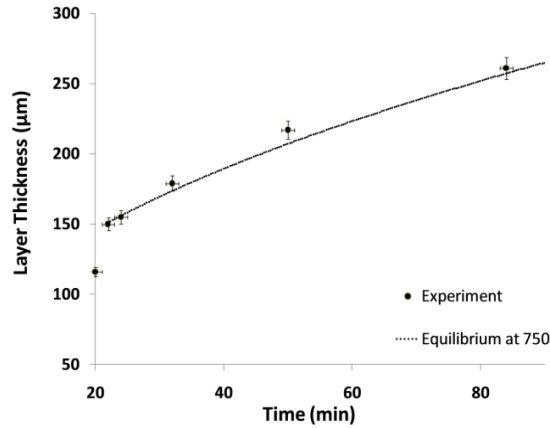
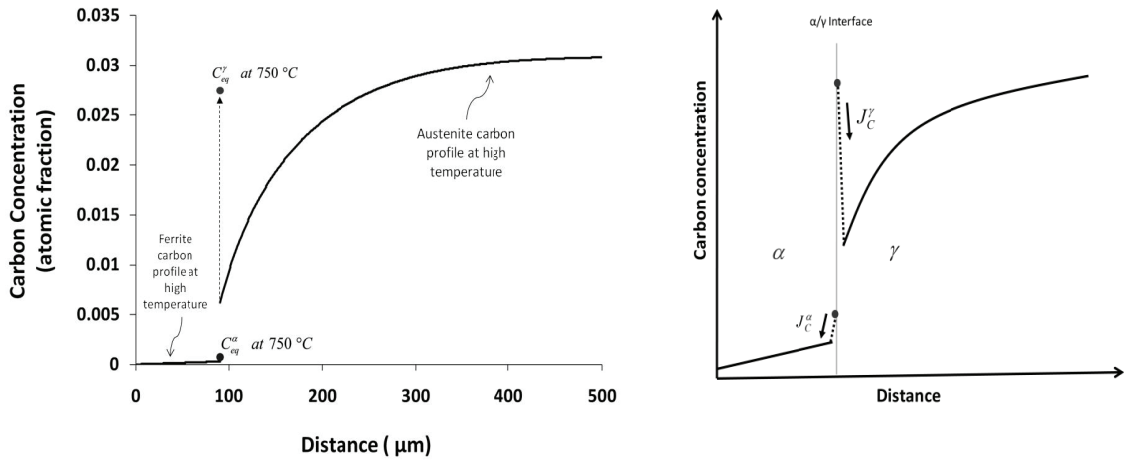


Figure 2-16: Temperature-jump data in Fe-C system. Samples were decarburized for 20 minutes at 850 °C and then were moved to 750 °C. The predicted kinetics assuming full equilibrium at 750 °C is shown by the dotted line.

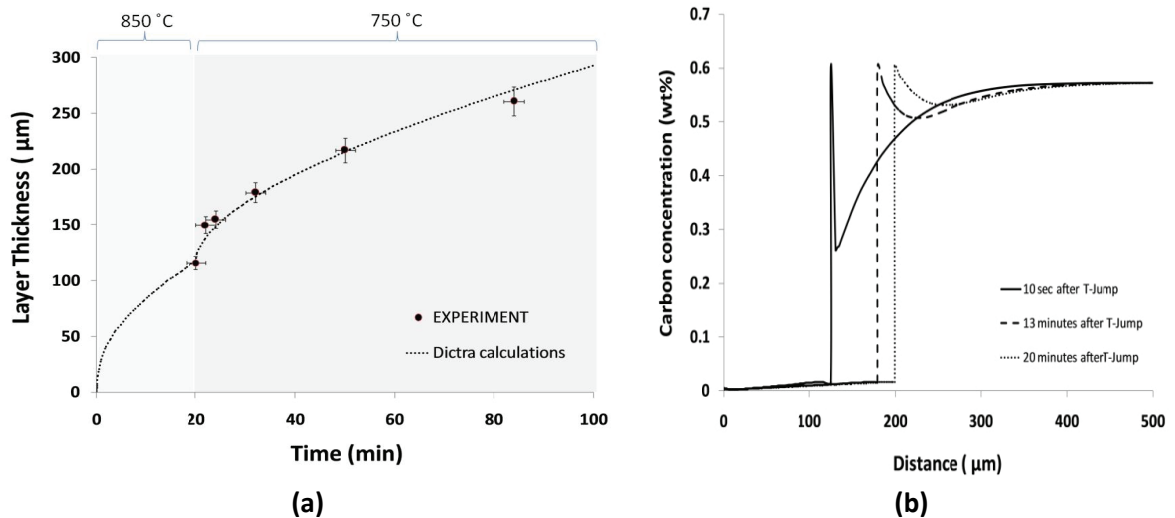
In Figure 2-16 the obtained experimental data is compared with the predicted kinetics assuming equilibrium carbon profiles at 750 °C (as if there has been no temperature change). It is clearly seen that the sudden temperature change has introduced a fast forward motion which cannot be explained by assuming equilibrium carbon profile immediately after changing temperature from 850 °C to 750 °C. However, it seems that after a short period of time (3-4 minutes) the concentration profiles are relaxed and normal equilibrium is attained at the interface *i.e.* equilibrium profiles can be used for assessing the growth kinetics.

To explain the fast forward motion, it was assumed that immediately after the temperature jump, carbon concentrations at the austenite and ferrite interfaces reach to their equilibrium value (at the second temperature *i.e.* 750 °C in this case). However, carbon profiles in bulk austenite and bulk ferrite cannot adjust themselves immediately and as a result old profiles from the higher temperature (850 °C) will be inherited. This situation is schematically shown in Figure 2-17.



(a) (b)
 Figure 2-17: a) Interfacial carbon concentrations and carbon profiles immediately after temperature jump from 850 °C to 750 °C in Fe-0.65 C b) schematic of carbon fluxes in ferrite and austenite after changing the temperature

As seen in Figure 2-17b, such a sharp change in carbon concentration, results in a large carbon flux in both ferrite and austenite. However, this situation is eventually relaxed by time (due to diffusion of carbon in the bulk), but immediately after the temperature-jump and before reaching to the full equilibrium condition, one can expect a fast forward motion which decelerate by time. The calculated kinetics and the carbon profiles using DICTRA software are Figure 2-18 .



(a) (b)
 Figure 2-18: a) DICTRA predictions for T-Jump experiment in Fe-C system a) Layer thickness before and after temperature jump b) Carbon profiles in austenite and ferrite after temperature-jump

2.3.4.2 Ternary system (*Fe-C-Mo*)

a) Fast forward motion

Fe-0.27 wt% C- 4.72 wt% Mo is an ideal system for evaluating effect of the free energy dissipation on the transformation behavior after a sudden change in temperature. On one hand, as seen in Figure 2-19, extended ferrite region in this system makes it possible to start the decarburization process at very high temperatures approximately between 1100 °C to 1400 °C without any concern about carbide precipitation. On the other hand, it has been shown [76] that similar systems show a very deep bay in their TTT diagram at temperatures around 550-600 °C. It means that the decarburization process can be continued at this temperature region with no concern about allotrimorph ferrite precipitation at grain boundaries for around 24-25 hours.

So, an alloy was arc melted from high purity stocks of Fe, Mo and C. In order to break down the as-cast structure, the alloy was cold-rolled to a reduction of 50%, sealed under high vacuum and annealed for 72 hrs at 1100 °C. Small samples of approximate dimensions of 3x4x8 mm³ were then sectioned from the alloy. The surfaces of the samples were then polished using SiC paper down to a 4000 grit. Most samples were decarburized in the “as-polished” condition. In some cases, however, a thin layer of Fe (5 to 10 μm) was electroplated on the samples in order to avoid any preferential oxidation during the decarburization experiments.

The decarburization treatment involved the same steps as the binary Fe-C alloy except the decarburizing temperatures which were chosen to be 1178 °C for the first step (5 minutes) and 578 °C (around the bay temperature) for the second step (as shown in Figure 2-19).

Here it should be emphasized that, nucleation of the equilibrium phases in this alloy at around 578 °C happens very slowly (e.g. it takes more than 24 hours before appearance of any of these phases) and this provides us with enough time to conduct the decarburization process without any concern about precipitation of unwanted phases.

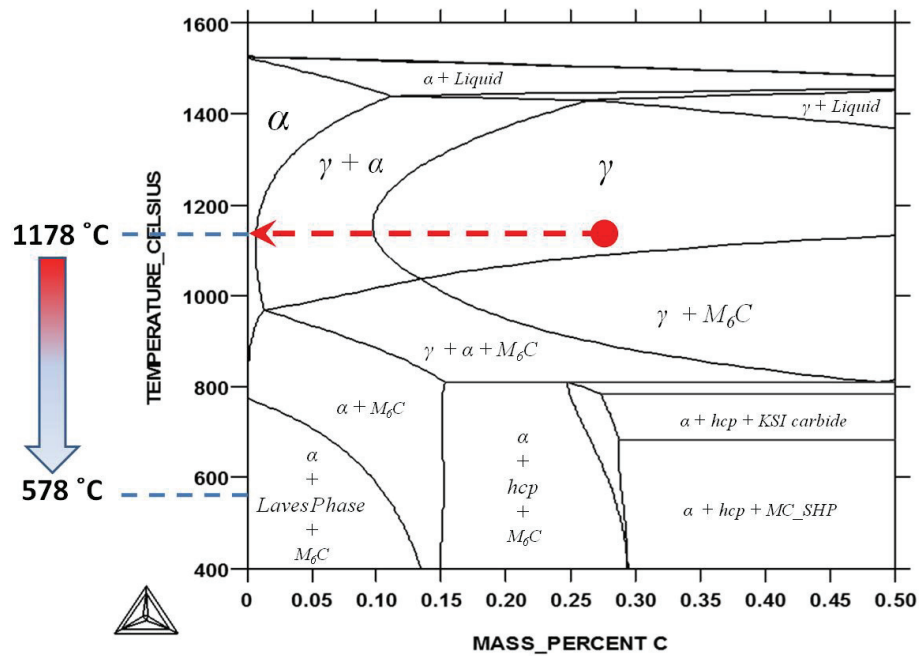


Figure 2-19: (Fe-4.72 Mo)-C binary phase diagram showing the temperatures at which decarburization was conducted

Similar to the binary case, the obtained results presented in Figure 2-20, system showed an acceleration in the interface velocity immediately after changing the temperature. It is believed that the main reason for the fast forward motion can be explained by the same argument used for the binary Fe-C alloy.

It is also seen that, similar to the binary case, the fast interface motion is followed by a very slow forward motion as if the interface is not moving. This part of the growth kinetics (*i.e.* very slow forward motion) can be explained by growth velocity calculations for isothermal decarburization at 600 °C (*i.e.* no temperature jump) without taking contribution of the free energy dissipation into calculations.

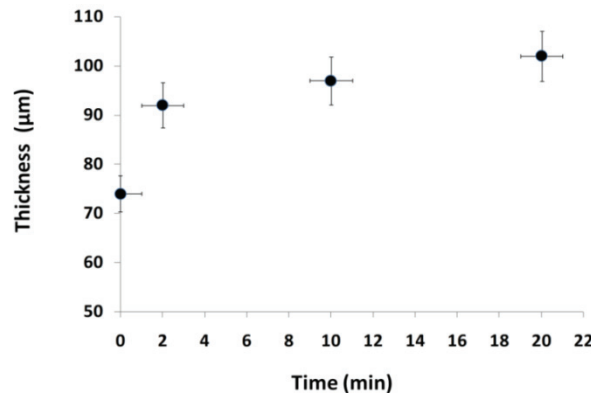


Figure 2-20: Experimental results for temperature jump from 1178 °C to 578 °C in Fe-0.27 C-4.72 Mo alloy

Nevertheless, it is still interesting to see the possible effect of the alloying element partitioning and free energy dissipation on the transformation kinetics.

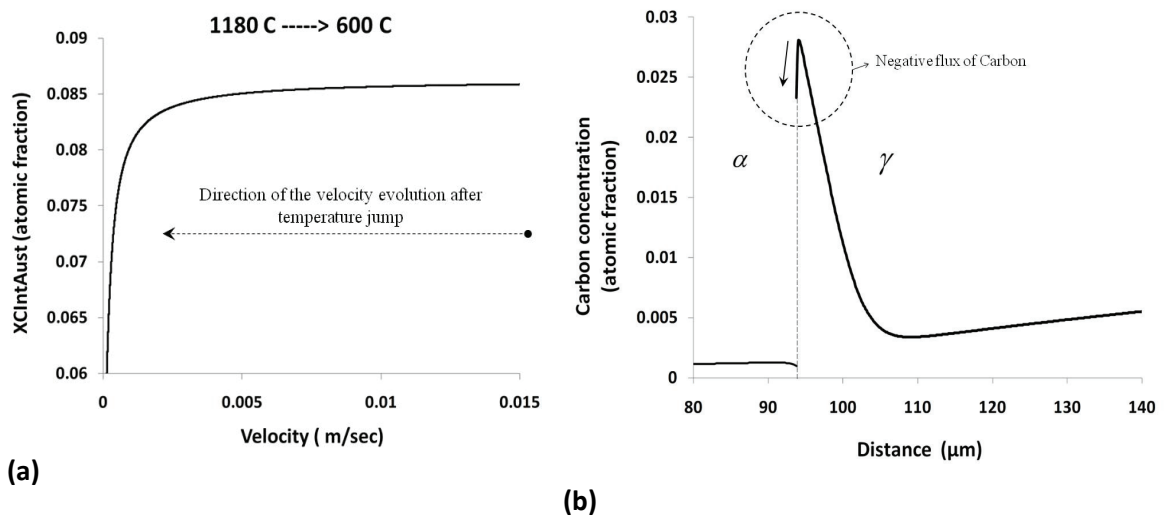


Figure 2-21: Modeling results for temperature-jump experiment in Fe-0.27C-4.72 Mo alloy. a) variation of carbon concentration at austenite interface ($X_{CIntAust}$), b) carbon profiles in ferrite and austenite after sudden change of carbon on the austenite side of the interface

Results of such calculations using the proposed model also showed that the fast forward motion (immediately after the temperature jump) is followed by stoppage of the interface. However, as presented in Figure 2-21, compare to the binary case, another mechanism is also in order at low velocities.

Based on these calculations, combination of fast partitioning of the Mo atoms (*i.e.* spike formation ahead of the interface or segregation of Mo atoms from austenite into the interface) and free energy dissipation, results in a fast change in carbon concentrations at the ferrite and austenite interfaces at low velocities. These changes create a negative net flux of carbon atoms at the interface (Figure 2-21b) which eventually leads to a negative velocity (stoppage of the interface).

b) Fast backward motion

Even though, the experimental observations can be more or less explained by the available models, it seems that there are still situations for which there are no clear answers.

In another attempt in line with further investigation for understanding interfacial boundary conditions, a similar set of temperature-jump experiments were performed on Fe-0.65 C-1.86 Mo alloy. Surprisingly, the obtained results showed that when the temperature is changed from 850 °C to 600 °C a fast forward motion is replaced by a fast backward motion amount of which seems to be a function of the thickness of the ferrite layer formed during the first step (*i.e.* thickness of the layer formed at 850 °C).

As seen in Figure 2-22, amount of backward motion in samples decarburized for 45 minutes and 5 minutes at 850 °C, has changed from $\approx 40 \mu\text{m}$ to $\approx 15 \mu\text{m}$, at 600 °C respectively. This indicates a possible relationship between the backward motion and thickness of the ferrite layer formed in the first step of decarburization.

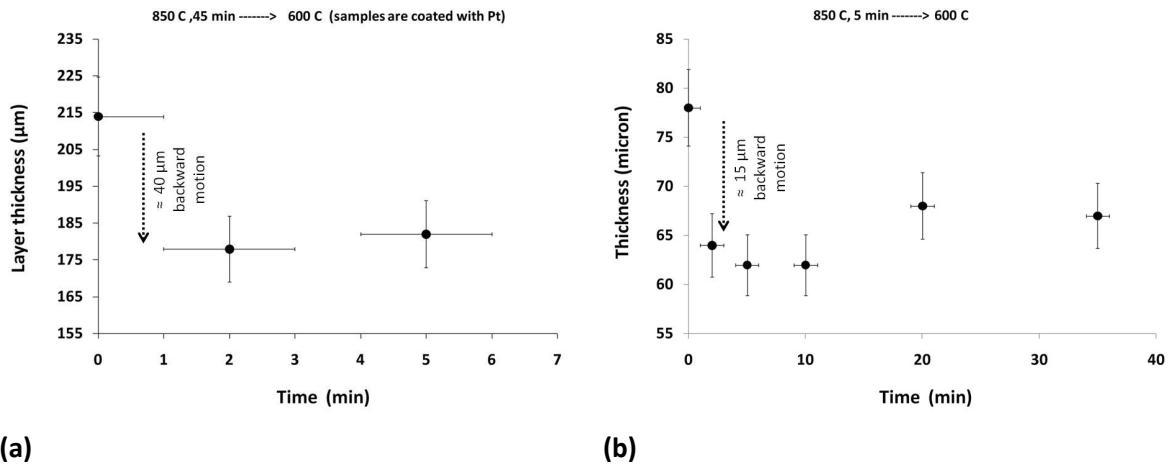


Figure 2-22: Experimental observation for temperature-jump from 850 °C to 600 °C in Fe-0.65C-1.85 Mo alloy. a) 45 minutes at 850 °C and jump to 600 °C, b) 5 minutes at 850 °C and then jump to 600 °C

Figure 2-23a presents a micrograph of this alloy (Fe-0.65 C-1.86 Mo) in which position of the interface immediately before and 2 minutes after temperature-jump are indicated. As seen, a series of ferrite islands are left behind the interface during this backward motion. At this point, there is no clear explanation for these observations. Answer to this question can probably shed more light on our understanding of interfacial processes during austenite to ferrite transformation.

Here, it is worth mentioning that according to the phase diagram of (Fe-1.86 Mo)-C, presented in Figure 2-23b, carbide precipitation may potentially be responsible for such a behaviour. In general, appearance of carbide particles in the structure can introduce some

sudden changes in the shape of the carbon profiles by changing the equilibrium interfacial carbon concentrations. As a hypothetical example, the ferrite interfacial carbon concentration may be quickly changed to its equilibrium value with the carbide particle (instead of being in equilibrium with austenite).

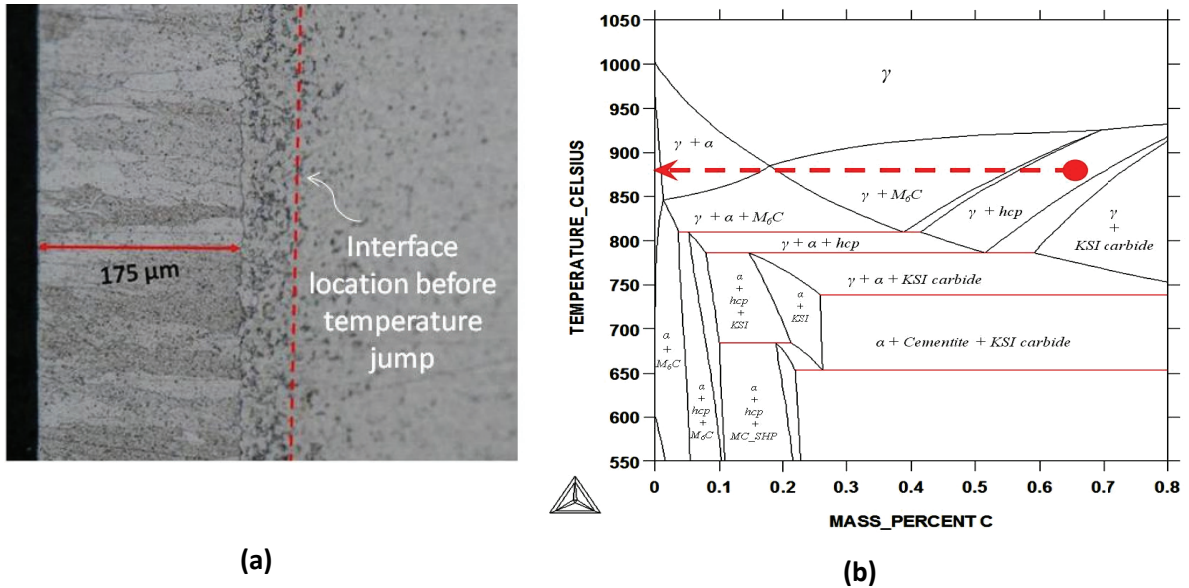


Figure 2-23: a) Interface location before and after temperature jump from 850 C to 600 C in Fe-0.65C-1.85 Mo alloy. It shows that some ferrite islands are left behind when the interface moves backward b) (Fe-1.86 Mo)-C phase diagram showing possibility of carbide formation during the T-jump experiment from 850 °C to 600 °C

So, these types of changes may potentially play an importance role in the backward motion of the interface. However, this hypothesis requires more in depth investigation in the future. For example, one can employ high resolution SEM or TEM extraction replica to see if there is any carbide formation occurring in the system or not.

3. DISCUSSION

3.1 Key Features of the Model:

A model for planar ferrite growth in Fe-C-X systems was presented in Section 2. The model self-consistently incorporates alloying element diffusion across the interface and the dissipation associated with it, the evolution of the corresponding carbon concentrations at the interface, the carbon diffusion in the bulk phases and the ferrite growth rate. The model may be viewed as a hybrid of the earlier approaches presented by Odqvist *et al.* [33, 34] and Hutchinson *et al.* [6]. The model considers a discrete jump approach at the interface in the spirit of the models of Hutchinson *et al.* [6] and Lucke and Stuwe [45] and it incorporates dissipation using the approach of Odqvist *et al.* [33, 34]. The model differs from the earlier approach presented by Hutchinson *et al.* [6] in two important ways; the first is that dissipation due to solute diffusion in the interface is taken into account and the second is that convection is described in terms of Eq. (2.1) as opposed to the probability term used earlier [6]. The key differences in comparison to the model of Odqvist *et al.* are the discrete nature of the jumps, the smaller cross-boundary diffusion coefficients, the finite grain size and the consideration of the driving force and dissipation over the interface only. Table 3-1, provides a summary of the parameters used in the present model compared to earlier ones for the case of precipitation in Fe-Ni-C at 700 °C. While the predictions of the present model are similar to those of Hutchinson *et al.* for the case of the Fe-Ni-C system, a key difference is the size of the Ni spike in austenite. In the

treatment of Hutchinson *et al.* the temporary cessation of ferrite growth for some alloys lying within the no-partitioning envelope (*e.g.* alloy containing 2.76 wt% Ni) was due to the rapid kinetics of Ni spike development and the subsequent lowering of the carbon contact condition in the austenite below that in front of the interface.

Table 3-1: summary of the parameters used in the present model compared to earlier models by Odqvist *et al.* [33, 34] and Hutchinson *et al.* [6] for the case of precipitation in Fe-Ni-C at 973 K (700 °C)

	Hutchinson <i>et al.</i> [6]	Odqvist <i>et al.</i> [33, 34]	Present Model
Driving Force	Across the interface	For the whole system	Across the interface
Dissipation	Not included	For the whole system	For the interface only
Diffusion coefficients within interface	$\text{Sqrt}(D_{\alpha} \times D_{\gamma})$	7.4E-13 m ² /s	Three jumps with coefficients of: D_{α} , $\text{Sqrt}(D_{\alpha} \times D_{\gamma})$ and D_{γ}
Diffusion Model within interface	* Discrete * transient	* Continuum * Steady-state	* Discrete * Steady-state
Interface Thermodynamics	N/A	*Liquid mixing model, with FCC interaction parameters $dL \sim 2.5RT$	* Modified description of FCC. * $dL \sim -2\text{kJ/mole}$

In the present model, both dissipation and spike build up contribute to the drop of the carbon concentration at the austenite side of the interface which leads to the cessation of ferrite growth. As a result, a much smaller spike is predicted prior to the cessation of ferrite growth in the present model compared to that of Hutchinson *et al.* [6]. This point is

illustrated in Figure 2-6a, which shows an example in which the cessation of ferrite growth occurred without an appreciable buildup of the Ni spike in austenite. The dominant contributor to the stoppage of ferrite growth in this case is energy dissipation (solute drag). Interestingly, similar calculations for an alloy with 2.08%Mn-0.095%C at the same temperature, Figure 2-6b, suggest an important role of spike build up. It can be seen in Figure 2-6b that energy dissipation has already peaked prior to the cessation of ferrite growth which suggests that the change of carbon concentration due to dissipation is not responsible for the stoppage. On the other hand, the height of the spike continued to build up and in this case, it led to the arrest of ferrite growth. The difference between the two alloys is probably due to the fact that the diffusion coefficient of Mn is nearly 40 times that of Ni which aids the development of the spike in the Mn alloy. An important consequence of this comparison is that the relative contributions of spike build up and energy dissipation to the cessation of ferrite growth is very sensitive to the choice of diffusivities. The general trend, however, is that the combined effect of these two processes result the arrest of ferrite growth.

The predictions of the present model also differ from those of Odqvist *et al.*, because of the differences in binding energies and diffusivities used. In addition, the Odqvist model was applied to precipitation in semi-infinite specimens compared to the application to finite spherical specimens in this work. This is an important difference critical in explaining the effect of grain-size on transformation kinetics and is described in section 3.3.

3.2 Critical Assessment of the Model:

The cross-interface diffusivities have been set to values determined directly from the known diffusivities in the bulk phases and are hence not adjustable parameters. The only parameter that is adjusted is the binding energy of the solute to the interface and this has been chosen on the basis of segregation data to grain boundaries. This model has been tested on six different systems: Fe-Ni-C and Fe-Mn-C, which are examples where the interaction between the alloying element and the interface is thought to be weak, but there exists a significant chemical potential difference for the substitutional element between the ferrite and austenite of bulk compositions, Fe-Mo-C, where the interaction with the interface is large, but the chemical potential difference across the interface is negligible, and finally on Fe-Cr-C, Fe-Si-C and Fe-Cu-C alloys in which both the interaction with the interface and the chemical potential differences across the interface might be important.

These systems allow a rigorous test of two origins of energy dissipation at the interface that occur in such systems - energy dissipation due to the cross-interface diffusion necessary for spike accumulation and energy dissipation due to diffusion in the interface alone where there is a strong interaction with the interface.

Two sets of experimental data were chosen for model validation – ferrite precipitation data, and ferrite growth data under decarburization conditions. These choices of data for comparison are not only significant in the fact that they provide a wealth of data under

different diffusion geometries, temperatures and alloy compositions, but also because the interface velocity ranges that are sampled in typical decarburization experiments are at least an order of magnitude slower than those in precipitation experiments. Since the dissipation due to diffusion in the interface is velocity dependent, this aspect of the data adds strength to the comparison between model and experiment. For both alloy systems and for both sets of experimental data, very good agreement between experiment and model was achieved. This indicates that the essential features of the model are probably correct.

A key test of the model was the correct prediction of the arrest of ferrite growth as a function of temperature and composition during precipitation in Fe-Ni-C and Fe-Mn-C alloys. The binding energy and cross-interface diffusivities which captured ferrite precipitation in Fe-Mn-C also provided an excellent fit of the decarburization kinetics of the Fe-Mn-C system. In particular, the model captured the close-to-parabolic ferrite growth kinetics under decarburization conditions. Interestingly, the experimental kinetics are occasionally very close to the predictions of the LE-NP model (e.g. [38] and [54]). These observations should be interpreted with care as illustrated in Figure 2-8 and Figure 2-9, which show the decarburization kinetics along with the parameter:

$$P_{Spike} = \frac{X_{Interface} - X_{PE}}{X_{LENP} - X_{PE}} \quad (3.1)$$

where $X_{Interface}$ is the instantaneous Mn concentration at the austenite interface predicted by the model and X_{PE} and X_{LENP} are the Mn concentration sat the austenite interface under PE and LENP conditions, respectively. This parameter (P_{Spike}) varies from 0 in the case of PE to 1 in the case of LENP. It can be seen than in the case of decarburization at 825 °C, the parameter is close to 1, meaning that the full LENP spike has developed and that the observed kinetics are indeed LENP kinetics. In contrast, at 755 °C, only a partial spike has developed. While the experimental data is close to the LENP predictions at 755 °C, the present model suggests that, in fact there is only a partial spike and the kinetics is due to the effect of dissipation on the interfacial conditions, *i.e.* LENP kinetics may be observed because there is a real spike of a magnitude close to that of the LENP model, or because the free energy dissipated due to alloying element diffusion across the interface gives rise to kinetics that look like LENP. Of course, the spectrum of combinations of spike and energy dissipation will also exist.

A second important comment needs to be made concerning the Fe-Mn-C system. In earlier works [38, 54], PE kinetics were reported at high temperatures in this system and the concept of a reduced capacity of the moving interface for Mn was introduced to fit the results. Unfortunately, it is difficult to assess the above observations in the absence of a reliable thermodynamic description of the Fe-Mn-C system at the above temperatures. The presence of PE at high temperature was based on calculations of the LENP and PE limits using the TCFE2 database. The modified thermodynamic description, in Appendix 1;

suggests that none of the high temperature observations reported earlier is PE. If the new database is employed, all of the earlier observations can be fitted using the present model without employing the capacity concept. We have therefore refrained from further discussing these high temperature results until a more reliable thermodynamic description is developed and agreed upon.

In the case of the Fe-Mo-C system, the apparently constant dissipation during decarburization was shown to be a natural consequence of a slowly varying dissipation with time (and interface velocity) giving a ferrite growth rate very close to parabolic.

3.3 Grain Size Effect in Precipitation:

The role of soft impingement in precipitation and the associated effect of grain size on the ferrite volume fraction are illustrated in Figure 3-1, which shows the predicted evolution of an alloy containing 2.41%Ni and 0.078%C transformed at 700 °C for grain size of 10, 20, 50, 100 and 500 μm . It is clear from these simulations that the buildup of the Ni spike is very slow at this temperature and that the transition to LENP would take very long times that are unlikely to be encountered experimentally. This conclusion is similar to that reached by Odqvist *et al.* who modeled the transition from PE to LE-NP using a semi-infinite geometry. The role of soft impingement is critical for understanding the behavior of finite specimens because it leads to a rapid decrease in interface velocity. The drop in the Ni concentration associated with this rapid decrease in velocity finally leads to the flattening or inversion of the carbon profile in the vicinity of the interface and the

arrest of ferrite growth. The predicted ferrite fractions when growth stops are 0.85, 0.84, 0.84, 0.84, 0.82 and 0.75 for samples in which the grain sizes are 5, 10, 20, 50, 100 and 500 μm , respectively. Several points are worth emphasizing at this stage:

- It is difficult to explore the evolution of the kinetics and contact conditions at low velocities using typical precipitation experiments (grain size 20-100 μm) because these velocities are only accessible after soft impingement. A key advantage of the decarburization method is that it permits one to easily access velocities below 1.10^{-8} m/s and estimate the operating contact conditions at these velocities. It is thus possible to observe the transition from PE to LENP experimentally under appropriate decarburization conditions.
- The ferrite volume fraction appears to be independent of grain size over a wide range of conditions. Goune *et al.* have reported experimental data that confirms this prediction. The reason for the apparently constant ferrite volume fraction is that the arrest of ferrite growth is triggered by the impingement of the carbon concentration profiles and the associated rapid decrease in velocity. Using the Zener approximation it is possible to show using a global carbon balance that the impingement of the carbon profiles as a function of grain size will occur at essentially the same ferrite volume fraction.

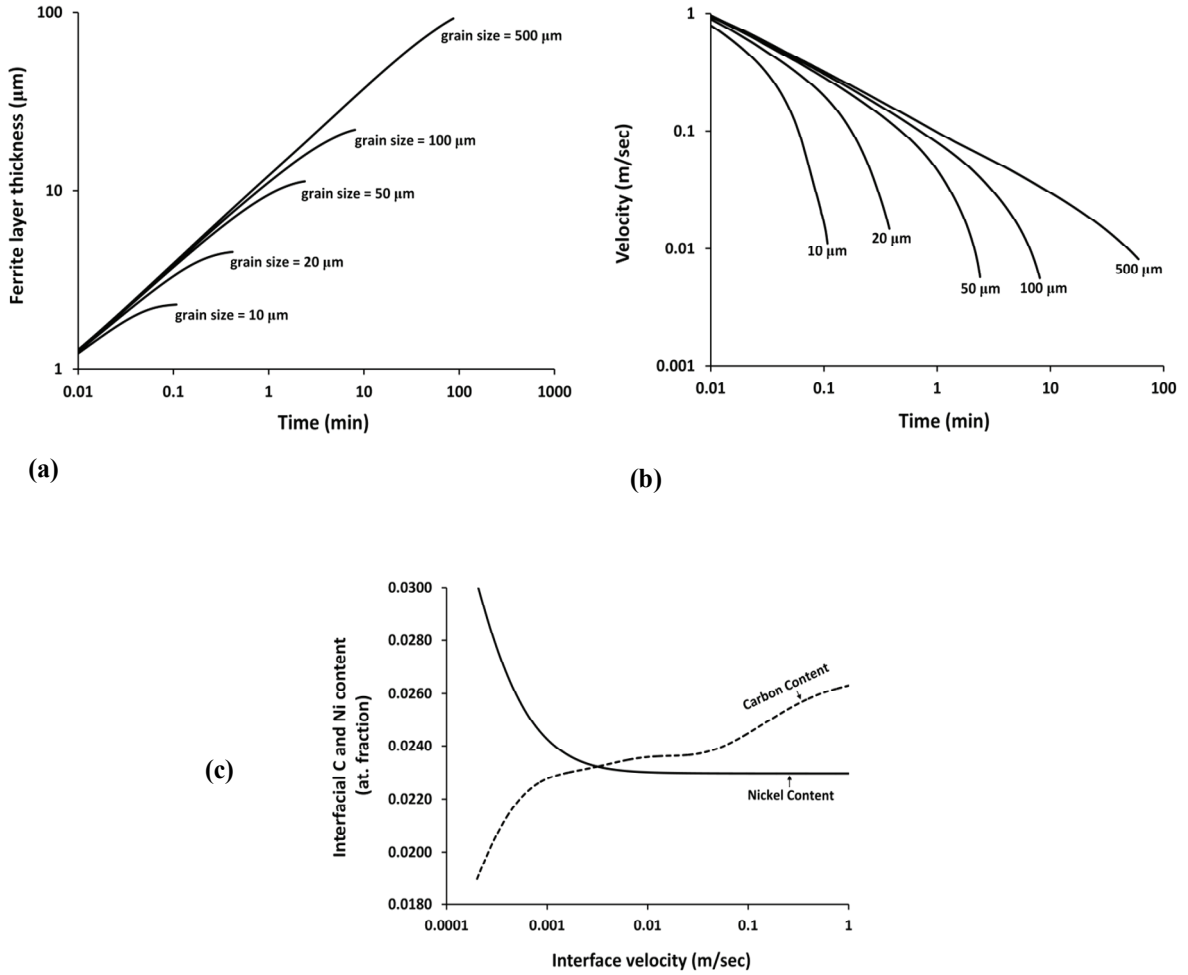


Figure 3-1: Predicted evolution of ferrite layer in an alloy containing 2.41% Ni and 0.078% C transformed at 700 °C for grain size of 10, 20, 50, 100 and 500 μm. a) Thickness of the ferrite layer vs. time b) Interface velocity vs. time c) evolution of austenite nickel and carbon concentration vs. interface velocity

However, one should be careful as there might be situations at which impingement of carbon profiles is not the underlying reason for arrest of the ferrite growth. In other words, in some cases stoppage of the interface due to the formation of the substitutional alloying element spike ahead of the migrating interface may occur before impingement of the carbon profiles. Such situations are more likely to be seen at higher temperatures and in samples with large austenite grain sizes. For example, recent publication by Liu et.al [77] confirms that the prior-austenite grain size does

have an effect on pro-eutectoid ferrite fraction but, this effect diminishes gradually with decreasing transformation temperature. It shows that, the importance of the initial austenite grain sizes increases at high temperatures.

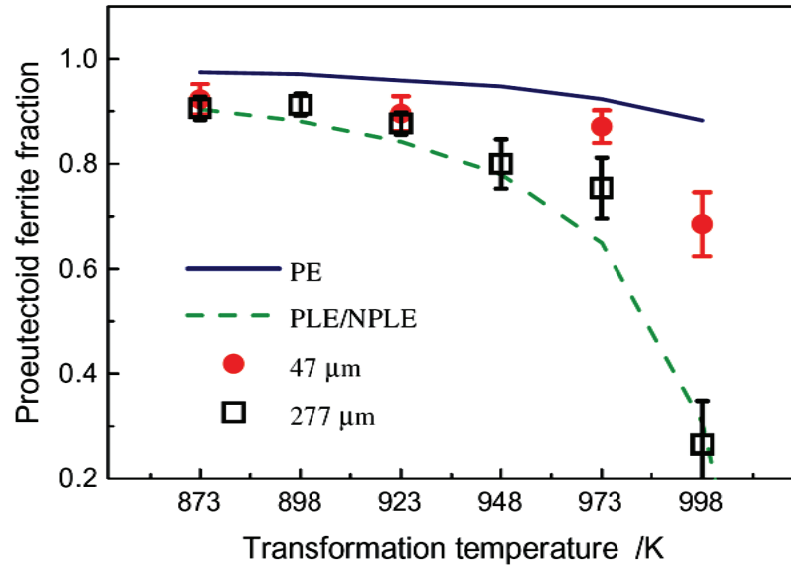


Figure 3-2: Effect of the precipitation temperature and prior austenite grain size on final ferrite volume fraction in Fe-2Mn-0.05C alloy. Dotted line shows the ferrite fraction predicted by assuming LENP boundary conditions and the solid line shows the ferrite fraction predicted by assuming PE boundary conditions [77]

4. CONCLUSIONS

A new model was presented for the interaction of prototypical alloying elements (a strong carbide formers, Mo, Si and Cr, austenite and ferrite stabilizers, Mn, Ni and Cu) with migrating ferrite-austenite interfaces in alloy steels. The model owes much to and is considered an advance on several previous efforts to describe quantitatively this fundamental aspect of microstructure development in steels.

The elements of the new model consist in: a multiple discrete-jump approach to the trans-interface transport of substitutional solute; the incorporation of the Gibbs energy dissipation associated with the kinetic interfacial solute profiles; and the assignment of a temperature-independent binding energy of each of the solutes to the interface. The frequencies of diffusive jumps within the interface region are systematically derived from volume diffusion data in the parent phases. The fast-diffusing interstitial carbon is considered to be in local equilibrium at all times.

The challenge for the present model lies in the self-consistent description of recently acquired data on ferrite growth in the decarburization of ternary Fe-C-Mo, Fe-C-Mn, Fe-C-Si, Fe-C-Cr and Fe-C-Cu alloys over a range of compositions and temperatures, as well as the precipitation of proeutectoid ferrite from Fe-C-Ni and Fe-C-Mn austenite. The latter includes a signature quantity, the volume fraction of ferrite formed after extended isothermal reaction. This quantity, resulting from a cessation of fast ferrite growth, proved elusive in previous modeling studies. It is shown that the model satisfactorily predicts this quantity, including its dependence on austenite grain size. Of course, once initial growth

has ceased, interfacial tie-lines will begin to shift and alloying element diffusion profiles develop in both ferrite and austenite phases, as suggested by [32] and [78]. The present model will then no longer apply. Reports of alloying element spikes based on microanalyses of specimens for which initial fast growth has ceased are therefore complementary to the model results discussed here, but they are not directly germane.

The kinetic evidence for spikes" buried in austenite" and their interaction with moving interfaces as reported by Chen and van der Zwaag [64], [65] appears to be consistent with the present model's suggestion of a rapid transition to full local equilibrium in Fe-C-Mn at higher temperatures.

The "adjustable parameters" employed in the current work are the solute binding energy and trans-interface diffusivity. However, the requirement that the characteristics of ferrite growth during decarburization and precipitation in Fe-C-Mn be reproduced places severe limits on the choices of these parameters for that system. Similarly, for Fe-C-Ni and Fe-C-Mo, the range of solute binding energies yielding viable solutions is strongly constrained.

An outcome of the present work is a suggestion for the resolution of a troubling paradox, the reported transition to a long-lived paraequilibrium state with increasing temperature in Fe-C-Mn alloys. It is considered that the accepted thermodynamic database is suspect at these highest temperatures. A suggested revision, consistent with experimental data,

that does not materially influence the computed phase equilibria at lower temperatures, is presented in Appendix 1:

Another important prediction of interest lies in the examination of the variation of the alloying element composition in the parent austenite as a function of time and temperature. The question of the “alloying element spike” in austenite has remained a challenge for more than a half-century. Although the present estimates are meant to be qualitative rather than definitive, they suggest that the complete spike will exist only at the highest transformation temperatures and that in general growth may occur with only a fractional spike.

We conclude that the present model, while remaining limited in certain aspects (it refers to the motion of planar, “incoherent” interfaces, for example), is able to answer a substantial number of outstanding questions in this long-standing area of research. In particular, the successful prediction of cessation of rapid ferrite growth depends on the incorporation of solute drag and of carbon diffusion field impingement effects.

5. Future works

Even though the current version of the developed model has been able to predict the experimental observation in a rather wide range of temperatures and compositions successfully, there are still some limitations which are worth to be addressed in the future versions of this model. Some of the possible steps in line with improvement of the model are listed below:

1. From practical point of view, one may want to extend application of this model to more industrially favorable alloying systems with more complicated chemistries. It means that, the interaction of each alloying elements with the interface and other alloying elements present in the system should be considered.
2. Also, extending its application to lower temperature regions, where Widmanstatten ferrite and bainite formation are expected, will be another challenging objective which can significantly improve applicability of this model. In this regard, as the first step, it is suggested to extend the model to a mixed-mode model in which importance of both diffusional process and structural changes are taken into account.
3. It is worth to pay attention to the fundamental problems exist in the Murray-Landis algorithm (finite difference approach) for calculating the carbon concentration profiles in austenite and ferrite. It seems that, it would be necessary to either find an alternative algorithm for such calculations or apply some

modifications to the current Murray-Landis version used in the present study to improve numerical accuracy and computational efficiency. Some of the problems exist in Murray-Landis algorithm are explained by Chen *et.al* [65] in their paper on mixed-mode model for kinetics of ferrite and austenite growth in cyclic transformation experiments. For example, it is well known that that due to some approximations used to simplify the calculations, solute conservation rule and mass balance is not fully satisfied (specially for large supersaturations) [3].

4. Backward motion of the interface during temperature jump experiments in the present study is still an unsolved mystery which is worth more in-depth investigations.

Appendix 1:

The modified thermodynamic description of Fe-Mn-C at high temperatures

The phase equilibria between ferrite and austenite in the Fe-Mn system were experimentally investigated by Troiano and McGuire [79], Hillert [80] and Srivastava and Kirkaldy [81]. The last authors reported the 95% confidence interval of their measurements as +/- 3%. The experimental data is summarized in Figure Ap1-1 along with the thermodynamic model due to Huang [82] which is the basis of the TCFE2 database of ThermoCalc. It is clear from the comparison that the pioneering treatment of Huang [82] systematically underestimates the solubility of Mn in ferrite at high temperatures. The discrepancy is, arguably, insignificant for most applications. In the present case, however, the difference between the experiments and model predictions at 822 °C is sufficient to change the interpretation of the decarburization data at 825 °C; PE is predicted if the description of [79] is used, while LENP would be predicted if one modified the description to fit the experimental data of Srivastava and Kirkaldy [81] at 822 °C. We have, therefore, modified the description of [82] in order to produce a better fit of the experimental data as shown by the solid curves in Figure Ap1-1. The modifications were limited to, namely:

$$\Delta L(\text{bcc, Fe,Mn:Va;0}) = 4007.8 - 4.44 T(\text{k}) \text{ J/mole}$$

Here, ΔL is the difference between the L parameter used in the new description and that used in the original TCFE2 .

This description was used for all calculations on the Fe-Mn-C system in this contribution. A more thorough examination of the thermodynamics, including new experimental data between 822 °C and 900 °C seems necessary in order to reach definitive conclusions as to the operating interfacial conditions during decarburization at high temperatures.

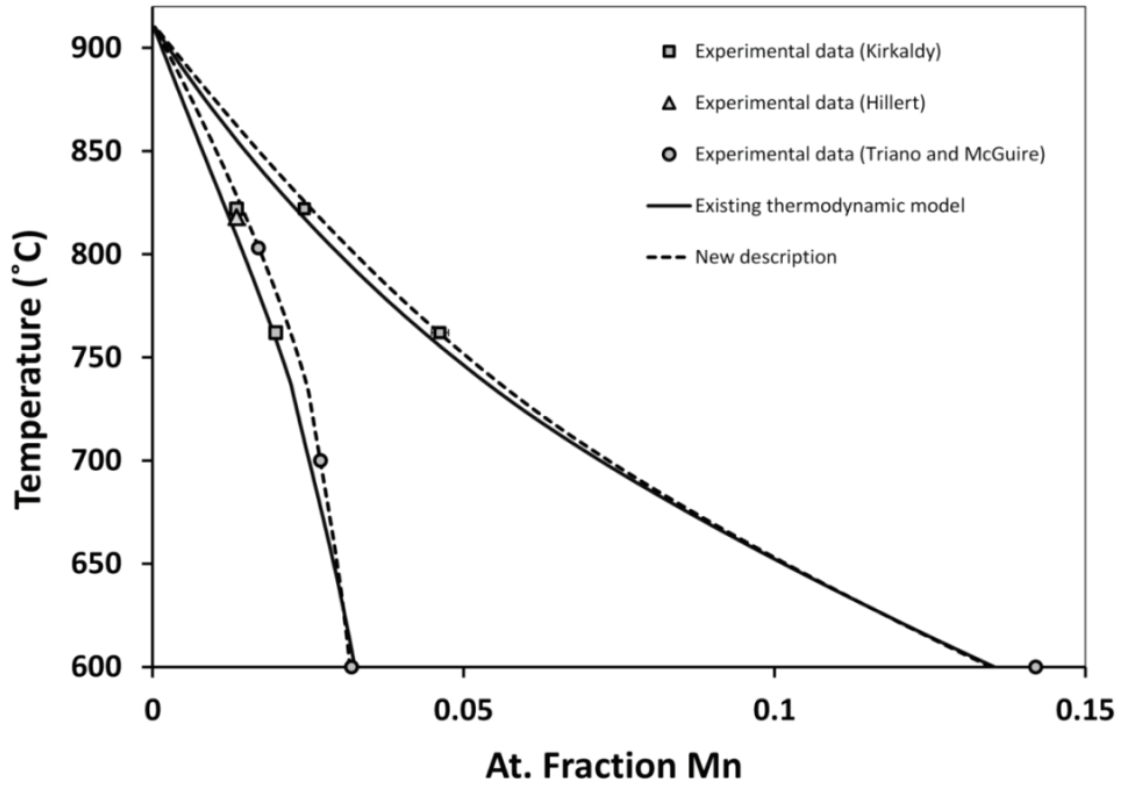


Figure Ap1-1: portion of the Fe-Mn-C phase diagram. Experimental data points along with the calculated phase boundaries using thermodynamic models by Huang [82], Srivastava and Kirkaldy [81] and the modified version of Huang's description.

Appendix 2: Two-jump vs. Three-jump model

As explained in section [1], in the model it was assumed that the interface to consist of four atomic planes (as shown in Figure 2-2), and diffusion from one side of the interface to the other side involved 3 jumps: one jump between ferrite and the interface, another jump between two atomic planes within the interface and finally a jump between the interface and austenite.

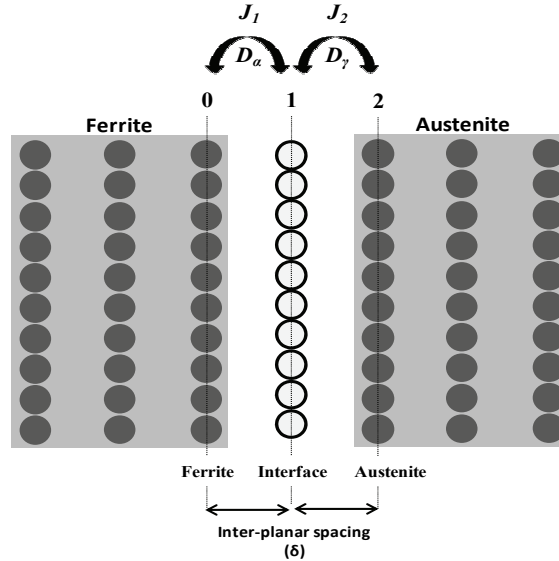


Figure Ap2-1: Two-jump model in terms of atomic planes (0,1,2) and diffusivity values D_α and D_γ for jumps from ferrite into the interface (J_1) and from austenite into the interface (J_2)

Contribution of the second jump within the interface in the total dissipation of free energy is a key question which is worth to be analysed. In other words, it would be interesting to see what would be the difference between value of the free energy dissipation predicted by a two-jump model, in which no atomic jump happens within the interface, and predicted value in the three-jump model (original model). Schematic of such a two-jump model is presented in Figure AP2-1.

To do so, a series of calculation, with two atomic jumps and three atomic jumps, were performed on Fe-0.51 Mo-0.54 C system at 717 °C, 806 °C and 825 °C. In all cases the bulk ferrite diffusion coefficient (D^α) and the bulk austenite diffusion coefficient (D^γ) were used for jumping from ferrite into the interface and from austenite into the interface, respectively. In the case of the three-jump model the geometric average was used for jumping within the interface.

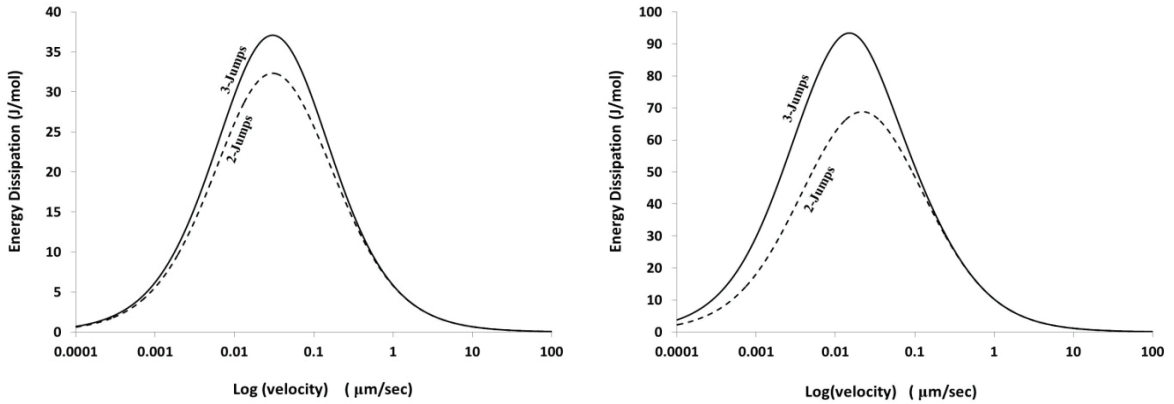
Moreover, effect of the depth of the potential well at the interface (E) has been analysed by changing E from 15 KJ/mol to 20 KJ/mol. Results of these calculations are presented in Figure Ap2- to Figure Ap2-.

As seen in these figures, while at very high and very low velocities both models predict the same value for dissipation of free energy, at intermediate velocities, which are usually encountered in experiments, deviation between the two models becomes rather significant.

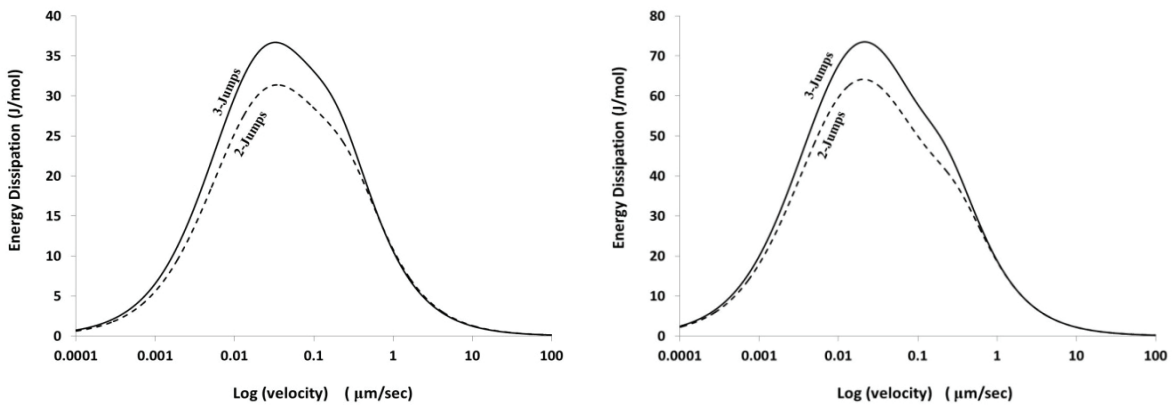
However, in the case of the two-jump approach, one can still fit the experimental data by treating diffusivity values (D_1 and D_2) as adjustable parameters. In other words, bulk austenite and bulk ferrite diffusivities should be replaced by other values which can be determined by iteration.

Also, simultaneously it is shown in these figures that the effect of the potential well depth at the interface is more pronounced on the predicted dissipation values during transformation. In other words, introduction of a small change in this value may make a

big difference in the predicted kinetic by these models. For example, as seen in these figures, dissipation value has been almost doubled by changing the potential well from 15 KJ/mol to 20 KJ/mol.



(a) (b)
 Figure Ap2-2: Effect of the second jump within the interface on free energy dissipation during austenite to ferrite transformation in Fe-0.51 Mo-0.54 C system at 717 °C. The dotted-line represents results without the second jump (two-jump model) and the solid line represents results including the second jump (three-jump model). a) $E=15$ KJ/mole b) $E=20$ KJ/mole



(a) (b)
 Figure Ap2-3: Effect of the second jump within the interface on free energy dissipation during ferrite grain growth in Fe-0.51 Mo-0.54 C system at 717 °C. The dotted-line represents results without the second jump (two-jump model) and the solid line represents results including the second jump (three-jump model). a) $E=15$ KJ/mole b) $E=20$ KJ/mole

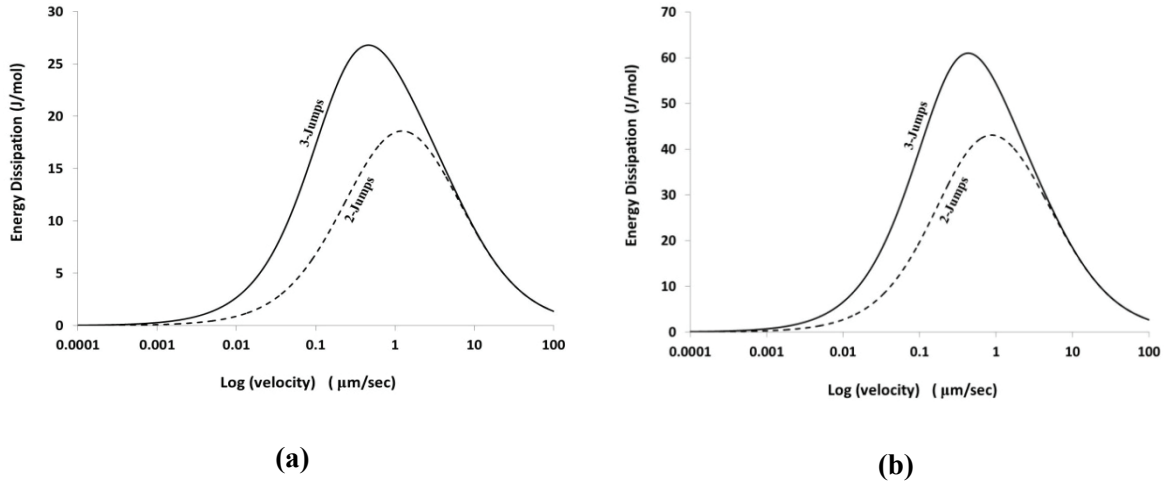


Figure Ap2-4: Effect of the second jump within the interface on free energy dissipation during austenite to ferrite transformation in Fe-0.51 Mo-0.54 C system at 806 °C. The dotted-line represents results without the second jump (two-jump model) and the solid line represents results including the second jump (three-jump model). a) $E=15$ KJ/mole b) $E=20$ KJ/mole

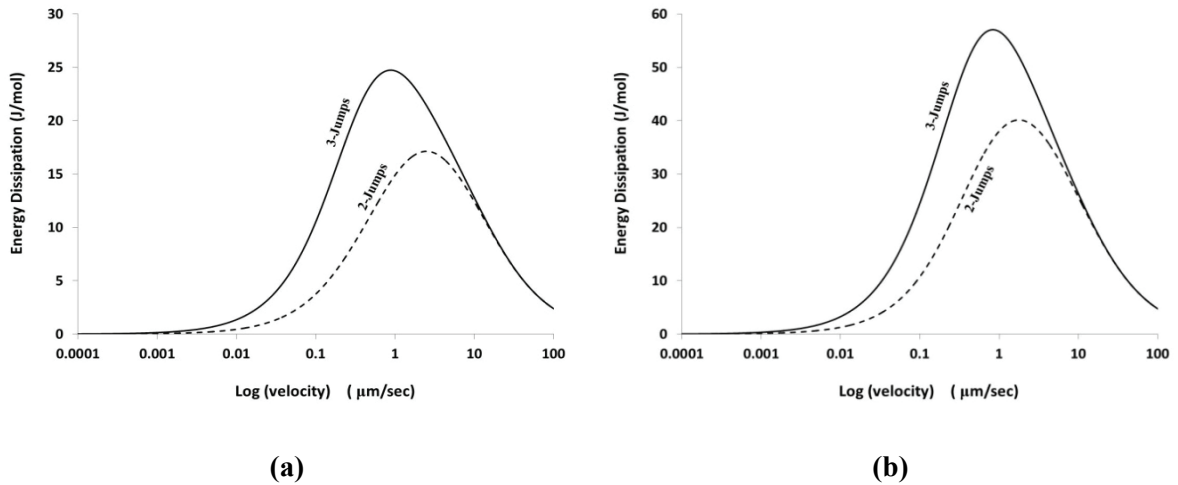


Figure Ap2-5: Effect of the second jump within the interface on free energy dissipation during austenite to ferrite transformation in Fe-0.51 Mo-0.54 C system at 825 °C. The dotted-line represents results without the second jump (two-jump model) and the solid line represents results including the second jump (three-jump model). a) $E=15$ KJ/mole b) $E=20$ KJ/mole

6. References:

- [1] C. Zener, *Journal of Applied Physics*, vol. 20, no. 10, pp. 950–953, Oct. 1949.
- [2] M. Hillert, *Acta Materialia*, vol. 47, no. 18, pp. 4481–4505, Dec. 1999.
- [3] A. Van der Ven and L. Delaey, *Progress in Materials Science*, vol. 40, no. 3, pp. 181–264, 1996.
- [4] M. Hillert, *Phase Equilibria, Phase Diagrams and Phase Transformations: Their Thermodynamic Basis*. Cambridge University Press, 2007.
- [5] J.-O. Andersson and J. Ågren, *Journal of Applied Physics*, vol. 72, no. 4, pp. 1350–1355, Aug. 1992.
- [6] C. Hutchinson, A. Fuchsmann, and Y. Brechet, *Metallurgical and Materials Transactions A*, vol. 35, no. 4, pp. 1211–1221, 2004.
- [7] Reynolds Jr. W.T, Enomoto, M., and Aaronson, H.I., “PROEUTECTOID FERRITE REACTION.,” in *Phase Transformations in Ferrous Alloys*, OH, USA, 1984, pp. 155–200.
- [8] T. Furuhashi and H. I. Aaronson, *Scripta Metallurgica*, vol. 22, no. 10, pp. 1635–1637, Oct. 1988.
- [9] Gary R. Purdy and J. Kirkaldy, *Trans TMS-AIME*, vol. 227, pp. 1255–66, 1963.
- [10] A. Phillion, H. S. Zurob, C. R. Hutchinson, H. Guo, D. V. Malakhov, J. Nakano, and G. R. Purdy, *Metallurgical and Materials Transactions A: Physical Metallurgy and Materials Science*, vol. 35 A, no. 4, pp. 1237 – 1242, 2004.
- [11] G. P. Krielaart, J. Sietsma, and S. van der Zwaag, *Materials Science and Engineering: A*, vol. 237, no. 2, pp. 216–223, Sep. 1997.
- [12] J. Sietsma and S. Van Der Zwaag, *Acta Materialia*, vol. 52, no. 14, pp. 4143 – 4152, 2004.
- [13] G. Purdy, “Diffusion and Dissolution-Controlled Transformation in Dilute Ternary Austenite,” PhD, McMaster University, Hamilton, Ontario, Canada, 1962.
- [14] M. Hillert, in *Suppl. Trans. ISIJ*, 1971, vol. 11, p. 1153.
- [15] H. Oikawa, J.-F. Remy, and A. G. Guy, *Trans. ASM*, vol. 61, p. 110, 1968.
- [16] C. R. Hutchinson, H. S. Zurob, and Y. Brechet, *Metall. Mater. Trans. A, Phys. Metall. Mater. Sci. (USA)*, vol. 37A, no. 6, pp. 1711 – 20, 2006.

- [17] H. S. Zurob, C. R. Hutchinson, A. Beche, G. R. Purdy, and Y. J. M. Brechet, *Acta Mater.*, vol. 56, no. 10, pp. 2203 – 11, 2008.
- [18] H. S. Zurob, C. R. Hutchinson, Y. Brechet, and G. R. Purdy, “A study of the austenite to ferrite transformation in Fe-C-X alloys using decarburization experiments,” in *Proceedings of an International Conference on Solid-Solid Phase Transformations in Inorganic Materials 2005*, Phoenix, AZ, United States, 2005, vol. 1, pp. 111 – 116.
- [19] D. Malakhov, “Lectures on Phase Transformation of Materials,” McMaster University.
- [20] D. V. Malakhov and G. R. Purdy, “Thermodynamic aspects and kinetic modeling of decarburization of steels in walking-beam furnaces,” in *Progress in Heat Treatment and Surface Engineering*, Gothenburg, Sweden, 2000, pp. 9 – 20.
- [21] O. Karabelchtchikova, “Fundamentals of Mass Transfer in Gas Carburizing,” PhD, Worcester Polytechnic Institute, Worcester, Massachusetts, United States, 2007.
- [22] J. Ågren, *Scripta Metallurgica*, vol. 20, no. 11, pp. 1507–1510, Nov. 1986.
- [23] A. Béché, H. S. Zurob, and C. R. Hutchinson, *Metallurgical and Materials Transactions A*, vol. 38, no. 12, pp. 2950–2955, 2007.
- [24] J.S. Kirkaldy, *Can. J. Phys.*, vol. 36, p. 907, 1958.
- [25] M. Hillert, “Paraequilibrium,” Swedish Institute for metal research, Stockholm, Sweden, 1953.
- [26] D. Coates, *Metallurgical and Materials Transactions B*, vol. 4, no. 4, pp. 1077–1086, 1973.
- [27] D. Coates, *Metallurgical and Materials Transactions B*, vol. 3, no. 5, pp. 1203–1212, 1972.
- [28] M. Hillert, “The Mechanism of Phase Transformation in Crystalline Solids,” Inst. of Metals, London, 33, 1969.
- [29] Purdy, G. R., Weichert, D. H., and S.Kirkaldy, J., *Trans AIME*, vol. 230, no. 5, pp. 1025–34, 1964.
- [30] M. Enomoto, *Metallurgical and Materials Transactions A*, vol. 37, no. 6, pp. 1703–1710, 2006.
- [31] G. R. Purdy and Y. J. M. Brechet, *Acta Metallurgica et Materialia*, vol. 43, no. 10, pp. 3763–3774, Oct. 1995.
- [32] A. Hultgren, *Trans. ASM*, vol. 39, pp. 915–1005, 1947.

- [33] J. Gilmour, G. Purdy, and J. Kirkaldy, *Metallurgical and Materials Transactions B*, vol. 3, no. 12, pp. 3213–3222, 1972.
- [34] M. Hillert, “Calculation of phase equilibria,” in *Phase Transformations: Papers presented at a seminar of the American Society for Metals, October 12 and 13, 1968*, Metal Park, Ohio, pp. 181–218, 1970.
- [35] D. V. Malakhov and G. R. Purdy, *Canadian Metallurgical Quarterly*, vol. 41, no. 2, pp. 231–242, 2002.
- [36] H. Guo, G. R. Purdy, M. Enomoto, and H. I. Aaronson, *Metallurgical and Materials Transactions A: Physical Metallurgy and Materials Science*, vol. 37, no. 6, pp. 1721 – 1729, 2006.
- [37] J. Odqvist, B. Sundman, and J. Agren, *Acta Materialia*, vol. 51, no. 4, pp. 1035 – 1043, 2003.
- [38] J. Odqvist, M. Hillert, and J. Agren, *Acta Materialia*, vol. 50, no. 12, pp. 3211 – 3225, 2002.
- [39] M. Hillert and B. Sundman, *Acta Metallurgica*, vol. 24, no. 8, pp. 731 – 743, 1976.
- [40] H. Guo and M. Enomoto, *Metallurgical and Materials Transactions A: Physical Metallurgy and Materials Science*, vol. 38, no. 6, pp. 1152 – 1161, 2007.
- [41] H. S. Zurob, C. R. Hutchinson, Y. Brechet, H. Seyedrezai, and G. R. Purdy, *Acta Mater.*, vol. 57, no. 9, pp. 2781 – 92, 2009.
- [42] C. L. Bauer, “Recent theoretical and experimental advances in the understanding of grain boundary migration,” in *Journal de Physique Colloque*, France, vol. 43, pp. 187 – 97, 1982.
- [43] E. Gamsjager, M. Militzer, F. Fazeli, J. Svoboda, and F. D. Fischer, *Computational Materials Science*, vol. 37, no. 1–2, pp. 94 – 100, 2006.
- [44] J. W. Cahn, *Acta Metallurgica*, vol. 10, no. 9, pp. 789–798, Sep. 1962.
- [45] K. Lucke and H. P. Stuwe, *Acta Metall.*, vol. 19, no. 10, pp. 1087 – 99, 1971.
- [46] K. Deter and K. Lucke, “The influence of defined small amounts of impurities on the recrystallization of aluminum,” Brown Univ., AFOSR-TN-56-103; AD-82016, 1956.
- [47] M. Hillert, *Zeitschrift fuer Metallkunde/Materials Research and Advanced Techniques*, vol. 96, no. 2, pp. 104 – 107, 2005.
- [48] M. Hillert, *Acta Materialia*, vol. 52, no. 18, pp. 5289 – 5293, 2004.

- [49] M. Hillert, J. Odqvist, and J. Ågren, *Scripta Materialia*, vol. 50, no. 4, pp. 547–550, Feb. 2004.
- [50] L. Zi-Kui and J. Ågren, *Acta Metallurgica*, vol. 37, no. 12, pp. 3157–3163, Dec. 1989.
- [51] M. Suehiro, Z.-K. Liu, and J. Ågren, *Acta Materialia*, vol. 44, no. 10, pp. 4241–4251, Oct. 1996.
- [52] M. Suehiro, Z.-K. Liu, and J. Agren, *Metallurgical and Materials Transactions A: Physical Metallurgy and Materials Science*, vol. 29, no. 13, pp. 1029 – 1034, 1998.
- [53] Z.-K. Liu, *Metall. Mater. Trans. A, Phys. Metall. Mater. Sci.*, vol. 28A, no. 8, pp. 1625 – 31, 1997.
- [54] M. Enomoto, *Acta Materialia*, vol. 47, no. 13, pp. 3533 – 3540, 1999.
- [55] M. Hillert, J. Odqvist, and J. Agren, *Scripta Materialia*, vol. 45, no. 2, pp. 221 – 227, 2001.
- [56] M. Hillert, *Acta Materialia*, vol. 47, no. 18, pp. 4481–4505, Dec. 1999.
- [57] G. Purdy, J. Ågren, A. Borgenstam, Y. Bréchet, M. Enomoto, T. Furuhashi, E. Gamsjager, M. Gouné, M. Hillert, C. Hutchinson, M. Militzer, and H. Zurob, *Metallurgical and Materials Transactions A*, vol. 42, no. 12, pp. 3703–3718, Sep. 2011.
- [58] C. R. Hutchinson, A. Fuchsmann, H. S. Zurob, and Y. Brechet, *Scripta Materialia*, vol. 50, no. 2, pp. 285–290, Jan. 2004.
- [59] K. Oi, C. Lux, and G. R. Purdy, *Acta Mater.*, vol. 48, no. 9, pp. 2147 – 55, May 2000.
- [60] Aaronson, H.I. and Domian, H.A., *Trans. metall. Soc. A.I.M.E.*, vol. 236, p. 781, 1966.
- [61] C. Capdevila, J. Cornide, K. Tanaka, K. Nakanishi, and E. Urones-Garrote, *Metallurgical and Materials Transactions A: Physical Metallurgy and Materials Science*, vol. 42, pp. 3719 – 3728, 2011.
- [62] E. S. Humphreys, H. A. Fletcher, J. D. Hutchins, A. J. Garratt-Reed, W. T. Reynolds Jr., H. I. Aaronson, G. R. Purdy, and G. D. W. Smith, *Metallurgical and Materials Transactions A: Physical Metallurgy and Materials Science*, vol. 35 A, no. 4, pp. 1223 – 1235, 2004.
- [63] M. Enomoto, N. Maruyama, K. . Wu, and T. Tarui, *Materials Science and Engineering: A*, vol. 343, no. 1–2, pp. 151–157, Feb. 2003.

- [64] H. Chen and S. van der Zwaag, *Philosophical Magazine Letters*, vol. 92, no. 2, pp. 86–92, 2012.
- [65] H. Chen, B. Appolaire, and S. van der Zwaag, *Acta Materialia*, vol. 59, no. 17, pp. 6751–6760, Oct. 2011.
- [66] H. Chen and S. Van Der Zwaag, *Journal of Materials Science*, vol. 46, no. 5, pp. 1328 – 1336, 2011.
- [67] W.D. Murry and F. Landis, *Trans. ASME*, vol. 81D, pp. 106–12, 1959.
- [68] B. Sundman, B. Jansson, and J.O Andersson, *Calphad*, vol. 9, p. 153, 1985.
- [69] M. Hillert, “Application of Gibbs energy-composition diagram,” in *Lectures on the theory of phase transformation*, Warendale, Pennsylvania, pp. 1–33, 1999.
- [70] C. W. Sinclair, C. R. Hutchinson, and Y. Bréchet, *Metall and Mat Trans A*, vol. 38, no. 4, pp. 821–830, Apr. 2007.
- [71] F. Fazeli and M. Militzer, *Metall and Mat Trans A*, vol. 36, no. 6, pp. 1395–1405, Jun. 2005.
- [72] H. Larsson and A. Borgenstam, *Scripta Materialia*, vol. 56, no. 1, pp. 61–64, Jan. 2007.
- [73] P. Bellon and G. Martin, *Phys. Rev. B*, vol. 66, no. 18, p. 184208, Nov. 2002.
- [74] P. Maugis and G. Martin, *Phys. Rev. B*, vol. 49, no. 17, pp. 11580–11587, May 1994.
- [75] Mingxing Guo and Hatem Zurob, “Internal report,” McMaster University, 2011.
- [76] K. . Wu, M. Kagayama, and M. Enomoto, *Materials Science and Engineering: A*, vol. 343, no. 1–2, pp. 143–150, Feb. 2003.
- [77] Z.-Q. Liu, G. Miyamoto, Z.-G. Yang, and T. Furuhashi, *Acta Materialia*, vol. 61, no. 8, pp. 3120 – 3129, 2013.
- [78] H. Guo and G. R. Purdy, *Metall and Mat Trans A*, vol. 39, no. 4, pp. 950–953, Apr. 2008.
- [79] A. R. Troiano and F. T. McGuire, *Trans. Am. Soc. Met.*, vol. 31, p. 340, 1943.
- [80] M. Hillert, T. Wada, and H. Wada, *J. Iron Steel Inst.*, vol. 205, p. 539, 1967.
- [81] K. K. Srivastava and J. S. Kirkaldy, *Metallurgical transactions. A, Physical metallurgy and materials science*, vol. 13 A, no. 12, pp. 2113–2119, 1982.

- [82] W. Huang, *Metallurgical and Materials Transactions A*, vol. 21A, no. 8, p. 2115, 1990.